SPECTROCHEMICAL ANALYSIS OF FOOD AND BIO SAMPLES USING LASER INDUCED PLASMA SPECTROSCOPY

BY

MOHSIN SARWAR

A Thesis Presented to the

DEANSHIP OF GRADUATE STUDIES

KING FAHD UNIVERSITY OF PETROLEUM & MINERALS

DHAHRAN, SAUDI ARABIA

In Partial Fulfillment of the
Requirements for the Degree of

MASTER OF SCIENCE

In

PHYSICS

MAY 2017

KING FAHD UNIVERSITY OF PETROLEUM & MINERALS

DHAHRAN- 31261, SAUDI ARABIA

DEANSHIP OF GRADUATE STUDIES

This thesis, written by **Mohsin Sarwar** under the direction his thesis advisor and approved by his thesis committee, has been presented and accepted by the Dean of Graduate Studies, in partial fulfillment of the requirements for the degree of **Master of Science in Physics.**

M. A. Gondal

Dr. M. A. Gondal
(Advisor)

Dr. Abdullah A. Al-Sunaidi
Department Chairman

Dr. Akhtar A. Naqvi
(Member)

Dr. Salam A. Zummo
Dean of Graduate Studies

عمادة الدراسات العليا
DEANSHIP OF GRADUATE STUDIES

Rgasmi

Dr. Khaled Gasmi
(Member)

4/6/17

Date

2017

This work is dedicated to the most precious blessing of ALLAH for me “my Mother”, who brought me in this position with her support, look after, encouragement, scarification and special prayers.

ACKNOWLEDGMENTS

As nothing can be happened without the will and help of ALLAH jalla shanahu, I am very much thankful to him for the completion of this study. Many many thanks to my respected supervisor Dr. M. A. Gondal to train, guide, encourage and motivate me throughout the present research. Respected committee members Dr. Akhtar Abbas Naqvi and Dr. Khalid Gasmi are specially acknowledged to help me in this research. The support by the Physics department and KFUPM is gratefully acknowledged. This work was supported under the project NO. RG 1421 by deanship of scientific research (DSR). Technical support from all laser group members specially Mr. M. A. Dastageer, Mr. Taoreed O. Owolabi ,Dr. Umair, Mr. Abul Lais, Mr M. Younas, my senior Mr. Habeeb and the technician Mr. Pillae to complete this study is also appreciated. ICP staff is also acknowledged for his great efforts. I am very much thankful to the chairman of Physics Department Dr. Abdullah A. Al-Sunaidi to recommend me in different departments for research. Special thanks to my wife to help and encourage during the whole research period. May almighty ALLAH give them best rewards of their support and efforts. Ameen!

Table of Contents

List of Tables

LIST OF FIGURES

LIST OF ABBREVIATIONS

LIBS: Laser Induced Breakdown Spectroscopy

LTE: Local Thermodynamic Equilibrium

ICP: Inductively Coupled Plasma

ICP-MS: - Inductively Coupled Plasma Mass Spectroscopy

GI: Gingival Index

PI: Plaque Index

CAL: Clinical Attachment Loss

PD: Pocket Depth

IUPAC: International Union of Pure and Applied Chemistry

ICP-OES: Inductively Coupled Plasma Optical Emission Spectroscopy

TRLIBS: Time Resolve Laser Induced Breakdown Spectroscopy

LAS: Laser Ablation Spectroscopy

LSS: Laser Spark Spectroscopy

UV: Ultra-Violet

Nd-YAG: Neodymium Yttrium Aluminum Garnet

KBr: Potassium Bromide

LA-ICP-MS: Laser Ablation Inductively Coupled Mass Spectroscopy

ICCD: Intensified Coupled Charged Device

NIST: National Institute of Standard and Technology

eV: Electron Volt

LIP: Laser Induced Plasma

ppm : Part Per Million

LOD: Limit of Detection

AAS: Atomic Absorption Spectrometry

HPLC: High-Performance Liquid Chromatography

HPCE: High-Performance Capillary Electrophoresis

PMT: Photomultiplier Tube

RF: Radio Frequency

NAA: Neutron Activation Analysis

SFDA: Saudi Food and Drug Authority

ABSTRACT

Full Name : [Mohsin Sarwar]

Thesis Title : Spectrochemical Analysis of Food and Bio samples using Laser induced Plasma Spectroscopy

Major Field : Physics

Date of Degree : May, 2017

The sensitivity and limit of detection (LOD) of our LIBS system, was optimized by study of dependence of LIBS signal intensity on plasma parameters [such as plasma temperature (T) and electron density (n_e)]. In addition, the LIBS signal intensity dependence on laser fluence and the delay time has also been investigated. Lastly in this study, we estimated the concentration levels of toxic and carcinogenic elements in various food and biological samples.

Toxic elements Mn, Cr and Ba detected in five different coffee samples and their concentrations were measured by using chemometric method, which was found to be: Mn (22.36 –27.74 mg/L), Cr (1.99 –2.13 mg/L) and Ba (3.18 –3.83 mg/L). The measured concentrations detected for these elements exceed the safe permissible limit set by the World Health Organization (WHO) and European Union (EU). In the second part of the study, we analyzed two samples of colon tissues: one healthy and another cancerous by using LIBS calibration free method. This study shows that Ca concentration decreases from 295858.61 ppb to 2700.92 ppb in cancerous colon sample as compared to the healthy colon

samples. Hence, calcium can be a good marker for the diagnosis of colon cancer. Another variational trend of the elemental concentration, which is also of considerable merit, is that Ba, Cr, Mn, V, Fe, and Na increased from healthy to cancerous tissues in ppb value of 58.61→534.64, 781.30→6780.82, 649.40→5937.43, 517.31→4866.83, 137.35→1282.12 and 831.58→1308.92 respectively while Cd, Cu, and Pb decreased from healthy to cancerous colon tissues in ppb value of 356.12→32.27, 410.86→371.30 and 1557.62→146.43 respectively.

Other analytical techniques such as ICP-MS or ICP-OES has been applied for comparison against, and validation of, our LIBS results. A good agreement was achieved between LIBS and aforementioned techniques.

نبذة مختصرة

ملخص الرسالة

الاسم الكامل: محسن سروار

عنوان الرسالة: التحليل الطيفي للمواد الغذائية والحيوية العينات باستخدام الليزر الطيفي البلازما

التخصص: علوم فيزيائية

تاريخ الدرجة العلمية: مايو، 2017

تم تحسين الحساسية والحد من الكشف (لود) من نظام ليبس لدينا من خلال دراسة الاعتماد على كثافة إشارة ليبس على المعلمات البلازما [مثل درجة حرارة البلازما (T) وكثافة الإلكترون (ن)]. وبالإضافة إلى ذلك، تم أيضا التحقق من الاعتماد ليبس كثافة الإشارة على فلوينس الليزر ووقت التأخير. وأخيرا في هذه الدراسة، قدرنا مستويات تركيز العناصر السامة والسرطنة في مختلف العينات الغذائية والبيولوجية.

تم الكشف عن العناصر السامة من و كر و با في خمسة عينات مختلفة من القهوة وتم قياس تركيزاتها باستخدام طريقة كيميائية تم العثور عليها من (22.36 -27.74 ملغم / لتر) و كر (1.99 -2.13 ملغم / لتر) و با (3.18 -3.83 مجم / لتر). وتتجاوز التركيزات المقاسة التي تم اكتشافها لهذه العناصر الحدود المسموح بها التي حددتها منظمة الصحة العالمية والاتحاد الأوروبي. في الجزء الثاني من الدراسة، قمنا بتحليل عينات من أنسجة القولون: واحدة صحية وسرطانية أخرى باستخدام ليبس طريقة المعايرة الحرة. أظهرت هذه الدراسة أن تركيز الكالسيوم ينخفض من 295858.61 جزء في البليون إلى 2700.92 جزء في البليون في عينة القولون السرطاني بالمقارنة مع عينات القولون السليمة. وبالتالي، يمكن أن يكون الكالسيوم علامة جيدة لتشخيص سرطان القولون. وهناك اتجاه مختلف آخر لتركيز العنصر، وهو أيضا ذو ميزة كبيرة، هو أن با، كر، من، V، في، و نا زاد من أنسجة صحية إلى سرطانية في قيمة بب من 517.31→4866.83, 649.40→5937.43, 781.30→6780.82, 58.61→534.64, 831.58→1308.92, 137.35→1282.12 على التوالي في حين انخفض سد، النحاس، والرصاص من صحية إلى الأنسجة السرطانية في قيمة بب من146.43→1557.62, 410.86→371.30, 356.12→32.27على التوالي.

تم تطبيق تقنيات تحليلية أخرى مثل إيكب-مس أو إيكب-أوس لمقارنتها، والتحقق من نتائج ليبس لدينا. تم التوصل إلى اتفاق جيد بين ليبس والتقنيات المذكورة أعلاه.

Chapter 1: Introduction

1.1. Nd: YAG Laser

In LIBS Nd: YAG (neodymium doped Yttrium aluminums garnet Nd:$Y_3Al_5O_{12}$) solid state laser is used. Nd is a lasing medium which replaces 1% of yttrium ion from YAG. This laser has a 1064nm wavelength which can be converted by a nonlinear crystal to 1/4 (266 nm) of the actual wavelength. This frequency quadrupling is done by placing a nonlinear material in the optical path of the laser beam, which is polarized. Dipoles emit electromagnetic radiation of almost double the absorbing frequency due to their vibrations. Primarily there are two types of Nd: YAG laser one is the continuous wave laser (low energy) and the second is a pulsed laser (high energy). In this research, we are using a pulsed laser which is powerful as compared to other continuous lasers.

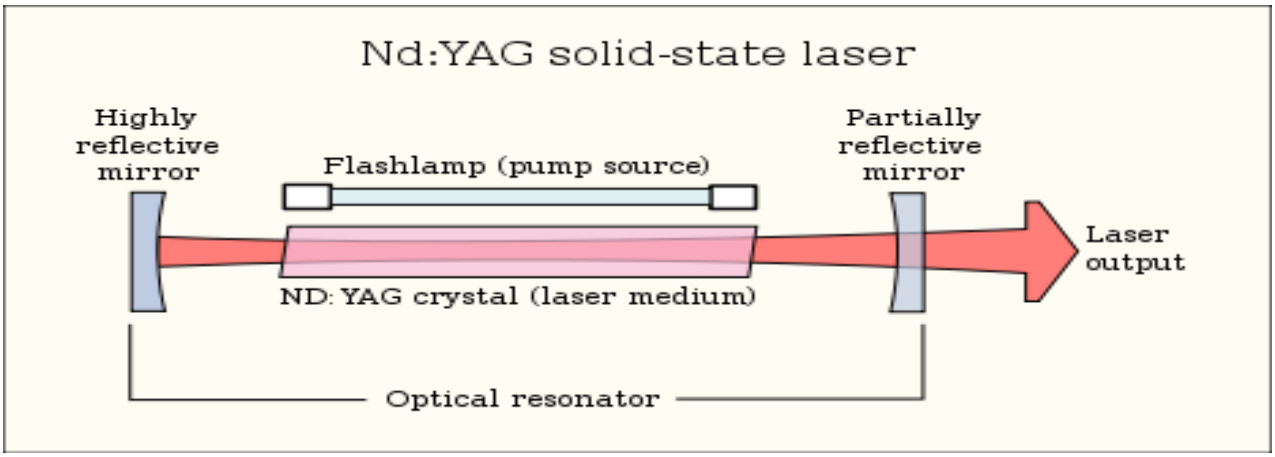

Fig. 1. 1: Schematic diagram of an ND: YAG laser [21]

The principle underlying the generation of high energy pulsed laser is Q switching, it is a technique by which a long pulsed laser can be changed into short pulsed laser to get more peak power of the laser beam. The laser of pulse width up to the order of nano seconds can

be produced by using Q switching. An electrically active opaque material is used between the lasing medium and partially reflected mirror. This shutter is used to attain maximum energy inside the cavity as there is no stimulated emission during that time in the active medium. When maximum population inversion occurs in the lasing medium, this opaque material is momentarily taken out to allow photons to escpe; after transmission, these photons undergo multiple reflections and are responsible for stimulated emission. When the metastable state becomes completely depopulated the opaque material again becomes active. In this way, we can obtain a high power pulsed laser.

LIBS technique has been applied successfully to analyze the elemental compositions of many objects like tea, marble stone, cemented walls, cinnamons, milk, lipsticks and many others. In biomedical applications using samples such as hair, blood, nails, tissues, bones, kidney and gallbladder stones, teeth can be studied etc. that's why LIBS technique has proved its worth to be amongst the powerful techniques to analyze different compounds. Briefly, LIBS has the following advantages over other techniques of atomic emission spectroscopy.

- Very little sample is needed.
- All states of matter can be analyzed, as well as both conductive and nonconductive samples.
- No waste is generated as very small amount of sample is ionized.
- Capability of analysis in a harsh environment by remote analysis.
- Atomization and excitation are done in one step.
- Capable of multi elemental analysis.

A unique property of the LIBS is that samples do not need to fluoresce, IR or Raman active. Very little sample preparation is required and in some experiments, no sample preparation is required at all and LIBS can analyze all states of matter with in a very short time. Extensive research has been conducted to study the prospects of using LIBS for biomedical and food sciences applications using samples such as hair, blood, nails, tissues, bones, body stones, teeth, tea, coffee, and vegetables etc. Hence, it could be a good bio and food samples diagnostic technique after ensuring repeatability and accuracy compared to already established diagnosis procedures.

Due to this uniqueness, LIBS have been applied for both quantitative and qualitative analysis in areas such as space exploration [1]–[3], medical and forensic field [4]–[8], industrial application [9], [10]and cultural heritage [11]–[15].

Hence, LIBS is a good medical diagnostic technique to ensure repeatability and accuracy compared to already established diagnosis procedures and it could be a good technique to ensure hygiene levels of different food materials.

1.2. LIBS THEORY

1.2.1 Principle of LIBS

LIBS is also known as time settle laser instigated breakdown spectroscopy (TRLIBS), Laser Ablation Spectroscopy (LAS), Laser Induced Plasma Spectroscopy (LIPS) and Laser Spark spectroscopy (LSS). Molecules radiated or retained the photons as per the quantum mechanical laws. Because of retaining a photon, an electron energizes to higher state yet the ideal state for an electron is the ground state so to refill the lower states it de-excite by

transmitting the light, this light will be a marker for the basic investigation. There are a few databases which manage these unique finger print wavelengths of the radiated light to investigations the material. The LIBS framework in light of vaporization, excitation, and ionization of the material and after that catching the light originating from it and after that investigation the analyte qualitatively and in addition quantitatively [16], [17]. When the fluence of the applied laser become higher than the ionization potential, ionization potential then overcomes and we acquired particles and electrons [18]. Low energy electrons are first ionized those are in external energy levels and then the electrons from the inner shells are ionized [19], [20]. Free bound process is a procedure in which an energized particle produces energy because of interaction while moving quick close to an electron or a cation. As the electrons rely on the discrete energy levels similarly energy originating from them is additionally some sort of discrete, which is a delegate for a unique component.

When plasma is generated due to the laser interaction with the sample, light emitted is caught which comprises of the information like characteristics wavelengths, intensity and broadening phenomena in peaks of transition lines. Doppler broadening (each particle emit light which can be slightly red or blue shifted resulting into broadening that dominate the linear shape) is due to the thermal motion of electrons and the Heisenberg's uncertainty principle is responsible for the natural broadening. Stark effect is due to the electric field produced when the fast moving electrons passing across slow moving ions, broadening due to Stark effect is dominating the other kind of broadenings [21]. Wavelengths, intensity of the specific wavelengths and their shapes are the key features to determine the plasma parameters like electron density and plasma temperature [22], [23].

1.2.2. LIBS as an Analytical Technique

Because of numerous remarkable properties of the LIBS, it is accepted as a well-established strategy for investigating of all states of matter. Photo interaction of the LIBS with the material is the most imperative component which separates it for the rest of the conventual procedures in which material ought to be required in the refined hardware. Plasma is produced quite over the objective specimens with no different instrumentations. A standout amongst the most unique properties of LIBS is, it doesn't require any specimen preparation or extremely small sample is required as few μg is removed all the while. As the spatial resolution of 1-10 μm can be accomplished, it gives us a good Microanalysis.

Some of the issues in the LIBS which stops the LIBS for its quick spreading as an examination method, one of the fundamental issues is to make the homogeneous examples, additionally, there is likewise irregularity of the measure of removed mass which leads towards the change in the obtained intensity, self-absorption is additionally one of the principle issues in it, because of these issues we have a less precession between 5-10 %. matrix synchronizes additionally one of the major ordeals to confront in the exactness of our outcomes by LIBS. In short we can rundowns, deficiencies which constrain the LIBS, are extensive number of parameters, these parameters are originating from encompassing condition [24], [25] laser wavelength[26][27], chemical and physical properties of focused species[28]–[31], laser energy [32]–[34], laser pulse temporal duration, shape[25] and effect of magnetic field [35][36].

LIBS involves the generation of the plasma and configure it by applying the laser upon a material. The parameters must be optimized in LIBS include energy per pulse, the wavelength, pulse time, and the number of pulses per burst. LIBS is influenced by two

parameters mainly: laser-material interaction and plasma properties and development (plasma-matter interaction), for this reason, plasma behavior is a function of wavelength in a nanoseconds LIBS set-up. It is obvious that lower wavelength lasers such as 266 nm laser has higher ablation rate then the higher energy laser (i.e. 532 and 1064 nm)[37].

The production of nanosecond laser is based upon two main processes; the first is to excite electrons from the inner shells and the second is inverse bremsstrahlung in which electrons gain the energy in the process of ions and atoms collisions. The threshold for the formation of plasma is higher wavelengths that's why the infra-red region is more favorable for bremsstrahlung [38]. While the photoionization process is more favorable in the shorter wavelengths. Due to this reason, less energy is needed per area (fluence) for the ablation process [39]. Furthermore, inverse bremsstrahlung process increases the life time of the plasma produced but simultaneously increases the background as well. Longer wavelengths limit the inverse bremsstrahlung and also reduces the ablation rate and increases elemental fractionation (elemental fractionation is the redistribution of elements between solid and liquid phases which modifies plasma emission) [40].

The most widely recognized laser which is utilized is the pulsed Nd:YAG laser [41]. It is precise and exact in recording the spectrum, the fundamental mode of the Nd: YAG laser is 1064 nm and its pulsed width is in the vicinity of 6 and 15 ns. harmonics can likewise be created by this laser at 532, 355, and 266 nm. They are less intense and have shorter time pulse in the vicinity of 4 and 8 ns [42][43]. Different types of laser utilized for LIBS are CO2 or excimer laser which in IR and UV wavelength regime respectively. Ablation process consists of melting, sublimation, erosion, and explosion etc. and have different

fluence (having units J /cm2) thresholds [44]. The usual irradiance limit for solids, liquids, and aerosol is 10^{10} W/cm^2 and 10^{11} W/cm^2 for gasses [42].

Acquisition time and time delay are the imperative parameters those are fundamentally be worked as beginning plasma is in the continuum state [45]. This continuum radiation in the process can be controlled in experiments by several parameters, for example, pulse time, laser wavelength, sample features and surrounding weight. The time delay and integration time (gate window) are influenced by the laser wavelength. In LIBS sample is ignited with the high-energy laser beam. Formally plasma comprises of the atoms, ions, and electrons, recombination process occurs after some time by transmitting the characteristic wavelengths. Delay time is set to have the high line intensity and low background. For Nd: YAG laser both time delay and gate width are altogether of microseconds to nanoseconds [45].

1.2.3. Laser ablation

Laser ablation has been under consideration for the last 50 years. Absorption of energy by the target and removal of the material from the target is called laser ablation. When the applied laser energy exceeds the ablation threshold of the target material, a plasma is produced then. Physics behind the production of the plasma is highly sophisticated which involves vaporization, ionization, excitation plasma production and the expansion of the plasma. The plasma produced and the crater in the target is due to the highly intense beam of the laser which are dependent on different parameters like laser energy, pulse duration, target properties and some surrounding conditions. Two of the well-known analytical applications of laser ablation are LIBS and laser ablation inductively coupled mass spectroscopy (LA-ICP-MS). Usually, LIBS uses a Q-switched pulsed laser which

generates the plasma which is further collected by the optical lens and CCD or ICCD camera is used to record the spectrum. In LA-ICP-MS ablated mass is analyzed for isotope detection. Important aspects of the process are minimum power for the ablation, long or short pulse width, the rate at which the plasma is produced and the recombination of the particles by emitting the light. Minimum laser power density required to produce vaporization is given by

$$I_{\min} = \left(\frac{L_v \rho \kappa^{1/2}}{\Delta t^{1/2}} \right) w / cm^2 \tag{1.1}$$

Where, L_v is the latent heat of vaporization, ρ is the density of target material, κ is the thermal diffusivity of the target and $\Delta t^{1/2}$ is laser pulsed length [2], [46], [47].

1.2.4. How the Plasma depends on the target material

Significantly the target material affects the plasma produced, its mechanical, thermal and compositional properties influence the plasma. The relationship between ablated mass m(t) and heat conduction process is as given in the equation.

$$m(t) = A(aIt) + B(AI)^2 \tau^{3/2} \tag{1.2}$$

Where a is the energy coupling factor, A and B are proportionate to the material target thermal properties, τ is the laser pulse duration and I is the laser Intensity. For a plasma to be formed, the laser fluence must exceed a threshold value which is usually of the order of several Jcm^{-2} for nanosecond laser pulses. When the laser energy exceeds the latent heat of vaporization of the material, a plasma is produced. The threshold fluence (F_{th}) for evaporation is given by

$$F_{th} = \rho l_v a^{1/2} w^{1/2}, a = K / \rho C_p \tag{1.3}$$

Where ρ is the density of the sample, l_v is the latent heat of vaporization of the material target, a is the thermal diffusivity, w is the laser pulse width, C_p is the specific heat per unit mass and K is the thermal conductivity. It is observed that the threshold for vaporization of the hard materials such as teeth or other hard things is low but the threshold for the soft material is higher and this is due to the pulse rate. A reflecting surface absorbs laser energy effectively due to change of material at high temperature, which this is possible only at high laser intensity. The reflectivity of sample surface, specific heat, density, boiling and temperature influences the shape and size of the craters and is given by the following relation [33]

$$D = A(1-R) \Big/ \rho C_p T_b \tag{1.4}$$

Where D is the crater diameter, R is the reflectivity of the surface, A is the proportionality constant, and T_b is the boiling temperature.

1.2.5. Others Factors those influence the Plasma Parameters

The geometry of plasma and spatial discharge intensity profile are to a great extent subject to the density of laser power, optical alignment for laser centering, and emission collection from plasma plume spectrum acquisition. Henceforth, it is very desirable to comprehend the LIBS signal reliance on the optical alignment and the accumulation of emission for the recording of the spectrum. Cylindrical and spherical lenses were checked to ensure the efficiency of the lenses, it was revealed the cylindrical was more accurate in focusing the laser bean on the target sample. It is a usual practice that in the LIBS system a beam is bombarded perpendicularly on the target sample [49], but some researchers taking it on some angle. To prevent air breakdown, the lens is placed at the distance shorter than the

focal length of the lens [49][50]. As the plasma plume is governed by the strong explosion laws there are several changes occurring in the time evolution of the plasma production and expansion. Assuming a model which is one-dimensional, where the plasma spreading out is along the x-direction and the target surface is at x = 0, the distance x (t) reached at time t is given by

$$x(t) = K\left(\frac{E_l}{\rho_o}\right)^{m/2} t^m \tag{1.5}$$

Where E_l is the deposited energy by the laser during the process and ρ is the ambient gas density. The coefficient m depends on plasma expansion geometry which is equal to 2/3 for planar propagation and 2/5 spherical symmetry. Eq. (1.5) specifies that there is a decrease in the plasma speed with the passage of time. To avoid a damage caused by a large amount of heat, the optical fiber is placed for the collection of the light from the plasma at some millimeter away from the target. Optical fiber is placed at an angle to catch the maximum light from the plasma. For the maximum collecting efficiency various ways have been adopted, one is to use two optical fibers, one is for the collecting the light while the other is to send the light, in another technique both collection and transmission occurs with a single optical fiber, it is observed that a similar limit of detection is acquired with both techniques [52].

1.2.6. Influence of binding materials on Laser – solid interaction.

In the process of palletization a binding material also called a matrix is a an important part. Strong binding is required as the material must go through the highly intense laser beam which can break the material in the powder form. Due to consequences of all these concerns, it is required to choose as appropriate matrix as a binding material [32].

Homogeneity is one of the main requirement in the pellet formation process, as we will have only a small portion in contact with the laser, so it is necessary that all the samples which is added to the binding material should be ground and well mixed before the palletization process [36]. Selection of an appropriate binding material is also one of the requirements for good results, which can only be achieved in our case by homogeneous mixing of the target material. Experimentally tested binding material include Al, Ag, Potassium bromide (KBr), and starch. Bond strength is the parameter which measures strength between the binding material and the ablation resist, it is also strongly required that the bond strength of the material is necessarily uniform throughout the material. In one research, it was observed by M. A. Gondal et al one of the best binding material is KBr.

1.2.7. Qualitative Analysis

Qualitative analysis means to identify the elemental composition of the experimental sample. It is a very fast, simple and efficient work using LIBS. Spectral data which is acquired by the LIBS setup is compared with the different existing databases for the spectral line identifications. One of the mostly used databases is the NIST database, which stands for national institute of standards and technologies. It provides data for almost all the elements nearly the figure up to 100. Transitional lines wavelengths which are the characteristics wavelengths for the elements are compared with the finger print wavelengths given in the NIST database. The suggested wavelength resolution is 0.03 to 0.2 nm for identification of emission lines.

1.2.8. Plasma study as an ionization process

Plasma is the combination of electrons, atoms, and ions. Plasma production undergoes several processes. First it is the production of plasma by breaking the bonds which includes the shielding of the material with the plasma when the laser is ignited on the sample. This process is not favorable for measurement as there is self-absorption occuring due to this plasma shielding in the way. In the second stage, plasma goes into the atomic stage which is the most favorable stage for measurements as with the passage of time plasma cools down and atomic state attained. The last stage in the plasma life time is the stage when plasma cools down completely and coming back into the atomic state by maximum redistribution of the electrons to the elements, this state is not favorable as electron density and temperature here is not at the desired values for the evaluation of the spectrum. One can attain the desired state of the plasma by adjusting the parameters. While recording the spectrum we are acquiring the continuum (background) spectra but this decays faster than the spectral lines. If we want to brief our discussion during this section, optically thin plasma and local thermodynamic equilibrium are required during entire this process. Optically thin plasma is needed to attain some special purposes which are described in the forthcoming discussions. The intensity of radiation emitted by plasma is given by

$$I(\lambda) = \left(\frac{\varepsilon(\lambda)}{\alpha(\lambda)} \right) \left(1 - \exp[1 - \alpha(\lambda) L]\right) \tag{1.6}$$

Where $\varepsilon(\lambda)$ is the emissivity, $\alpha(\lambda)$ is the absorption coefficient in cm^{-1}, and L is the plasma length along the line sight of the observer.

There are many techniques to determine the LTE, one is the McWhirter criterion, which becomes satisfied when the rate of the collisional process is greater than the radiative process, which is mathematically represented by:

$$n_e \geq 1.6 \times 10^{12} T^{1/2} (\Delta E)^3 cm^{-3} \tag{1.7}$$

where n_e = electron number density and ΔE is the greatest possible transition energy for the shortest wavelength is used in the calculation of temperature T [52], and n_e, T & ΔE have units of cm^{-3}, K and eV respectively. LTE is required as all the information of the plasma is related to the temperature of the plasma, like the speed of the electrons, population of the levels and stages of the ionization. The classical Maxwell velocity distribution function F_m is given as

$$f_m(v)dv = \left(\frac{m}{2\pi k T_e} \right)^{3/2} \exp\left[-\frac{mv^2}{2kT_e} \right] 4\pi v^2 dv \tag{1.8}$$

Where m is the electron mass, and v is the electron speed. The relative population of energy levels, whether atomic or molecular in origin, are given by the Boltzmann distribution.

$$\frac{N_j}{N_o} = \left(\frac{g_i}{Z} \right) \exp\left[-\frac{E_j}{KT} \right] \quad \text{with respect to the ground state} \tag{1.9}$$

$$\frac{N_j}{N_o} = \left(\frac{g_i}{g_i} \right) \exp\left[-\frac{(E_j - E_i)}{KT} \right] \quad \text{for relative populations} \tag{1.10}$$

Where i and j refer to two energy levels, N_o is the total specie population; N_{ij} is the population of energy level E_{ij}, g_{ij} is the statistical weights of the levels $(2J_{ij} + 1)$; J is the total angular momentum quantum number of the term, and Z is the partition function.

Sometimes it is not the correct relation as when the ground state levels are closely packed multiplets occurs and in that case the partition function of the ground levels must be added.

1.2.9. Local Thermodynamic Equilibrium (LTE) and Optically Thin Plasma

Local thermodynamic equilibrium (LTE) is greatly required in the determination of the plasma for the qualitative analysis of the materials. LTE or the optically thin plasma is attained when the electron atom collision or electron ion collision is so fast such as to overcome the radiative process. LTE specifies the properties of the plasma such as temperature, the electron density of the plasma and number density of the material [16]. And the information of the temperature of the plasma plume is important as this determines the atomization, dissociation, and excitation of the materials [56]-[60]. LIP is characterized by the occurrence of the following processes, namely photo-ionization, collision ionization, collisional excitation, radiative and three-body recombination, radiative decay, de-excitation process and Bremsstrahlung process. As we acquired the plasma in LTE regime it will be governed by different types of distribution laws [53] namely, Maxwell distribution which describes the plasma particle, Boltzmann's statistic which describes the distribution of population in the energy level, Saha's equation which describes the ionization process, and the radiation density obeys the Planck's law [54][55]. the electron density which is required to be attained for overcoming the electrons in the atomic levels, this criterion was originally formulated by McWhirter and is now called McWhirter criterion [56][57]. One of the forms of this criterion is given in Eq. (1.7).

In the prevailing conditions, the population of the electrons in the energy levels can be described by the Boltzmann distribution law:

$$\frac{N_{k,z}}{N_z} = \frac{g_{k,z}}{p} \exp\left[\frac{-E_{k,z}}{K_b T}\right] \tag{1.11}$$

Where $N_{k,z}$, $E_{k,z}$, $g_{k,z}$ are the population, energy and degeneracy of upper energy level K respectively, N_z and p_z are the number density and partition function of the species in the ionization stage z, K_b is Boltzmann constant, T is the electron temperature. The integrated intensity I_z of atomic emission lines occurring between the upper energy level K and the lower energy level, I is the integrated signal intensity of the species in the ionization stage z in an optically thin plasma is given as:

$$I_z = \frac{hc}{4\pi\lambda_{kl,z}} A_{kl,} N_{k,z} L \tag{1.12}$$

Where h is plank's constant, c is the speed of light; L is the characteristics length of the plasma, $A_{kI,Z}$ is the transition probability and $\lambda_{kl,z}$ is the spectral line wavelength. By substituting Eq. (1.11) in Eq. (1.12), we have:

$$I_z = \frac{hc}{4\pi\lambda_{kl,z}} A_{kl,} L \frac{N_z g_{k,z}}{P_z} \exp\left(-\frac{E_{k,z}}{K_b T}\right) \tag{1.13}$$

Taking the natural logarithm of both sides of Eq. (1.13), we have:

$$In\left[\frac{\lambda_{KI,Z} I_z}{A_{KI} g_{KZ}}\right] = \frac{E_{kz}}{K_b T} - In\left[\frac{4\pi Z}{hcN_z}\right] \tag{1.14}$$

where ln is the natural logarithm, I_z is the integrated signal intensity of the spectral line occurring between upper level k and the lower level I of the species in the ionization stages

z in an optically thin plasma, K_b is the Boltzmann constant, T is the plasma temperature, $A_{ki,z}$ is the transition probability , $\lambda_{KI,Z}$ is the transition line wavelength, $g_{K,Z}$ is the degeneracy of the upper level k, P_Z is the partition function of the species in ionization stage z, L is the characteristic length of the plasma and all other symbols carry their traditional meaning[66]. The ideal condition for attaining the Boltzmann distribution is to obtain a straight line while plotting the left hand side of the previous equation against the energy of the upper level, while -1/KT provides the slope of the line. For the straight line acquisition, some of the entities have to be attained accurately such as well spaced energy level, accurate line intensities, and accurate transition probabilities [56], [57], [59]

Transition lines in the process of spectrum formation originally have zero-line width, but due to some other processes, it gets broadened to a certain extent. These processes are Doppler, instrumental, natural and stark broadening [23][60]. In this case, Stark broadening is the most prominent one and this is due to the electric field produced due to the collision of electrons and the ions. This creates the expansion in the levels of the elemental shells as well, which results in the shifting of the wavelengths. The line profile for Stark broadening is described by a Lorentzian function with a full width at half maximum $\Delta\lambda_{1/2}$ and electron density is related to the expression.

$$\Delta\lambda_{1/2} = 2w\left[\frac{n_e}{10^6}\right] + 3.5\left[\frac{n_e}{10^6}\right]^{1/4} + \left[1 - \frac{3}{4}N_D^{-1/3}\right]w\left[\frac{n_e}{10^{16}}\right]A^0 \qquad (1.15)$$

where w is the electron impact factor, n_e is the electron density, A is the ion broadening parameters and N_D is the number of particle in Debye sphere [23], [60]. The first term on the right-hand side of Eq. (1.15) represents the broadening due to electron contribution and second term is due to ions contribution. For non-hydrogenic ions, stark broadening is

mainly due to electron impact, since the perturbation by ions are negligible compared to that of electron. Therefore, the equation reduces to the form:

$$\Delta\lambda_{1/2} = 2\omega\left[\frac{n_e}{10^{16}}\right] \tag{1.16}$$

where ω is an electron impact parameter which is a function of the temperature and only changes by a factor of two over the temperature range of 10,000- 80,000K. The stark broadening profile is one of the great tools to determine the electron density with in an acceptable range of error.

1.2.10. Quantitative Analysis

LIBS provides the quantitative analysis of the samples, i.e. the concentration of the elements (composition of the material in parts per million) [16]. There are several ways to detect the concentration of the elements inside the sample with the raw data acquired by the LIBS technique, these ways including the calibration method, calibration free method, chemo metric method etc. The emission line intensity of plasma is given by the equation below:

$$I = \left[\frac{h\nu_{ji} N A_{ji} g_i}{Q}\right] \exp^{\left(-E_j/KT\right)} \tag{1.17}$$

h= planks constant, V_{ji} = transition frequency from state j⟶ i, A_{ji}= Einstein coefficient for spontaneous emission between j and i, N= population density of atom exited by plasma in the ground state, E_j = energy of the upper level of the atom, g_i = Statistical weight of the upper

level, Q= Partition function, T= electron temperature and K= Boltzmann constant.

1.2.11. Limit of Detection

It specifies the minimum amount of the analyte which can be analyzed with the help of some analytical technique for example in our case LIBS. So, it's a very important quantity to be measured as it tells us the accuracy of our results as well. The limit of detection is estimated as 3σ divided by slope ($\Delta c/\Delta x; x = signal$) of the calibration curve. The limit of detection is given as:

$$LOD = 3\left[\frac{\sigma}{S}\right] \tag{1.18}$$

where σ is the standard error of the experimental calibration data, and S is the sensitivity which is given by the ratio of intensity to the concentration.

1.2.12. Precision and Accuracy in LIBS results

The accuracy of LIBS is determined how close we are from the actual results; in our case, we are comparing our results of LIBS with standard techniques of ICPMS and ICPOES (described in preceding sections). The relative accuracy is calculated as follows

$$Error = \frac{\left|x_m - x_{atv}\right| + SD \times t_{0.975}/\sqrt{n}}{x_{atv}} \tag{1.19}$$

Where $|x_m - x_{atv}|$ is the difference between the measured value x_m and the acceptable value (x_{atv}), SD is the standard deviation of LIBS measurement, n is the number of measurement, $t_{0.975}$ is the t value at 2.5 % error confidence.

CHAPTER 2: Objectives

2.1. Objectives of this work

- To optimize various LIBS parameters and estimation of plasma parameters (electron density and plasma temperature).
- To assembled a UV pulse laser induced breakdown spectrometer for detection and elemental analyses of toxic element in food products.
- To assemble a LIBS sensor and optimizing it for trace element analysis for biological samples.
- Cross validation of LIBS results using standard techniques like ICP-MS, ICP-OES and XRF technique.

CHAPTER 3: LITERATURE REVIEW

3.1. Literature Review

The first time LIBS technique was introduced in the early 1960s when it was applied on solid material, ablated material was excited with the help of electric discharge sparks [61], which showed massive potential to be a powerful analytical technique for multi-element analysis. From the 1980s onward, remarkable progress has been made in both laser and detector technology, as these instruments are rather cheap and reliable for research and analysis in laboratories. Hence, this analytical technique is rapidly growing in popularity for the quantitative and qualitative analysis of various types of samples [62].

Over several decades, there has been a perpetual quest to enhance the LIBS technique, since LIBS exhibits attractive features such as sensitive multi-elemental detection, rapid response for online monitoring, easy sample preparation for in situ measurements, high spatial resolution for surface mapping, and standoff operation capacity for remote sensing [61][63], which are advantageous over other available elemental analysis techniques. These features have been garnering growing interest, leading to the application of LIBS in increasingly-diverse domains [64], [65].

Laser-induced breakdown spectroscopy (LIBS) is a powerful analytical technique that has been proved useful in many applications [66]. LIBS can be applied easily in the investigation of the elemental composition of a wide range of samples such as metals, rocks, soil, explosives, cosmetics, air and may more in spite of their state: liquid, solid or gas [81]. Extensive research has been conducted to study the prospects of using LIBS for biomedical applications using samples such as blood, tissues, body stones, teeth, nails, etc.

[67]. The main advantage of the LIBS technique is that it requires very little sample preparation and delivers fast results. Hence, it could be a good medical diagnostic technique after ensuring repeatability and accuracy compared to already established diagnosis procedures.

Heavy metals have been implicated in the pathogenesis of various cancers, but data on colon cancer and heavy metals exposure is lacking. Of the few studies, one is by Emre et al. who compared blood samples from healthy individuals to those with metastatic colon cancer measuring levels of heavy metals and noting higher levels in the cancer group [68]. Colorectal cancer [CRC] is presumed to involve a complex array of inherited susceptibility and environmental DNA genotoxic exposure, yet mostly no genetic predisposition is found and etiology continues to remain elusive. New observational studies suggest a strong association of lifestyle and dietary intake specifically consumption of processed red meat, saturated fats, alcohol and sedentary life style as possible contributors to the development of CRC. Although challenging, for the first time we could employ a highly precise Laser Induced Breakdown Spectroscopic technique to measure levels of heavy metals directly in CRC tissue.

Investigations of fingernails using LIBS with the aim of finding a promising tool for medical diagnosis has also been studied. For example, an investigation to find an association between elements in fingernails and osteoporosis was performed by Bahreini et. al. [69]. Moreover, Bahreini et. al. used LIBS to discriminate between patients with diabetes mellitus and normal healthy humans [26]. In addition, the same group examined using LIBS as a method to determine alcoholic and doping subject [70]. Hosseinimakarem

and Tavassoli[71] used LIBS spectra of fingernails to discriminate healthy patients with those suffering from hyperthyroidism and high blood pressure

Innumerable investigators have used LIBS in fingernail analysis. Qualitative analysis of the detection of calcium in human hair and nails was performed by Haruna et. al. [54]. A more extensive analysis was conducted by Rusak et. al. [72] where they performed a quantitative analysis of the elements calcium, magnesium and zinc present in human fingernails using LIBS through the investigation of two different standards for calibration purposes. Driven by the promising results reported in the literature mentioned above, the aim of this work is to apply LIBS as a diagnosing method for the vitamin-D deficiency which is a very common illness in Saudi Arabia [73][74].

Laser induced breakdown Spectrometry LIBS was used to detect elements qualitatively and quantitatively in the various brands of tea samples used locally and internationally, using 266 nm pulsed UV laser by Gondal et. al. [52] LIBS spectra for the range of 200-900 were taken for 5 different tea samples and almost all the elements were identified present in them. The major toxic elements detected in several brands of tea samples were chromium, bromine, and minerals like calcium, iron, potassium and silicon.

Laser induced breakdown spectroscopy (LIBS) was applied for the detection of carcinogenic elements like bromine in four representative brands of loaf bread samples and the measured bromine concentrations were 352, 157, 451, and 311 ppm, using Br I (827.2 nm) atomic transition line as the finger print atomic transition. [75] LIBS system was used to find out the concentration of toxic elements such as chromium in hair dyes available in the local market. [76] Chromium 427.5 nm wavelength was used to calibrate and find out

the concentration of our dyes samples. For this line, the limit of detection 1.2 ppm was achieved by our LIBS detection system, due to which we could detect chromium concentration in the range of 5–11 ppm in the commercial hair dyes available on the local market.

UV nanosecond (LIBS) has been deployed to detect trace chemicals contained in fresh vegetable (including fruits, stem, and roots) by Vincent Juvé et al [16], which was purchased from the local market. He used the 4^{th} harmonic of Nd:YAG laser (266 nm; energy = 10 mJ; repetition rate = 10 Hz). The fiber optics used have high transmittance in the 200 to 850 nm interval. The root spectrum was captured from the interior to the exterior of the root, whereas the stem spectrum was recorded at various heights (from lower to upper part) of the plant; the fruit spectrum was recorded over the entire volume of the fruit. A meticulous analysis of the spectral lines was identified by reference to the NIST database and yielded 422 lines as follows: 391 lines were emitted by ionic and atomic species, 9 lines by molecules (C_2 and CN), and 22 lines were ghost lines. In brief, UV nanosecond LIBS has proven its efficacy in identifying trace elements, for instance, organic, metallic, and nonmetallic substances. It is a potent tool for detecting and analyzing trace element in raw vegetables, with the potential for extrapolation to other food stuff.

Josef Kaiser et al uses LIBS for the detection of trace element in the matrices of various organic samples: microbiological, flora and fauna. LIBS is still not a very well-established technique for analyzing bacterial and animal samples. In the first reported instance of the usage of LIBS for distinguishing between healthy and cancerous tumor cells from a canine histological section, the concentration level of trace element in it was found to vary significantly between the healthy and tumor cells. To enhance LIBS performance, analyses

were performed under elevated pressures and cryogenic temperatures of -196 ^{o}C. A few elements detected in the tumor are aluminum, calcium, copper, iron, magnesium, potassium and sodium. This work has decisively demonstrated the capability of LIBS in detecting trace element in biological samples and diagnosing ailments.

LIBS has been used to determine the level of Ca concentration by Edilene C. Ferreira et al [77], wherein 16 different commercially-available cereal samples from Brazil were chosen based on differences in grain type, sugar and flavor composition. These cereal specimens were vigorously pounded to form homogeneous samples using a cryogenic mill model MA 775 (Marconi), and the LIBS spectra were captured using Ocean Optics LIBS2500 system (gate pulse energy = 50 mJ; pulse duration = 8ns). In this study, the wavelength interval was 391.4 - 398.4 nm with particularly focusing on the following finger print wavelengths: Ca II at 393.3 nm. 7 known calcium concentrations of 16.02, 37.21, 68.62, 124.7, 1288, 3734 ppm were prepared in the breakfast cereals matrix for calibration, to deduce the Ca concentration in all the samples.

M.A Gondal et al [78] applied LIBS to determine the concentration of toxic elements in 4 different brands of lipsticks available in the local Saudi Arabian market. Since lipsticks are fluids, pretreatment is called for before analyzing it with the LIBS technique. To remove the liquid portion from the lipstick samples, they were heated to 105 ^{o}C before being frozen in a freezer and then were cut to circular shapes having 1 cm diameter, which allows easy fitting into the LIBS sample holder. After acquiring the various lipstick spectra, the harmful elements found in these lipsticks samples: Pb, Cd, Zn, and Cr. Subsequently, calibration curves for these 4 elements were attained by preparing standard samples with fixed concentrations for each element. Conventional ICP analyses reaffirmed the accuracy of the

LIBS findings, as both sets of results agreed with each other. In retrospect, perpetual use of these cosmetics may cause increased heavy metal build-up within the ocular system in the human body in excess of the acceptable limit.

CHAPTER 4: Experimental Methodology

Well assembling and optimizing of the LIBS setup is required to have a good signal to noise ratio. All the mechanism for setup, optimization techniques and how to operate the LIBS were taken from the literature. All the experimental details are given in upcoming sections.

4.1. General Description of LIBS Setup

A pictorial description of the LIBS setup is illustrated in fig. 3.1. LIBS set-up comprises the following components: a source of a pulsed laser, a spectrophotometer, ultrafast electronic circuits, a computing device and an intensified charge coupled device (ICCD). For this study, we applied an intense laser beam on the coffee samples, and the above-mentioned elements were determined by matching the observed wavelengths with their fingerprint wavelengths, which were obtained from the database published by NIST (National Institute of Standards and Technology). Quantitative analysis was conducted using gravitational search algorithm based support vector regression (GSA-SVR) advanced hybrid chemo-metric. To validate the LIBS results, the elemental concentration values were also quantified using Inductively coupled plasma mass spectrometry (ICP-MS). The LIBS data were acquired using the following settings: a spectrophotometer with high resolution (Andor SR 500 i-A, which boasts a resolution of up to 0.1 nm) equipped with a grating (whose groove density is 600 lines cm^{-1}) together with an optical fiber mounted at 45^0 angles relative to the horizontal plane. An Andor iStar ICCD camera was synchronized with the laser pulses to control the delay time. The latter is defined as the duration elapsed from the point of ignition of the laser to the opening of the gate of the ICCD camera. The

gate pulse width is the spectrum recording time after each laser pulse. The spectrometer used has a resolution of 0.1 ns and it has the capacity to work at different delay times. Other parameters can also significantly influence the results, such as the accumulation number (which is the number of pulses imparted at the sample, captured and averaged by the ICCD camera) which was 30, the delay time which was set at 200 ns and the gain which was maintained at 200.

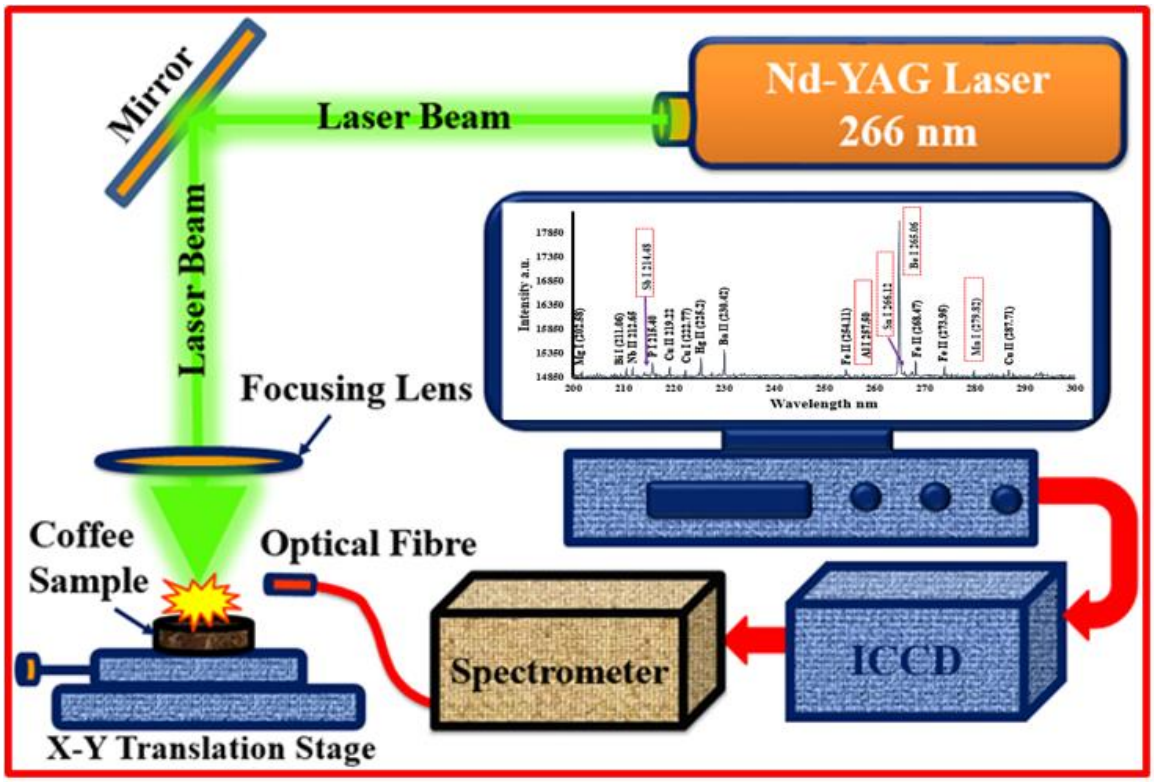

Fig. 4. 1: Illustrate the LIBS setup in KFUPM

LIBS comprises many components but main source is the laser. Laser ignites the material for the study and plasma is produced just above the material which is further used for elemental analysis. Parameters related to the laser in LIBS setup is its energy per pulse, time duration (pulse width), wavelength and number of pulses per burst. It is a very usual

practice to use nanosecond laser in the laboratories related to the LIBS, so that's why we will mainly discuss this laser in the following [79].

4.2. The LIBS Emission collecting system

In LIBS collecting system is not so much complicated as we are dealing here with light, a miniature convex lens is used to collect, converge and send to the optical fiber. This optical fiber attached lens is placed at an angle of 45^0 to the plane perpendicular to the surface of the sample. Collected light signal are sent to the ICCD camera for further processing. This collected system is adjusted upon a three dimensional translator for easy alignment of the lens to collect the maximum signal from the spark [82].

4.3. ICCD Camera.

Integrated charged coupled Device, abbreviated as ICCD camera, which is a very complicated, well oriented device to catch the signals in the form of light. This camera is specially assembled for highly sensitive imaging; it is an extension of the formerly used camera CCD. This camera has the ability to catch instantaneous actions in spite of the signals beams highly intense or faint. One of the main features of this device is, it provides time resolved imaging by adjusting the gate time delaying. Gate time delay is the phenomenon in which user can adjust the timing for opening the window of the ICCD camera for capturing the signals. We are adjusting the timing according to our signal requirement in ICCD camera in this way we are acquiring a good signal to noise ratio.

4.4. LIBS spectrometer

One of the main and a bit sophisticated device used in LIBS system is its spectrometer. It works by offering better resolution of the signals from the spark in the form of spectrum. As for the as large range of spectra is dealt one should have a spectrometer with special features, just like it should cover a wide range of light with the high resolution to give a sharp image of closely spaced transition lines. It should also have good quantum efficiency over the whole range of the spectral region. Spectrum is the key to analyzing all the composition of the analyte, so spectrometer should have high data acquisition and read out time.

In our laboratory, we are using a spectrometer of high resolution 500 mm spectrograph (Andor SR 500i-A) with a grating groove density of 1200 lines /mm. This spectrometer is taking the spectrum from the ICCD camera which is already discussed. This a very good device which generates a very good well resolved spectrum in the range of 200-900 nm.

4.5. Focusing Lens

For focusing the laser beam on the target sample, a converging lens is used, either spherical or cylindrical. By converging the laser beam one can easily achieve threshold irradiance, which is the minimum irradiance for the ablation of some normal material and it is reported > 10^7 W/cm^2, even can easily be exceeded with the help of some modest fluence of the laser. Converging laser after passing through the lens has the Gaussian intensity profile and its radius is given by

$$w_o = \frac{f\lambda}{\pi D/2} \tag{4.1}$$

f is the focal length of the lens, λ is the wavelength of laser and D is the diameter of the laser beam before focusing. Eq. (4.1) shows that with the high-energy laser and lens with the less focal length will give a higher density of the focusing laser. One of the advantages of the shorter focal length lens is it is good for the localized spark for the good resolution results. Longer focal length lens gives large focal volume and similarly, high energy laser is required to ignite the sample. Longer focal length lens is being used preferably where it is dangerous to put the lens near the examined sample.

4.6. Target holder

One of the main parts of the LIBS setup is its target holder, a clear picture of the target holder can be seen in the fig. 4.2. In the case of LIBS experiment, it is necessary to provide a fresh surface to the laser beam for plasma production, otherwise, crater is produced at the surface of the sample. This crater is not favorable in the LIBS measurements, as spectra are very badly effected due to the light absorbed inside the crater. So, to avoid this kind of problem it is necessary to have a rotational target holder, either manual or electrically the holder is rotated.

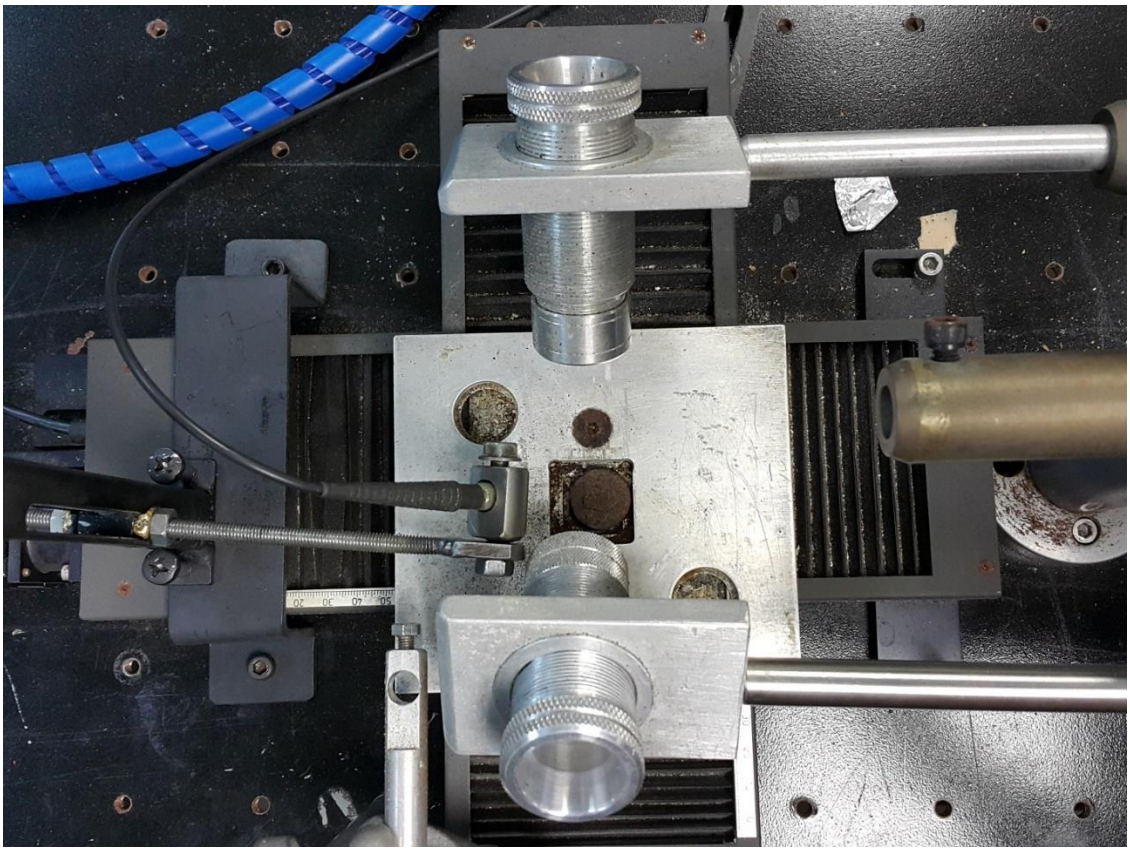

Fig. 4. 2: LIBS target holder

4.7. Inductively coupled plasma mass spectrometry (ICP-MS)

One of the well-known and previously mostly used analytical technique is the ICP-MS**.** Its components description is given as nebulizer, plasma torch, spray chamber, interface and a detector**.** The representation diagram of these components is portrayed in Fig. 4.3. In this technique, light is acquired from the atoms and ions by discharging them with the radio frequency. Only liquid or gaseous form of the analyte can be analyzed by it, while solids can be retained after the proper procedural digestion. The analyte is first changed in the form of aerosols and then in plasma state finally. These states of analyte are acquired in ICP-MS by attaining the temperature of 10000 K, due to this much high temperatures solutions can be moved inside the gasses or air as atoms and particles. A peristaltic pump

is used to process the solution by passing it through the nebulizer at few ml/min, highly pressurized argon gas is passed through the resultant solution which converts it into a fine aerosol. The fine droplet is attained of with diameter about 5 µm inside the spray chamber. This processed droplet from the spray chamber is sent towards the plasma torch using the injector [83]. Plasma torch is used to convert these tiny droplets into the cations, these cations are then passed to the spectrometer through the connecting pipe having the pressure of 1-2 torr. These ions are then entered the main vacuum chamber where the electrostatic lenses are ready to process it further. These electrostatic lenses (ion optics) separate the charged species from the neutral and provide the charged particle to the ion detector. At last these ions are detected and signals are converted into the electrical pulses by the detectors. Then these signal were handled to get the concentration of the of the elements using a different set of traditional methods [83]. The ICP-MS device is as portrayed in Fig. 4.4.

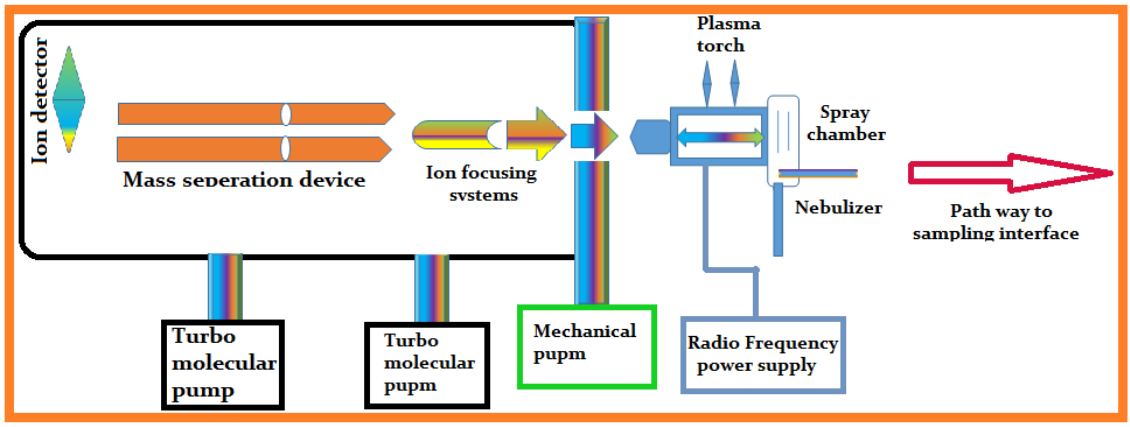

Fig. 4. 3: Schematic diagram of ICP-MS setup

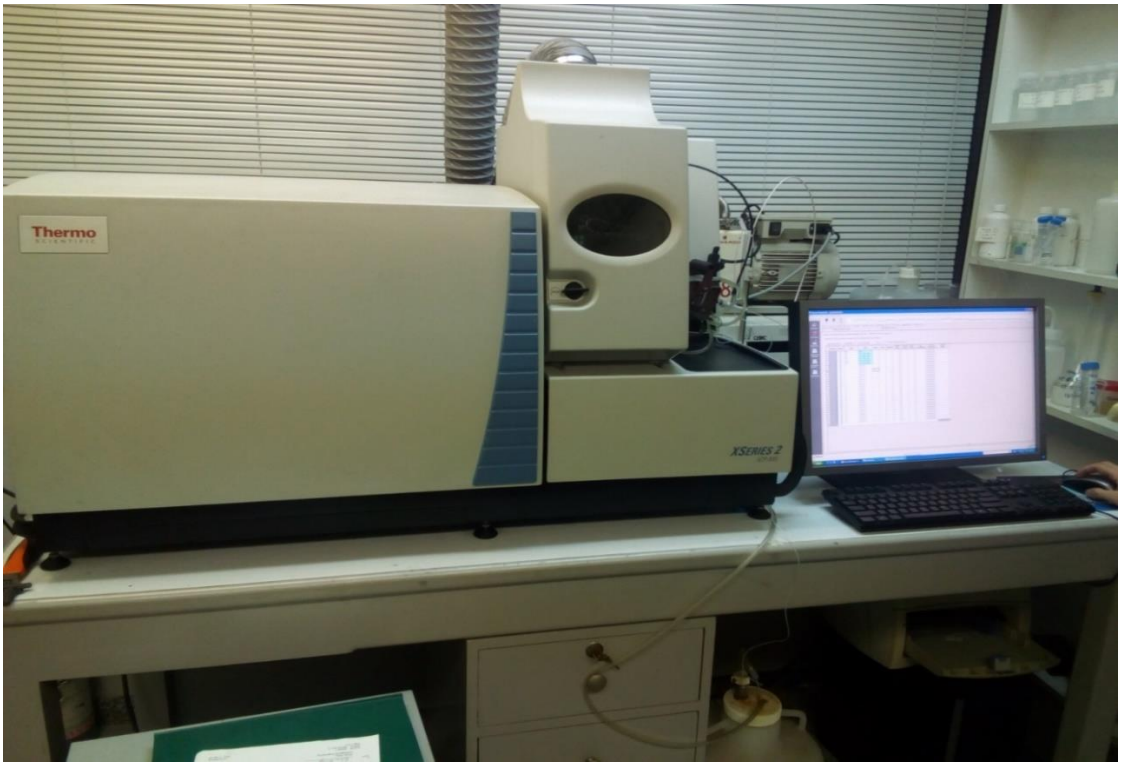

Fig. 4. 4: Inductively Coupled Plasma Mass Spectrometry

4.8. Preparation of Samples

As we are doing research here for the toxic elements in the food products and variations in the elemental concentration in the healthy and cancerous tissues. For better results from the LIBS, it is required to have a well grinded, homogeneous mixed and appropriately shaped by applying the pressure from the hydraulic press samples. While the colon samples do not require palletization by compressing in the hydraulic press but we made the tissues in the shape of the sample holder to fit the samples in the holder after freezing it to avoid the splashing of blood.

4.8.1. Preparation of coffee Sample for LIBS

In this work, five commercially available brands of coffee samples were acquired from the local market in Dhahran, Saudi Arabia. The LIBS technique requires samples to be compacted into pellet form prior to analysis. For the higher efficiency and sensitivity of analysis with the LIBS, the binding material for making the pellets should be appropriately selected [84]. This can be acquired by homogeneously mixing the material under analysis with suitable binders, such as cellulose, Ag, Al, potassium bromide (KBr), starch or poly (vinyl alcohol). These pellets were formed as follows: first, the coffee samples were ground into finely-powdered form and shaken vigorously in a closed bottle to ensure the sample homogeneity. Then, each (of 5) sample was individually filled in a hollow cylindrical dye (diameter = 2 cm; thickness = 2 mm); the dye was pressed by applying a hydraulic load of 7 to 10 metric tons for a duration of 1 to 3 minutes, which resulted in round-shaped, highly-compact pellets that could be fitted in the sample holder of the LIBS setup, as shown in the Fig. (5.1f, g, h, i, j). fortunately, the pellets are sufficiently compressed and firm so to obviate the need for any binder, and they remain intact when subjected to high-energy laser pulses. Contaminations to the samples were prevented by placing the pellets in a desiccator before the LIBS analysis.

4.8.2. Sample Preparation for (ICP-OES)

For the analysis of the coffee samples using ICP-OES technique, the samples were prepared as follows: 0.01 g of coffee powder was stirred in 5 mL of HNO_3 (99% purity, Fisher scientific), to ensure the samples dissolve well into the solution. Next, the solution was heated at 60 ^{o}C until a residual solution of 2 mL remained. After the solution cooled to room temperature, deionized (DI) water (40 mL) was added to it, for complete

dissolution of the coffee samples. The resultant solution was heated up to 45 ^{o}C, whereupon it was held for 2 hours, and thereafter allowed to cool. The solution obtained thereafter was filtered into a volumetric flask to sift out undissolved sediments, after which doubly-DI water was put in until the solution attained a volume of 50 mL. The solutions were thoroughly mixed to ensure proper homogeneity. At this point, the solution was ready for ICP-OES analysis. These steps were repeated for each of the coffee samples individually.

4.8.3. Acquiring of the colon samples and preparation for the LIBS analysis

This work has been done with the collaboration under the supervision of medical doctors from the Mohammed Al Dossary Hospital located in Al Khobar, Saudi Arabia. Both healthy and effected colon tissue samples were acquired from the aforementioned hospital. Samples were collected in a well secure sealed packet. Before applying LIBS, we freeze the samples to have good spectrum and avoiding the flying of blood which can decrease the efficiency of results during the experiment. Samples were converted in a good pallet like shape to fit in the LIBS sample holder.

4.8.4. Sample Preparation (ICP-MS)

10 mg of colon sample was stirred in 5 mL of HNO_3 (99% purity, Fisher scientific), to ensure the metals dissolve well into the solution. Next, the solution was heated at 55-60 ^{o}C until a residual solution of 2 mL remained. After the solution cooled to room temperature, deionized (DI) water (50 mL) was added to it, for complete dissolution of the coffee samples. The resultant solution was heated up to 45-50 ^{o}C, whereupon it was held for 2 hours, and thereafter allowed to cool. The solution obtained thereafter was filtered into a volumetric flask with whatman filter paper 4 to sift out undissolved sediments, after which doubly-DI water was put in until the solution attained a volume of 100 mL. The solutions

were thoroughly mixed to ensure proper homogeneity. At this point, the solution was ready for ICP-MS analysis. These steps were repeated for each of the colon samples individually.

4.9. Preparation of standard samples for calibration

Standard samples have been prepared and used for the determination of the toxic elements like Manganese (Mn), Chromium (Cr) and Barium (Ba) in coffee samples (1-5), by using the KBr as a matrix. It is surely taken into account that the mixing should be homogeneous after well grinded the analyte material in the matrix. Analyte used with the known concentration such as Manganese oxide, Potassium dichromate and Barium sulphate for Mn, Cr, and Ba respectively. The calibration standard sample concentrations that were prepared for Mn were (a) 10 ppm (b) 20 (c) 30 (d) 40 (e) 50,(f) 100 for Chromium (Cr) were (a) 10 (b) 20 (c) 30 (d) 40 (e) 50 (f) 100 and for Ba were (a) 10 (b) 20 (c) 30 (d) 40 (e) 50 (f) 100. A special cylindrical dye of 2 cm in diameter and 2 mm thickness is operated for the palletization process under the hydraulic press of the pressure 10-15 metric tons**.**

4.10. Quantitative analysis of LIBS spectra using GSA-SVR model

The quantitative analysis of the acquired LIBS spectra was conducted using gravitational search algorithm based support vector regression GSA-SVR hybrid chemo-metric. The model was developed using the spectra of the standard samples of different brands of coffee samples. Since our focus in coffee, the study is with toxic elements such as chromium, barium, and manganese, so these elements concentrations were estimated using the model, the spectra of chromium, barium, and manganese standard were used in building the above-mentioned model. Thirty-eight data sets were used for the modeling and the results obtained from statistical analysis of the dataset.

The need for non-linear modeling technique for correlating the intensity with the concentration becomes significant. The choice of SVR based chemo-metric is due to its excellent performance in the presence of few data-points[85]. The hyper-parameters of SVR are optimized using GSA. The influence of the convergence of the model on the number of initial population is presented in Fig. 5.6. The figure shows that the initial number of the agent has no significant effect on the exploration and exploitation ability of the model. To reduce the model's complexity, ten numbers of agents are finally used for model development and implementation.

The results achieved through the quantitative analysis obtained using the developed GSA-SVR chemo-metrics are compared with the results of toxic elements obtained from the standard analytical technique like ICP-OES.

4.11. Fundamental principles of CF-LIBS for analysis of LIBS spectra

The second technique used to measure the concentrations of the elements from the data acquired by the LIBS technique is the calibration free method (CF-LIBS). The hypothetical background of the calibration free algorithm as proposed by A. Ciucci and his group rely heavily on the plasma conditions as well as the experimental method of operation [86]. Apart from the assumption that the composition of the plasma truly represents that of the material to be ablated prior to the ablation, the plasma should also be in a condition of local thermodynamic equilibrium. The optical thinness of the radiation source is also significant and should be maintained for successful execution of the algorithm. Generally, normal LIBS operating conditions uphold optically thin plasma condition for trace element while self-absorption correction needs to be incorporated in the calibration free algorithm to

enhance minor element quantification. Consider an atomic species s (neutral or singly ionized species), the transition between two energy levels E_i and E_j which gives raise to the observed integral line intensity I_λ^{ij} (measured in photon/s cm^3) is defined by equation (4.2).

$$I_\lambda^{ij} = N_s A_{ij} \frac{g_i \exp\left(-E_i / K_B T\right)}{U_s(T)} \tag{4.2}$$

Where:

λ = transition wavelength

g_i = degeneracy of the ith level

N_s = emitting atomic number density (particle/cm^3) for each species

A_{ij} = transition probability of the given line intensity

$U_s(T)$ = partition function of s species at plasma temperature T

K_B =Boltzmann constant

T = plasma temperature

In the actual experimental set-up, the efficiency of the collecting system is factored as a scaling parameter for the measured intensity. Equation (3.2) can be modified as presented in equation (4.3).

$$I_{\lambda}^{ij*} = FC_s A_{ij} \frac{g_i \exp\left(-E_i / K_B T\right)}{U_s(T)} \tag{4.3}$$

Where I_{λ}^{ij*}, F and C_s respectively represent the measured integral intensity, the experimental parameter (it accounts for plasma volume, density and the optical collection efficiency of the data acquisition system) and the emitting atomic species concentration. It should be noted that changes in experimental conditions such as laser energy focusing and so on can affect the parameter F and care should be taken while collecting signal for several shots of laser or while repeating the experiment.

For the algorithm implementation, the parameters g_i, A_{ij} and E_i are to be extracted from NIST data base while F T and C_s are to be obtained from the experimental data. From the logarithm of equation (4.3) , a straight line equation presented in equation (4.4) can be obtained.

$$y = mx + Q \tag{4.4}$$

Where $y = In\frac{I_{\lambda}^{ij*}}{A_{ij} g_i}$, $x = E_i$, $m = -\frac{1}{K_B T}$ and $Q_s = In\frac{C_s F}{U_s(T)}$

A two-dimensional space defined in equation (3.4) is called Boltzmann plane and each species in the plasma has a specific Boltzmann plane. Therefore, each LIBS line can be well represented in Boltzmann plane. The concentration of each of the species can be easily determined from the Boltzmann plot intercept after which the plasma temperature can be determined. In order to avert uncertainty in the measurement and further improve the accuracy of the algorithm, several lines can be used for determining the concentration of a

particular species while the experimental parameter F is factored in this case. Equation (4.5) and (4.6) respectively details how the experimental factor and the concentration of atomic species are determined.

$$\sum_s C_s = \frac{1}{F}\sum_s U_s(T)\exp(Q_s) \tag{4.5}$$

$$C_s = \frac{U_s(T)\exp(Q_s)}{F} \tag{4.6}$$

The total concentration of a given element in the plasma is presented in equation (3.7)

$$C_{tot}^{element} = C_I + C_{II} \tag{4.7}$$

Where C_I and C_{II} are the concentrations of singly ionized and neutral species respectively.

Another method of determining the concentration of one species of a given element after the concentration of the second species is known is to use Saha-Boltzmann equation presented in equation (4.8). Also, the electron density (N_e) can be determined using the concentration of element with known species concentration.

$$\frac{N_e N_c(II)}{N_c(I)} = 6X10^{21}\frac{g_{II}}{g_I}\exp(\frac{-E_c(I)}{T}) \tag{4.8}$$

Where $N_c(II)$ and $N_c(I)$ represents the population of the ground state of the singly ionized and neutral species respectively while g_{II} and g_I respectively represent their degeneracy. The ionization potential of the singly ionized species in the ground state and the plasma temperature are respectively represented in the equation as $E_c(I)$ and T .

4.12. Precaution taken during the experiments.

(1) Cleaning and drying of all the equipment are highly demanded throughout the experiment.

(2) The desiccator is used to place the samples to avoid exposed to outside contaminations.

(3) Homogeneity in the mixing is required to have the good results and from the recorded spectra.

CHAPTER 5:

LIBS ANALYSIS OF FOOD AND BIOLOGICAL SAMPLES

This section is the brief description of our results from the MS research. **W**e will discuss in detail the application of LIBS in the detection of the toxic element and comparative detection of the nutritional element in food products, such as coffee. And the varying trend of elemental concentration in healthy and affected tissues of the colon for the diagnosis of the colon cancer. The plasma parameters for each product were also studied for verification of Local Thermodynamic Equilibrium (LTE).

5.1. Determination of toxic elements in different brands of coffee using laser induced breakdown spectroscopy with advanced hybrid chemometric quantitative analysis

It is reported recently that 40% of the world's population consumes coffee as part of their lifestyle, or for the stimulating effects arising from caffeine [87]. The coffee tree traces its roots back to a region now known as Ethiopia, where it's believed that coffee trees were first harvested several millennia ago. However, the first reported instance where coffee was commercially grown comes from fifteenth century Yemen. Commercially, it was made popular by the Arabian tribes and spread rapidly throughout the entire Arabian Peninsula. It was introduced to Europe by Venetian traders in 1615 which triggered the development and proliferation of coffee shops [88]. These coffee outlets often served as important meeting points for both business and social needs across Europe. The coffee beverage is obtained from roasted beans of the coffee tree and has an alluring taste, flavor and health benefits, which accounts for its widespread popularity. Besides caffeine, it contains a

myriad of vitamins like E, PP, B1, B2, and B9, in addition to minerals such as K, Mg, Zn, Na, Fe, Cu, and P, and phenolic acid which have anti-oxidative properties [89][90]. However, determination of the purity of coffee is very significant for optimizing its full benefits and avoiding its toxic danger. This work determines the purity levels of five different brands of coffee samples using LIBS and quantifies a number of toxic elements present in the samples using a novel hybrid chemo-metric (our grouped developed software).

In an effort to determine the purity of coffee using the spectroscopic technique, Pohl et al [87] reviewed the elemental variation in the different types of coffee like in green, ground and roasted coffees using different analytical methods which include INAA, FAAS, FOES, ICP-OES, DPASV, and ETAAS. Furthermore, Mehari et al. [91] analyzed six different coffee samples using ICP-OES and the elemental constituents obtained from their analysis include phosphorus, sulfur, copper, iron and manganese which are among the toxic elements. It is worth mentioning that this is a pioneer study whereby LIBS has been selected to find the elemental concentration of coffee samples. Here the toxic elements detected from the LIBS spectrum are quantified using gravitational search algorithm based on support vector regression (GSA-SVR) advanced hybrid chemo-metric.

LIBS technique is based on irradiation of the test sample with highly energetic laser pulse which generates the plasma due to ablation, melting, atomization and ionization of the target surface. Laser-induced plasma is responsible for the emission of spectral lines due to de-excitation of the excited atoms as neutral and ionic transitions. Finger-print spectral lines are used to identify the constituent elements, and their spectral line intensities can be used to calculate the concentrations as for other spectroscopic techniques. For the

confirmation of our LIBS results, we conducted the analysis of coffee samples using the standard technique inductively coupled plasma optical emission spectrometry (ICP-OES). LIBS results are well in agreement with the results of ICP-OES.

In this research, we analyzed a series of five different commercially-available brands of coffee samples which were acquired from the local market in Dhahran, Saudi Arabia. The samples are hereafter called as Sample 1: Cafe Najjar Classic; Sample 2: Hamwi Coffee; Sample 3: Nescafé Cappuccino; Sample 4: Bayouni Coffee and Sample 5: Nescafe Classic. In particular, the focus of this study is on the detection of toxic elements such as Manganese, Barium, and Chromium. The samples are characterized by LIBS and the results were further confirmed by the results achieved by using ICP-OES. Our results are a well in comparable range with ICP-OES and it is confirmed that LIBS technique can be considered as one of the most important emerging material characterization technique with its unique properties upon the other existing techniques, such as simplicity, versatileness, rapidity and affability of its experimental set- up and ability of multi-elemental analysis with negligible sample preparation.

In our LIBS analysis, Support vector regression (SVR) has been applied for quantification of toxic elements. SVR has recently attracted attention as a chemo-metric tool owing to its excellent generalization and predictive capability in handling problems that are not linear [92][93][94]. Its main features in many applications can be attributed to non-convergence to local minima and excellent pattern acquisition using few data-points and descriptive features [85]. SVR hyper-parameters which include the regularization factor, epsilon and kernel option play a significant role in the algorithm performance and were optimized in this present work using a novel gravitational search algorithm (GSA). GSA is a population-

based heuristic algorithm that locates the optimum solution using Newtonian mechanics [95].Utilization of this hybrid model (GSA-SVR) for LIBS spectral analysis enhances the accuracy of the results obtained from LIBS data. Furthermore, the LIBS results were counter verified using the standard analytical technique of ICP-OES and the results of ICP-OES were in reasonable agreement with the results acquired by our LIBS.

Fig. 5. 1: An illustrated view of palletization of the coffee samples. (a, b, c, d, e) as acquired from the market. (f, g, h, i, j) pelletized form of coffee samples.

5.1.1. Quantitative and qualitative analysis.

The LIBS spectra of the 5 samples were acquired within the 200 to 800 nm range with the following parameters: 200 ns delay time, 266 nm laser wavelength and 17.54 J laser energy. The standard NIST database was used for identification of the spectral lines. The existence of each element was confirmed using three or more fingerprint wavelengths of each element, together with the alternative confirmatory spectroscopic technique of ICP-OES,

to ensure a high degree of reliability for our data. We obtained both quantitative and qualitative information for the elements present in the coffee samples. The spectral line intensities from the LIBS spectra were used to evaluate the concentration of each element in the sample by using GSA-SVR based model [84], such findings were compared with those from the standard technique of ICP-OES, which are presented in table 5.5. Standard samples of fixed concentrations were prepared to find the concentration of the desired toxic elements by using the advanced hybrid chemometric algorithm. The transitions lines used to determine the concentrations of each element are: for Mn I 279.48nm, for Cr II 428.97nm and for Ba II 614.17nm as indicated in Fig. 5.2. Furthermore, the concentration of each element is depicted in Table 8.5. The LIBS experiments were carried out under ambient conditions, hence lines from some atmospheric gasses such as oxygen, nitrogen etc. were also observed [93].

Our LIBS elemental analysis of the various coffee samples reveals that the concentration of all the above mentioned elements exceeds the maximum permissible limits set by the World Health Organization (WHO) [Mn: 0.5, Cr: 0.05, Ba: 0.3 ppm] and European Union (EU) [Mn: 0.05ppm, Cr: 0.05ppm, Ba: not mentioned] [96], as mentioned in Table. 5.5 and European Union (EU), as portrayed in Table 5.5. Specifically, the following trends were observed for Mn (Sample 1 > Sample 4 > Sample 2 > Sample 5 > Sample 3), Cr (Sample 1 > Sample 4 > Sample 2 ~ Sample 3 ~ Sample 5) and Ba (Sample 4 > Sample 1 > Sample 5 > Sample 2 > Sample 3). The samples are characterized by LIBS and the results were further confirmed by the results achieved by using ICP-OES.

Optically thin plasma and local thermodynamic equilibrium (LTE) conditions were satisfied due to high electron density and Maxwellian distribution of the velocity. To detect

LTE and optically thin plasma, spectral line intensities can be used in the following relation.

$$I_{ik,z} = \frac{A_{ik,z} g_{i,z} L N_z}{\lambda_{ik,z} U_z(T)} \exp\left(-\frac{E_{i,z}}{KT}\right) \tag{4.1}$$

Where $I_{ik,z}$ = signal intensity arising from electron transiting from higher-energy state i to lower-energy state k for an atom in an ionization state z, $E_{i,z}$ = higher energy state, $g_{i,z}$ = statistical weight of $E_{i,z}$, $\lambda_{ik,z}$ = spectral line wavelength, $A_{ik,z}$ = transitional probability, K = Boltzmann constant and T = temperature of plasma, L = characteristic length of plasma and N_z = density of emitting atom [97].

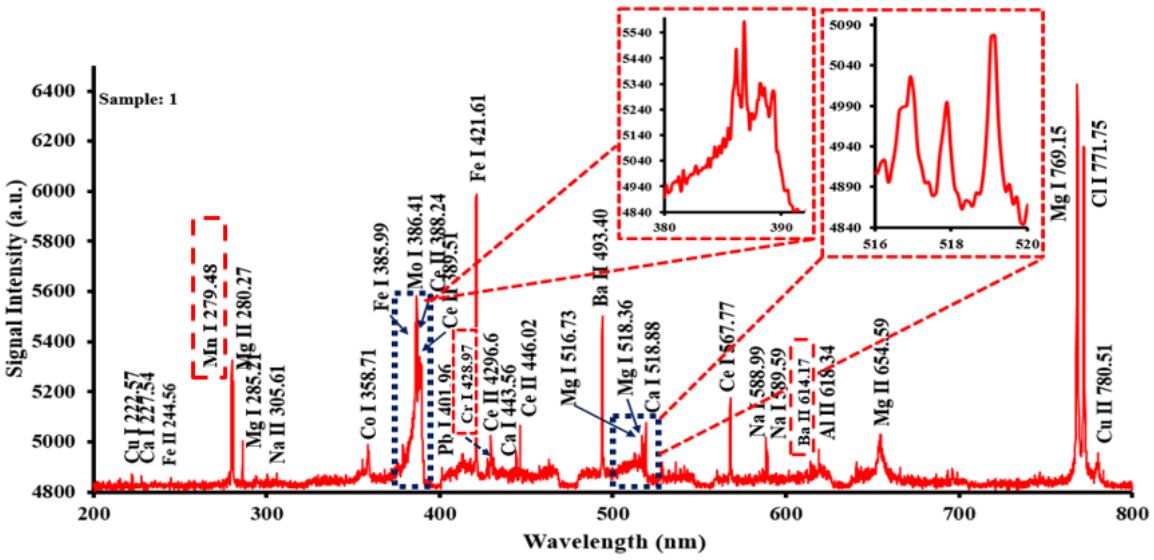

Fig. 5. 2: LIBS spectrum of sample 1 in the range 200-800 nm by applying the laser of 266 nm wavelength, 400 ns is the delay time and 17.54 J laser energy.

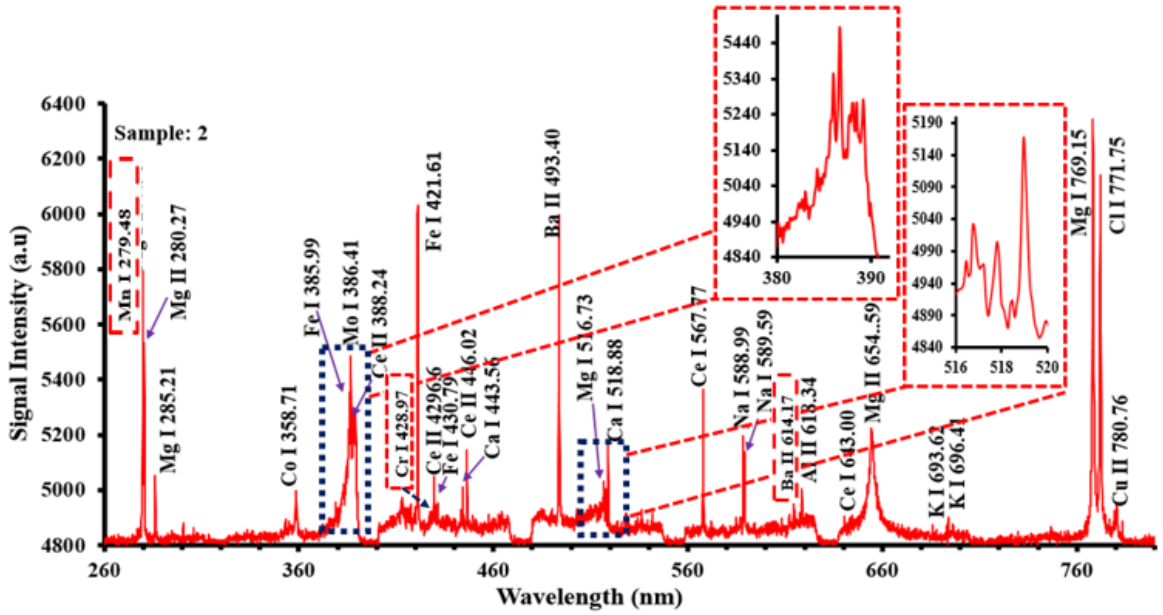

Fig. 5. 3: LIBS spectrum of sample 2 in the range 200-800 nm by applying the laser of 266 nm wavelength, 400 ns is the delay time and 17.54 J laser energy.

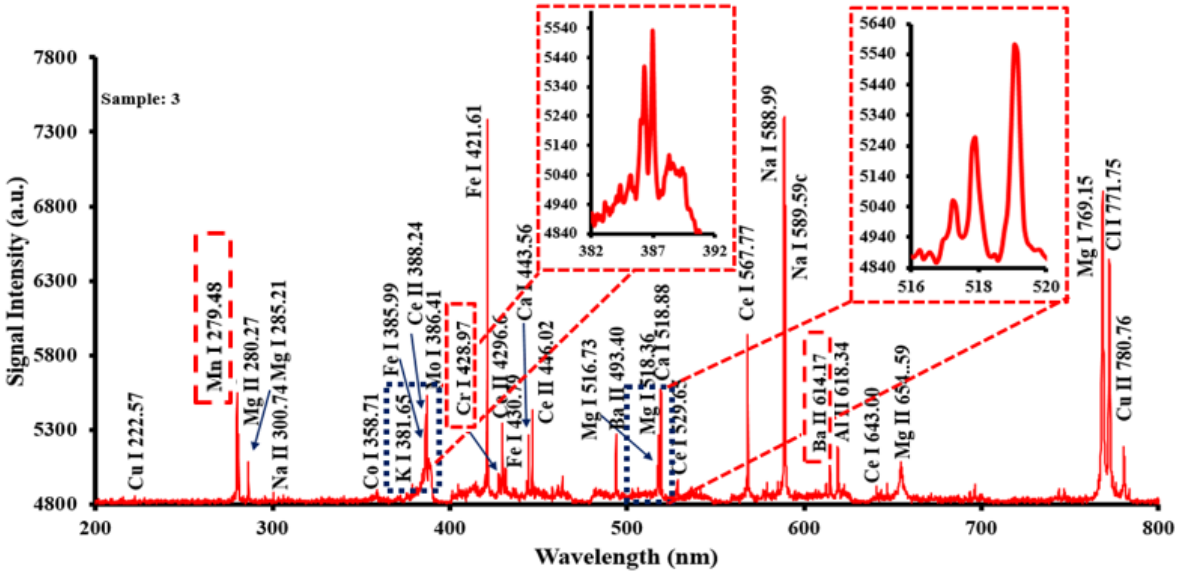

Fig. 5. 4: LIBS spectrum of sample 3 in the range 200-800 nm by applying the laser of 266 nm wavelength, 400 ns is the delay time and 17.54 J laser energy.

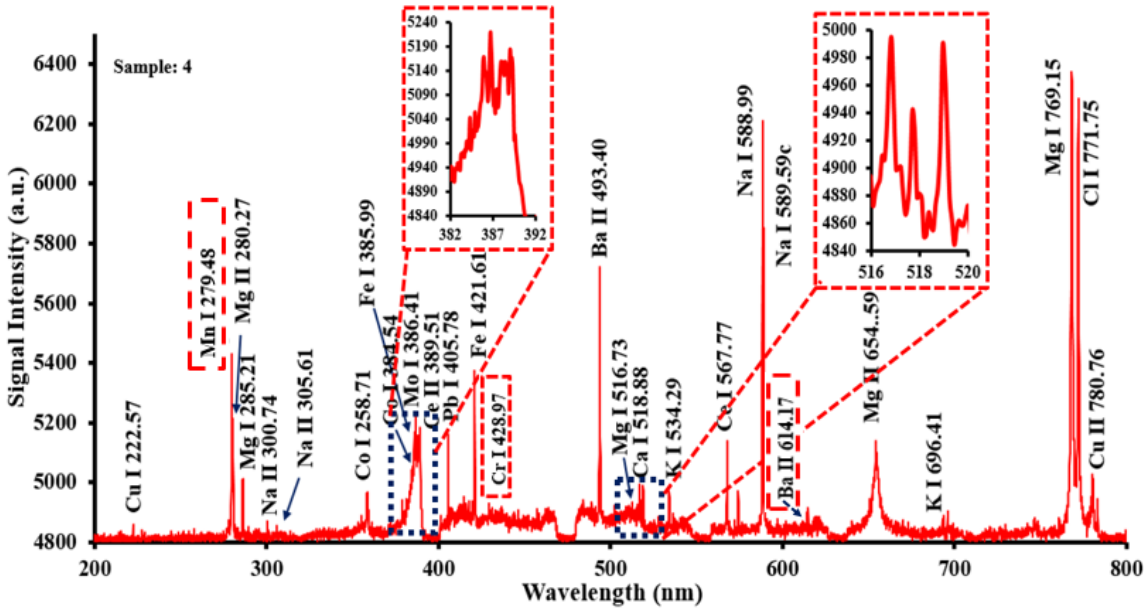

Fig. 5. 5: LIBS spectrum of sample 4 in the range 200-800 nm by applying the laser of 266 nm wavelength, 400 ns is the delay time and 17.54 J laser energy.

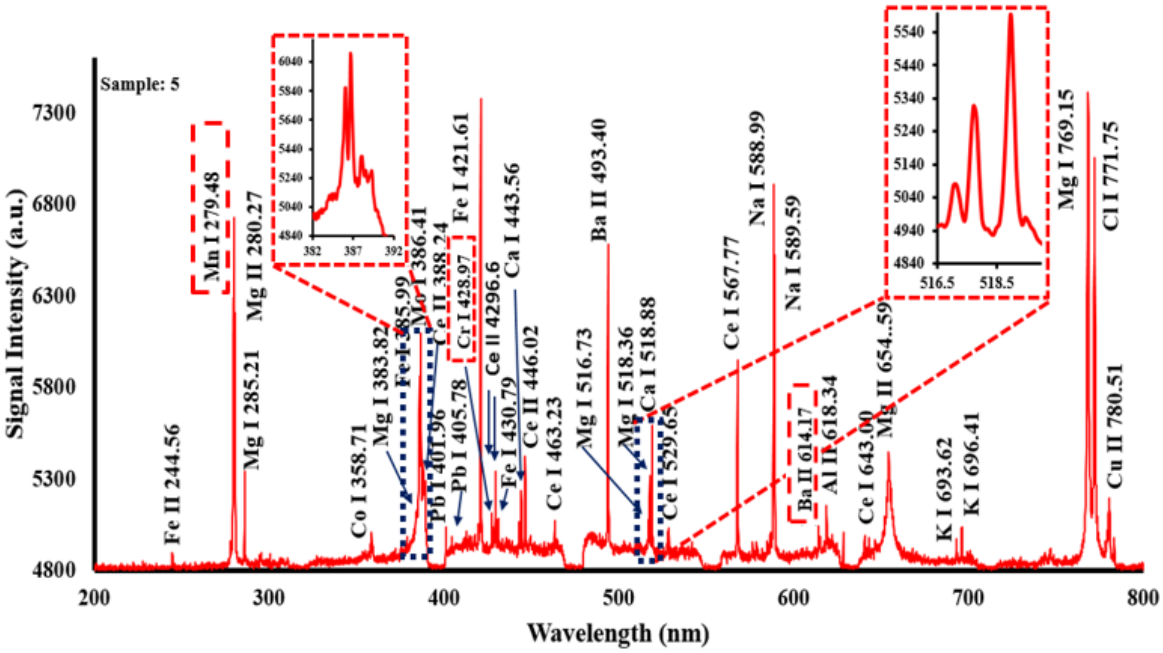

Fig. 5. 6: LIBS spectrum of sample 5 in the range 200-800 nm by applying the laser of 266 nm wavelength, 400 ns is the delay time and 17.54 J laser energy.

5.1.2. Plasma temperature and electron number density.

The entire plasma generation process in LIBS is highly complicated and comprises various steps, for instance, ablation, atomization, dissociation, electronic excitation, and ionization. Two critical parameters, the temperature of the plasma and electron number density, are vital to understanding the formation dynamics of the laser-induced plasma (LIP), and to enhance its sensitivity. In detail, LIP formation comprises the following steps: collisional excitations, photo- and collisional ionization, radiative and three-body recombination, radiative decay, de-excitation process and Bremsstrahlung scattering radiation. When the plasma plume is in LTE regime, it consists of a multitude of species whose properties can be modeled by several equilibrium laws. These include Maxwell's distributions, which characterizes the velocity distribution of the plasma particles; Boltzmann statistics, which characterizes the population in various energy levels; Saha's equation, which characterizes the ionization process, and Planck's law, which governs radiation intensity. The foremost condition which determines whether the plasma is in the LTE regime is that the collisional process must dominate the radiative process. On the other hand, if the excitation and de-excitation rates due to the collisional and radiative process are equal, the plasma is in partial local thermal equilibrium (PLTE) regime. The plasma electronic temperature is obtained using the Boltzmann eq. (4.2)

$$\ln\left(\frac{I_{ik,z}\lambda_{ik,z}}{g_{i,z}A_{ik,z}}\right) = -\frac{E_{i,z}}{KT} + constant \tag{4.2}$$

By computing the left-hand side and plotting it against $E_{i,z}$ for the spectral lines in the ionization state z, the slope 1/KT served to obtain the temperature. Above equation 4.2 was applied to the strong lines of Mg I at 518 nm, 384 nm, 769 nm and 285 nm as illustrated in the figure (5.3a). Plasma temperature was calculated to be 10254 K for the above-

mentioned parameters. For the accurate analysis, local thermal equilibrium (LTE) must attain for the optically thin plasma otherwise, self-absorption may occur in the process and one cannot determine precisely the accurate concentration of the element. The parameters $A_{ik,z}$, $g_{i,z}$ and $E_{i,z}$ were taken from the references [97][98]. The most common used methods to determine the LTE condition are electron energy distribution function (EEDF) and McWhirter criterion. In the preceding section, reference was made to the plasma as being in the LTE regime. The LTE regime is very critical to ensure that the plasma becomes optically thin, failing which self-absorption may occur and prevent an accurate concentration determination of various elements. To avoid the LIBS signal intensity reduction of various atomic transitions induced by self-absorption, the requisite conditions are an optically thin plasma and the LTE regime. These conditions were tested for EEDF and McWhirter criteria, and these latter criteria necessitated the estimation of the electron number density. The EEDF condition holds when electron number density $(n_e) > 10^{16} cm^{-3}$ and kT< 5eV, whilst the McWhirter criterion remains satisfied when the rate of the collisional process is greater than the radiative process, which is mathematically represented by:

$$n_e \geq 1.6 \times 10^{12} T^{1/2} (\Delta E)^3 cm^{-3} \qquad (4.3)$$

where n_e = electron number density and ΔE is the greatest possible transition energy for the shortest wavelength is used in the calculation of temperature T [52], and n_e, T & ΔE have units of cm^{-3}, K and eV.

The spectral lines of plasma broaden due to the Stark effect (which consists of splitting of energy levels due to electric field induced by the plasma, with FWHM $\sim$ 0.1-1), the

Doppler effect (resulting from thermal movement of the ions with FWHM ~ 0.01-0.1 nm), the van der Waals effect (resulting from the van der Waals dipolar force with FWHM ~ 0.01 nm) and other instrumental reasons [87]. Here the plasma produced by the laser shows that at low temperatures and densities, the contributions from the Doppler and van der Waals effects are negligible. The primary contribution to the FWHM width in the LIBS spectra arises mainly from Stark broadening. The stark width parameter ω for Mg 285.21 nm line is 0.0041 nm [99]. As the Stark effect broadening dominates, we estimated the FWHM for the neutral line of Mg 285.21 nm to find the electron density of the plasma. Stark broadening is governed by a Lorentzian Function and its FWHM is directly proportional to the electron density, as per equation (4.4).

$$FWHM\,(A^0) = 2\omega\left(\frac{n_e(cm^{-3})}{10^{16}}\right) \tag{4.4}$$

Where ω represents the FWHM at the calculated temperature for the electron density of $10^{16}cm^{-3}$ [52][100][16]. The calculated electron density for an FWHM of 0.27 nm for the Mg I line of 285.21 nm is $3.293*10^{17}cm^{-3}$. It is noteworthy that the calculated electron density meets the EEDF criterion for the LTE with the calculated electron density of $n_e \geq 10^{16}cm^{-3}$ and KT = 0.88 eV < 5 eV. Furthermore, the McWhirter criterion is also satisfied as the estimated electron density n_e is greater than the critical electron density of $1.45*10^{16}cm^{-3}$. Based on the parameters calculated above, it is apparent that the LIBS plasma is in the LTE regime.

Table 5. 1: Spectroscopic parameters of neutral Mg lines taken from NIST database for the plasma temperature estimation

Wavelength (nm)	**Signal Intensity (a.u)**	**Statistical weight**		**Transition Probability** $A_{ik}(s^{-1})$	**Energy of the Transition Levels (eV)**	
		g_i	g_k		E_i	E_k
518.36	515	5	3	5.61E+07	2.72	5.11
383.82	317	5	7	1.61E+08	2.72	5.95
769.15	258	5	7	2.66E+06	5.75	7.36
285.21	512	5	5	1.36E+08	2.71	7.18

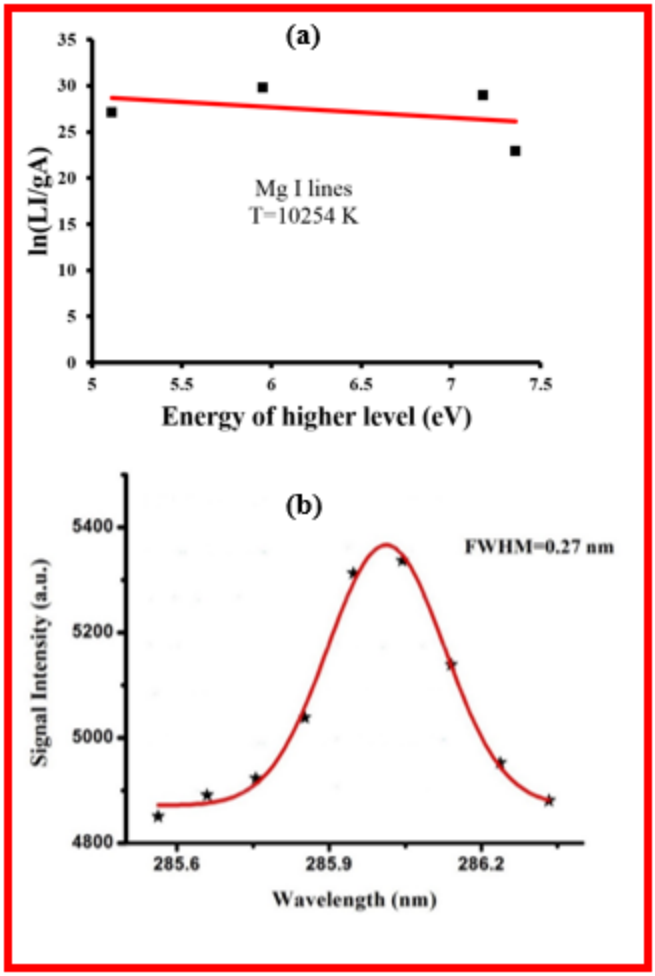

Fig. 5. 7: (a) Boltzmann plot drawn for Plasma temperature determination, spectral lines of the neutral lines of Mg were taken for the Boltzmann plot with plasma temperature detected 10254 K. (b) Particular Stark Broadened Profile of neutral atomic Mg at 285.21nm

5.1.3. Laser energy and Delay time effect on the Signal Intensity

Before using the LIBS setup for analysis of samples optimization of some parameters is necessary. These include the dependence of LIBS signal intensity on delay time and incident laser energy. Fig. (5.4a, 5.4b, 5.4c) depicts the LIBS signal intensity dependence on the incident laser energy, which shows a linear dependence trend. The increase in the LIBS signal intensity is obvious as the incident laser energy increases, more mass of the

sample ablated due to which LIBS signal intensity is increased and when laser energy is low, less mass is ablated so the signal intensity is decreased.

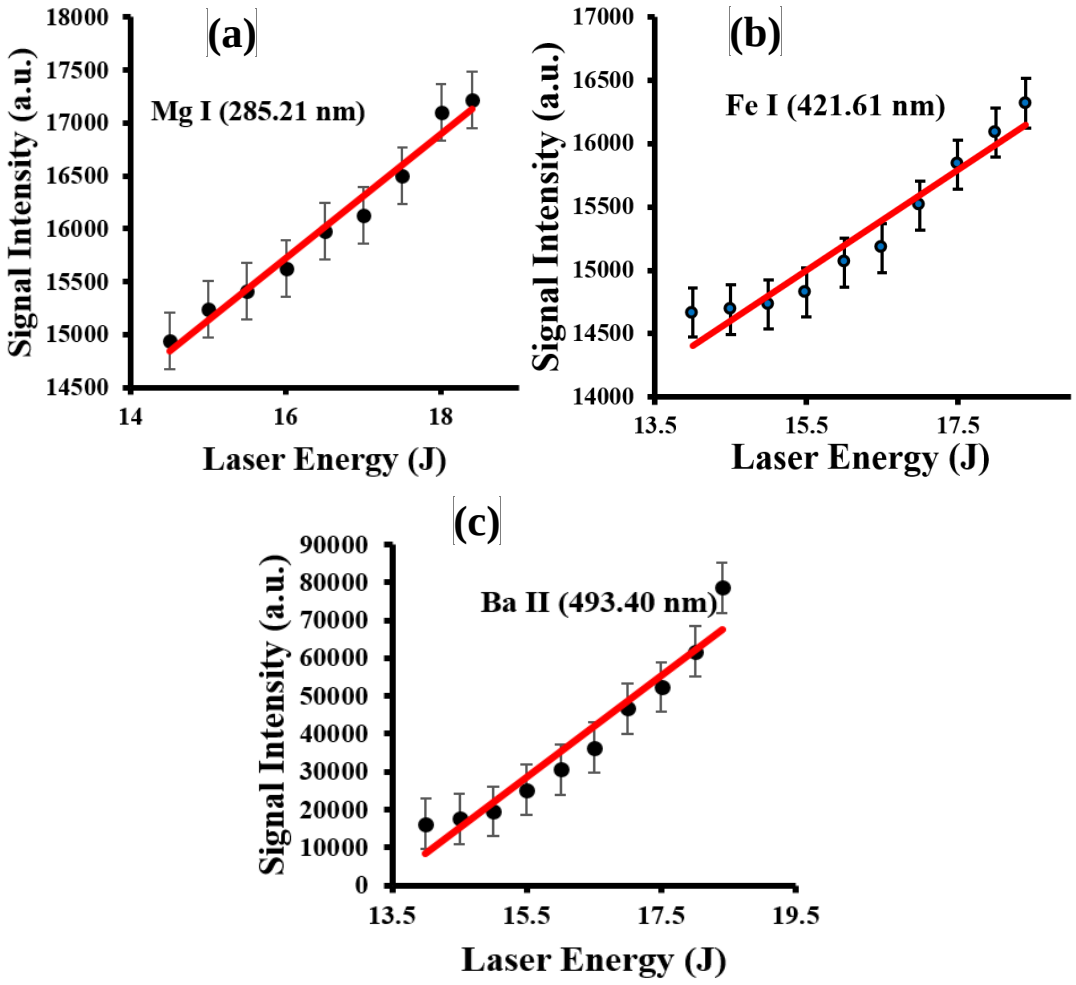

Fig. 5. 8: (a, b, c) Dependence of LIBS signal intensity on the Laser energy.

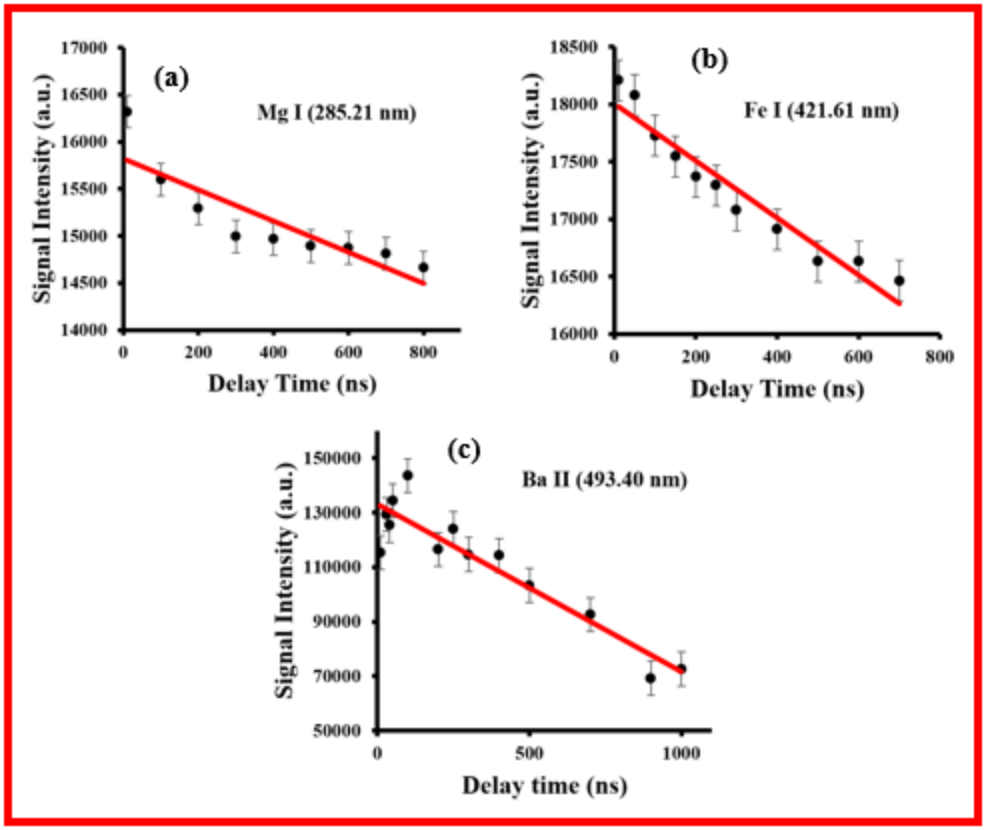

Fig. 5. 9: (d, e, f) Dependence of Laser Signal Intensity on Delay time.

From the fig. (5.5d, 5.5e, 5.5f) it is clear that signal intensity is inversely proportional to the delay time. In the beginning (few nanoseconds), the plasma is the hot (non-LTE regime) and ionic transitions dominates in most of the region of the spectrum so the LIBS spectrum in our case were recorded at 200 ns when the plasma has been cooled down to get the sufficient lines for the atomic transition which considered to be a good marker for the elemental analysis and moreover LIBS plasma has entered to the LTE regime.

5.1.4. Quantitative analysis of LIBS spectra using GSA-SVR model

The quantitative analysis of the acquired LIBS spectra was conducted using gravitational search algorithm based support vector regression GSA-SVR hybrid chemo-metric. The model was developed using the spectra of the standard samples of different brands of coffee

samples. Since our focus in this study is on toxic elements such as chromium, barium, and manganese, so these elements concentrations were estimated using the model, the spectra of chromium, barium, and manganese standard were used in building the above-mentioned model. Thirty-eight data sets were used for the modeling and the results obtained from statistical analysis of the dataset are shown in table 5.2.

The mean values presented in table 5.2 give useful insight regarding the content of the dataset while the discrepancies in the dataset are measured through the standard deviations. The correlation coefficients listed in table 5.2 show a weak correlation between the intensity and the elemental concentration. Hence, the need for non-linear modeling technique for correlating the intensity with the concentration becomes apparent. The choice of SVR based chemo-metric is due to its excellent performance in the presence of few data-points[85]. The hyper-parameters of SVR are optimized using GSA. The influence of the convergence of the model on the number of initial population is presented in Fig. 5.6.

Table 5. 2: Statistical analysis of the dataset used for model GSA-HSVR development

	Mean	Standard deviation	Correlation coefficient
Intensity (a.u)	1035.063	1655.855	0.248148
Wavelength (nm)	411.3573	115.3418	-0.39332
molar mass (g/mol)	302.3755	81.84988	-0.53318
Concentration(pp)	12.09342	14.28255	

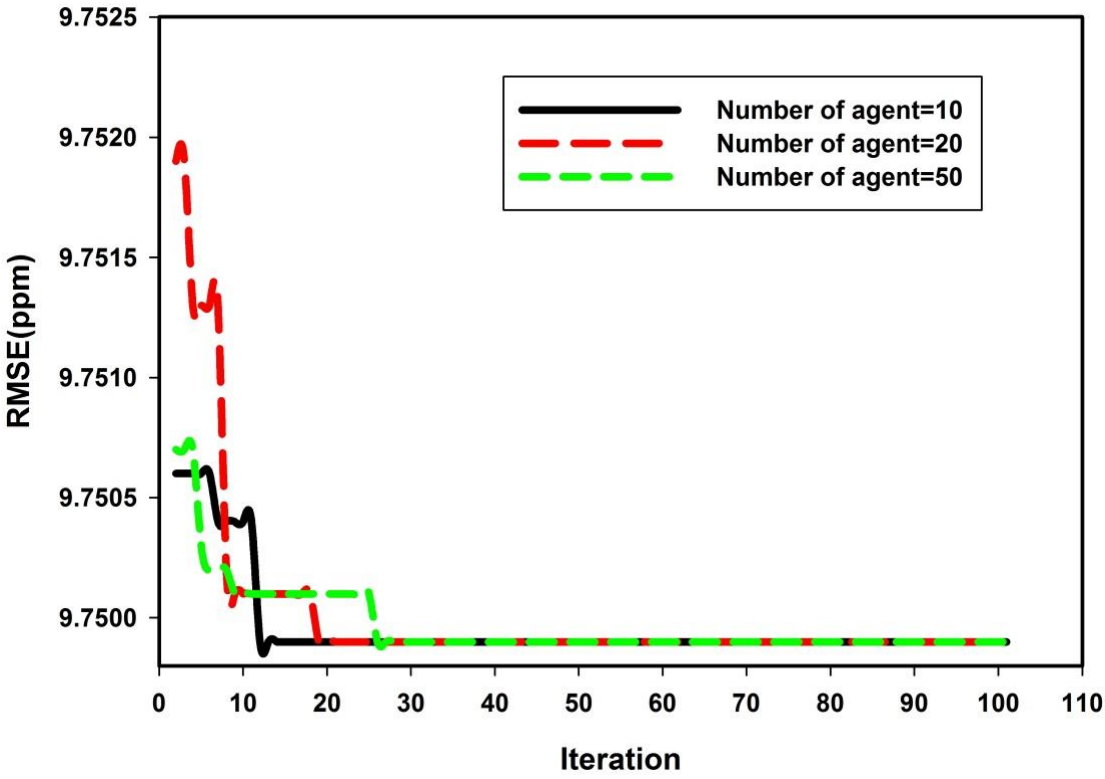

Fig. 5. 10: Effect of model convergence on initial number of agent

The figure shows that the initial number of the agent has no significant effect on the exploration and exploitation ability of the model. To reduce the model's complexity, ten numbers of agents are finally used for model development and implementation. In table 4.3, the optimum values of the model parameters are enumerated; these values enhance the reproducibility of the results. Table 5.4 shows the parameters that measure the generalization and predictive ability of the model.

Table 5. 3: Optimum values of the model parameters

model parameters	GSA-SVR
C	543.4553
Epsilon	0.2
Option	0.1542
Lambda	E-1
Kernel function	Polynomial
Number of agents	10
Alpha	20
Go	100

Table 5. 4: evaluation of the generalization and predictive capacity of the model

Parameters	GSA-SVR	
	Training	Testing
Correlation coefficient (CC) in %	67.53	95.74
Root mean square error (RMSE) ppm	10.3403	9.7499

The results achieved through the quantitative analysis obtained using the developed GSA-SVR chemo-metrics are compared with the results of toxic elements obtained from the standard analytical technique like ICP-OES and the comparison is depicted in table 5.5.

Table 5. 5: Comparison between the results of LIBS (GSA-SVR) and ICP-OES in ppm

Element	Samples	ICP	LIBS (GSA-SVR)
	Sam. 1	46.5	22.73
Mn	Sam. 2	22.5	24.40
	Sam. 3	3.5	22.36
	Sam. 4	23.8	23.10
	Sam. 5	8.9	27.74
Cr	Sam. 1	2.1	2.08
	Sam. 2	0.1	2.10
	Sam. 3	0.1	2.08
	Sam. 4	1.9	1.99
	Sam. 5	0.1	2.13
Ba	Sam. 1	3.2	3.27
	Sam. 2	1.2	3.49
	Sam. 3	0.7	3.83
	Sam. 4	4.4	3.18
	Sam. 5	1.5	3.68

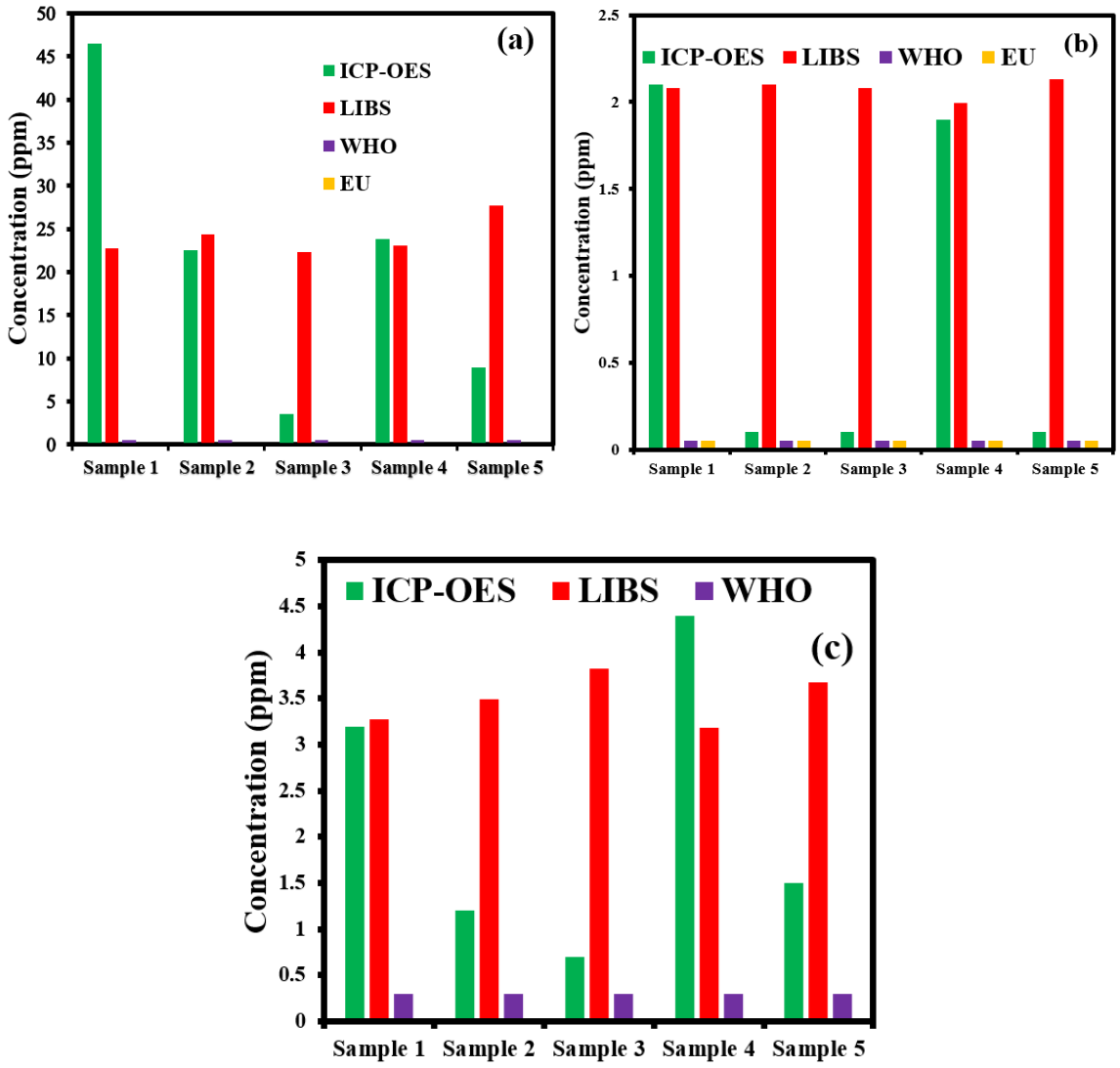

Fig. 5. 11: Bar charts of the comparison between ICP-OES, LIBS, maximum permissible limit by WHO and EU. (a). Shows the concentration of Mn. (b). Shows the concentration of Cr. (c). Shows the concentration of Ba.

5.2. Diagnosis of colon cancer by determination of variable concentration of elements in healthy and cancerous colon tissues using laser induced breakdown spectroscopy with calibration free quantitative analysis

It is reported that colon cancer is the 3rd most common cancer in women and 4th most common cancer in men [100]. It is noted that highest rate is in Europe, North America, and Oceania, and somehow lower in South America, Africa, and Asia (e.g. about 4 cases in 100 000 population in India), in Asia (i.e. Japan, Singapore, and Israel) also observed high rates. A major factor for this areal variation seems due to the factors like diet and physical activity and supposed to have a western living style [101]. 50–75% cancer can be reduced by alteration of some aspects, first by having a good diet, consistent physical working, and maintaining the appropriate mass. professional activity is also influenced greatly by the risk of colon cancer and it is seen that mostly the worker working in the field related to asbestos and wood dust and those are working in the cloth industry are honored the victims of colon cancer. Additionally, people working in the pesticide factories are also victim of colon cancer [102].

Large digestive organ growth is the last phase of a dynamic procedure of dysplastic change, happening most as often as possible in adenoma. Most colon growths likely emerge from benevolent neoplastic polyps [103]. It is experienced that 90% recovery has been achieved for the large instestime cancer in the early stages while its recovery chances reduced to 5% in advanced stages, almost after 5 years of intestine cancer [104].

Medical studies have evaluated that the early stage colon cancer can be controlled by the excess amount of taking Mg in diet, but for the advanced stages it can cause to increase the

malignancy [105]. It is aso reported that Ca, Zn and Cu provide good safety against the rectum cancer [106]. Klimczak et al. [107] demonstrated that the tendency of disturbed equilibrium in some of the elements like Mg and Cu can cause the colon cancer. MILDE et al. [108] reported for Cu, Mg, Se, and Zn in blood serum and colon tissue samples were examined by atomic absorption spectrometry (AAS). His results show that Se level decreased in colon cancerous tissues as compared to the healthy one while Zn was increased up to a small value in effected colon and Cu, Mg did not vary significantly. Bocca et al. [109] researched and reported that the metal concentrations in colorectal normal tissue presented a large range of dissimilarity: Ag, Au, Be, Bi, Co, Li, Sb, Tl, V, W, and Zr were under 50 ng g-1 ; As, Ba, Cd, Cr, Cs, Hg, Mo, Ni, Pb, Se, and Sn were in between the range of 100 to 500 ng g-1 ; Al, Cu, Fe, Mn, Sr, and Zn were from a some mg g-1 to 100 mg g-1 ; and Ca and Mg were the most discovered close to 1000 mg g-1.

In contrast to the earlier published works, to diagnose the colon cancer we are introducing a new technique here which is named as Laser induced Break down Spectroscopy (LIBS). Basics of the LIBS system is to analyses an analyte qualitatively and quantitatively from the recorded spectra of the laser induced plasma by utilizing the characteristics wavelengths, transition lines intensities and relative intensities [67][110][16]. Preciseness, multi-elemental recognition, fast results for online inspection, easily sample preparation for complete quantities, high resolution for exterior recording, and its ability for the remote sensing in harsh environments are the unique properties of the LIBS upon the existing analysis techniques [64][12]. Metallic alloys have been extensively used for quantitative analyses by LIBS system with the high degree of accuracy. [12], [19], [64]. Plenty of applications has been demonstrated with the LIBS system especially in the vicinity of

organic materials [111][112][113]. Applications of LIBS to organic materials were reported more recently, including quantitative analysis [114][115][116]. LIBS used the plasma as a marker for the analysis which is produced by a high intense laser beam which ignites the sample. Parameters those must be optimized in the LIBS system are laser intensity, laser pulse width, the diameter of the laser beam and the necessarily adjusting the laser on the surface of the target material. Usually, LIBS system doesn't require any complicated vacuum system for the analysis but it is expected efficiency will increase in a vacuum chamber. Self-absorption is one of the main problems in LIBS measurement which can be controlled up to a certain extent by acquiring of local thermodynamic equilibrium (LTE), which is evaluated thoroughly in our present research. In addition, using new emerging LIBS technique we worked for the precise and accurate results for the detection of colon cancer which are also somehow confirming as well as extending the previous results of conventional techniques. Results obtained from LIBS also confirmed by cross check with the results obtained by the conventional procedure after digestion of the sample using inductively coupled plasma mass spectroscopy (ICP-MS) analysis. Such direct comparison provides an assessment of the performance of LIBS, and especially of the procedure of calibration free method, to deal with different biological compounds.

5.2.1. Laser induced plasma parameters (electron temperature and density): their studies for optimization of LIBS analysis

Local thermal equilibrium (LTE) and thin plasma state are required to attain the good results from the LIBS setup, otherwise, there will be a drastic self-absorption. LTE is justified since the electron density is the high and Maxwellian distribution of the velocity.

To detect LTE and optically thin plasma, spectral line intensities can be used in the following relation.

$$I_{ik,z} = \frac{A_{ik,z} g_{i,z} L N_z}{\lambda_{ik,z} U_z(T)} \exp\left(-\frac{E_{i,z}}{KT}\right) \tag{4.5}$$

Where $I_{ik,z}$ = signal intensity arising from electron transiting from higher-energy state i to lower-energy state k for an atom in an ionization state z, $E_{i,z}$ = higher energy state, $g_{i,z}$ = statistical weight of $E_{i,z}$, $\lambda_{ik,z}$ = spectral line wavelength, $A_{ik,z}$ = transitional probability, K = Boltzmann constant and T = temperature of plasma, L = characteristic length of plasma and N_z = density of emitting atom[97].

The entire plasma generation process is highly complicated and comprises various steps, for instance, atomization, dissociation, and electronic excitation. Two critical parameters, the temperature of the plasma and electron number density, are vital to understanding the formation dynamics of the laser-induced plasma (LIP), and to enhance its sensitivity. In detail, LIP formation comprises the following steps: collisional excitations, photo- and collisional ionization, radiative and three-body recombination, radioactive decay, de-excitation process and Bremsstrahlung scattering radiation. When the plasma plume is in LTE regime, it consists of a multitude of species whose properties can be modeled by several equilibrium laws. These include Maxwell's distributions, which characterizes the velocity distribution of the plasma particles; Boltzmann statistics, which characterizes the distribution of the population into various energy levels; Saha's equation, which characterizes the ionization process, and Planck's law, which governs radiation intensity. The foremost condition which determines whether the plasma is in the LTE regime is that

the collisional process must dominate the radiative process. On the other hand, if the excitation and de-excitation rates due to the collisional and radiative process are equal, the plasma is in partial local thermal equilibrium (PLTE) regime. The plasma electronic temperature is obtained using the Boltzmann eq. (4.6)

$$\ln\left(\frac{I_{ik,z}\lambda_{ik,z}}{g_{i,z}A_{ik,z}}\right) = -\frac{E_{i,z}}{KT} + cons\tan t \tag{4.6}$$

By computing the left-hand side and plotting it against $E_{i,z}$ for the spectral lines in the ionization state z, we obtain the temperature from the slope 1/KT. Above Eq. was applied to the strong lines of Ca I at 616.90 nm, 646.25 nm, 649.37 nm and 643.9 nm as illustrated in the figure 5.8a. For the accurate analysis, local thermal equilibrium (LTE) must attain for the optically thin plasma otherwise, self-absorption may occur in the process and we cannot determine precisely the accurate element. The parameters $A_{ik,z}$, $g_{i,z}$ and $E_{i,z}$ were taken from [70], [71]. The most common used methods to determine the LTE condition are electron energy distribution function (EEDF) and McWhirter criterion. In the preceding section, reference was made to the plasma as being in the LTE regime. Why is it optimal to work in the LTE regime? It is to ensure that the plasma becomes optically thin, failing which self-absorption may occur and prevent an accurate determination of the identity of the various elements. To avoid getting spurious signals from atomic transitions induced by self-absorption, the requisite conditions are an optically thin plasma and the LTE regime. These conditions are tested for using EEDF and McWhirter criteria, and these latter criteria necessitate an estimation of the electron number density value. The EEDF condition holds when electron number density $(n_e) > 10^{16} cm^{-3}$ and kT< 5eV, whilst the McWhirter

criterion holds when the rate of the collisional process is greater than the radiative process, which is mathematically represented by:

$$n_e \geq 1.6 \times 10^{12} T^{1/2} (\Delta E)^3 cm^{-3} \tag{4.7}$$

where n_e = electron number density and ΔE is the greatest possible transition energy corresponding to the shortest wavelength is used in the calculation of temperature T [16], and n_e, T & ΔE have units of cm^{-3}, K and eV.

The spectral lines of plasma broaden due to the Stark effect (which consists of splitting of energy levels and the electric field induced by the plasma, with FWHM ~ 0.1-1), the Doppler effect (resulting from thermal movement of the ions with FWHM ~ 0.01-0.1 nm), the van der Waals effect (resulting from the van der Waals dipolar force with FWHM ~ 0.01 nm) and other instrumental reasons [116]. Here the plasma produced by the laser reveals that at low temperatures and densities, the contributions from the Doppler and van der Waals effects are negligible. The primary contribution to the FWHM width arises mainly from Stark broadening. The stark width parameter ω of this line is 0.000569 nm [33]. As the Stark effect, broadening dominates, we estimate the FWHM for the neutral line of Be I 265.06 nm to find the electron density of the plasma. Stark broadening is governed by a Lorentzian Function and its FWHM is directly proportional to the electron density, as per equation (4.8).

$$FWHM(A^0) = 2\omega\left(\frac{n_e(cm^{-3})}{10^{16}}\right) \tag{4.8}$$

Where ω represents the FWHM at the calculated temperature for the electron density of $10^{16} cm^{-3}$ [52][100][16]. The calculated electron density for an FWHM of 0.20 nm for the

Be I line of 265.06 nm is $1.757 * 10^{18} cm^{-3}$. It is noteworthy that the calculated electron density meets the EEDF criterion for the LTE with the calculated electron density of $n_e \geq 10^{16} cm^{-3}$ and KT = 0.05 eV < 5 eV. Furthermore, the McWhirter criterion is also satisfied as the estimated electron density n_e is greater than the critical electron density of $9.01 * 10^{14} cm^{-3}$. Based on the parameters calculated above, it is apparent that the LIBS plasma is in the LTE regime.

Table 5. 6: Spectroscopic parameters of neutral Mg lines taken from NIST database for the plasma temperature estimation

Wavelength (nm)	**Signal Intensity (a.u)**	**Statistical weight**		**Transition Probability** $A_{ik}(s^{-1})$	**Energy of the Transition Levels (eV)**	
		g_i	g_k		E_i	E_k
616.91	519	5	3	$5.61 * 10^7$	2.52	4.53
646.25	395	5	7	$4.70 * 10^7$	2.52	4.44
649.37	336	3	5	$4.40 * 10^7$	5.75	7.36
643.90	190	3	5	$9.00 * 10^6$	2.52	4.44

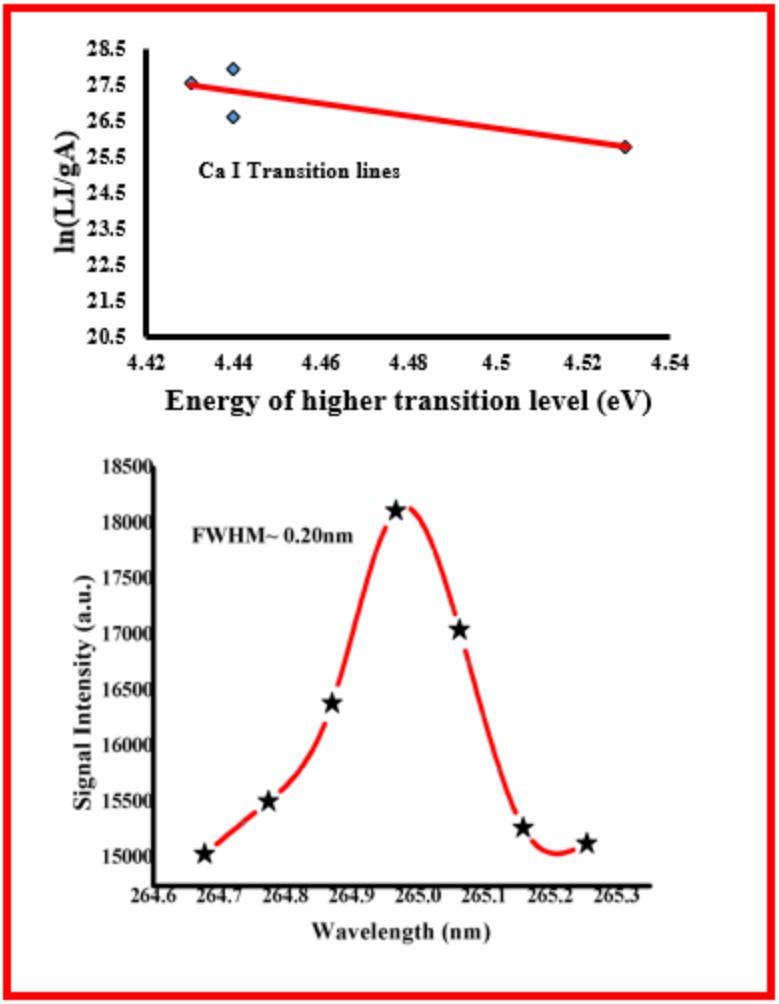

Fig. 5. 12: (a) Boltzmann plot drawn for Plasma temperature determination, spectral lines of the neutral lines of Ca were taken for the Boltzmann plot (b) Particular Stark Broadened Profile of neutral atomic Be at 265.06 nm.

5.2.2. Laser energy and Delay time effect on the LIBS Signal Intensity

Before using the LIBS setup, optimizing several parameters is necessary. These include the delay time and the energy. Fig. (5.10a, 5.10b) depicts the signal intensity as linearly increasing with increasing laser energy. We performed our experiment with the energy of 17.54 J, which is below the maximum energy achievable by our setup (18.40 J). This is a safety precaution, to prevent the setup from being damaged due to high laser intensities. It is obvious when the laser has the high energy we will acquire more ablated mass of sample due to which signal intensity increased and when energy is low, due to less ablation signal

intensity decreased. From the fig. (5.11a, 5.11b) it is revealed that signal intensity is inversely proportional to the delay time. In the beginning, the plasma is in the hot stage (non-LTE regime) and ionic transition overcome most of the region of spectrum so the results were taken at 200 ns when the plasma has cooled down to have the sufficient peaks for the atomic transition which can be a good marker for the elemental analysis and moreover LIBS plasma has entered the LTE regime.

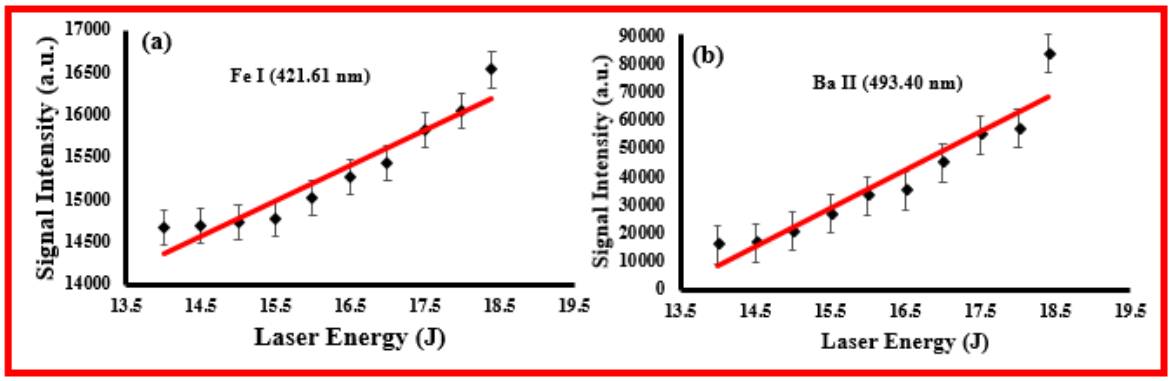

Fig. 5. 13: (a, b) Dependence of LIBS signal intensity on the Laser energy.

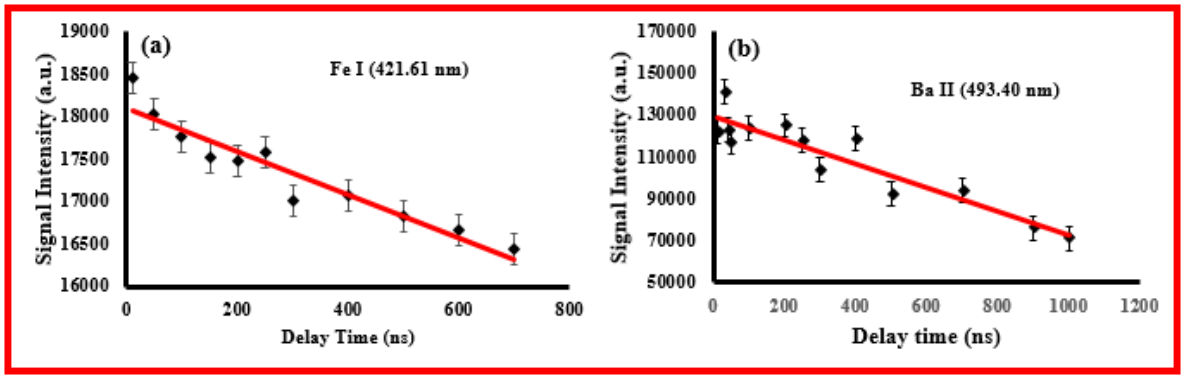

Fig. 5. 14: (a, b) Dependence of Laser Signal Intensity on Delay time.

5.2.3. LIBS Qualitative analysis of the colon samples

The LIBS spectra of the 2 samples were captured within the 200 to 800 nm range with the following parameters: 200 ns delay time, 266 nm laser wavelength and 17.54 J pulse

energy. The standard NIST database was used for identification of the spectral lines. The existence of each element was confirmed using almost three or more fingerprint wavelengths of each element, together with the alternative confirmatory spectroscopic technique of ICP-MS, to ensure a high degree of reliability for our data. Elements detected in colon tissues with slightly or some drastically varying in concentration those are confirmed from the ICP-MS analysis are Ag, Al, Ba, Be, Ca, Cd, Co, Cr, Cu, Fe, K, Li, Mg, Mn, Mo, Na, Ni, Pb, sb, Sn, Sr, Ti, V and Zn with the wavelengths 338.40, 257.65, 652.74, 264.97, 616.36, 360.92, 345.14, 425.31, 510.78, 386.04, 769.68, 670.84, 516.46, 279.89, 386.14, 588.83, 351.39, 374.11, 214.24, 266.02, 460.82, 365.15,437.63, and 307.41nm respectively as indicated in Fig.5.11.. The LIBS experiments were carried out under ambient conditions, hence some atmospheric gasses such as oxygen, chlorine etc. were also observed [93].

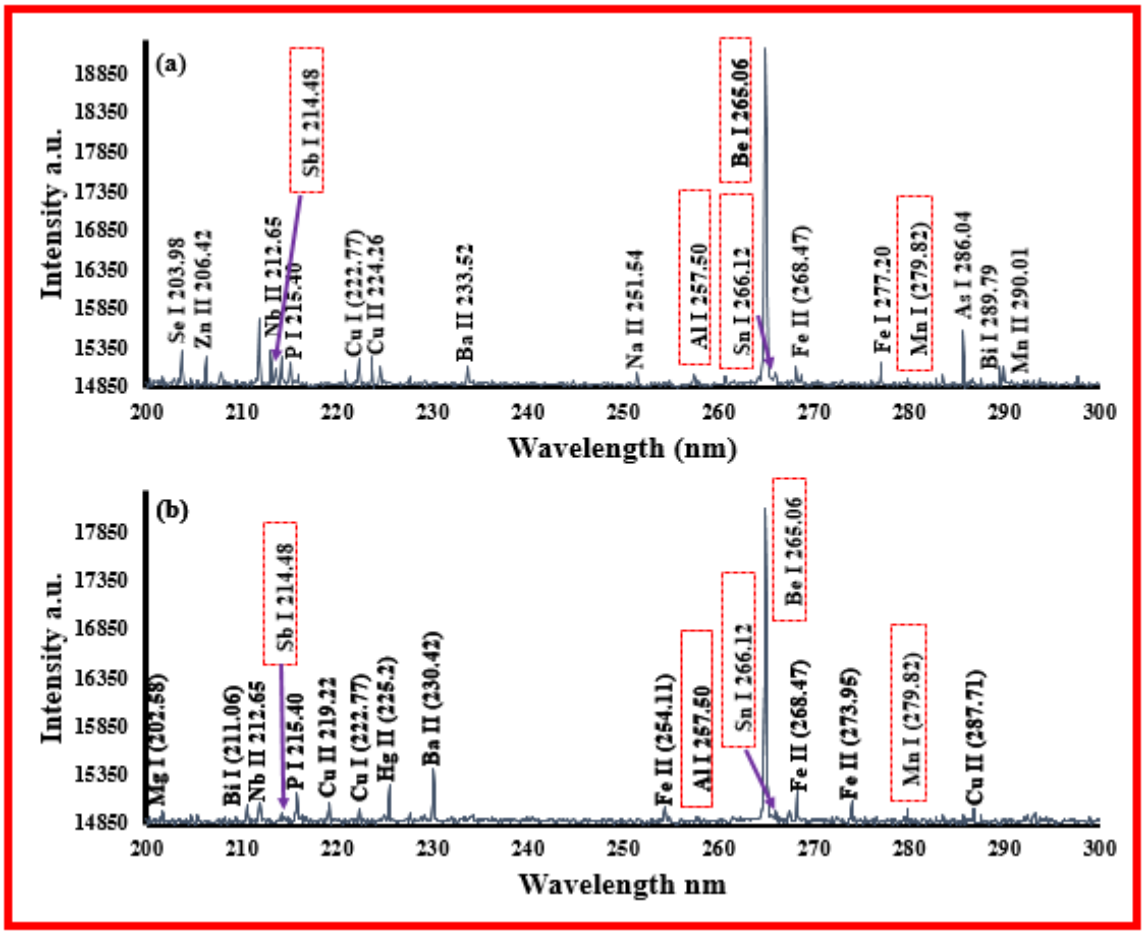

Fig. 5. 15: Spectra illustrated a comparison between health and cancerous tissues in between 200-800 nm (a represents healthy and b represents cancerous)

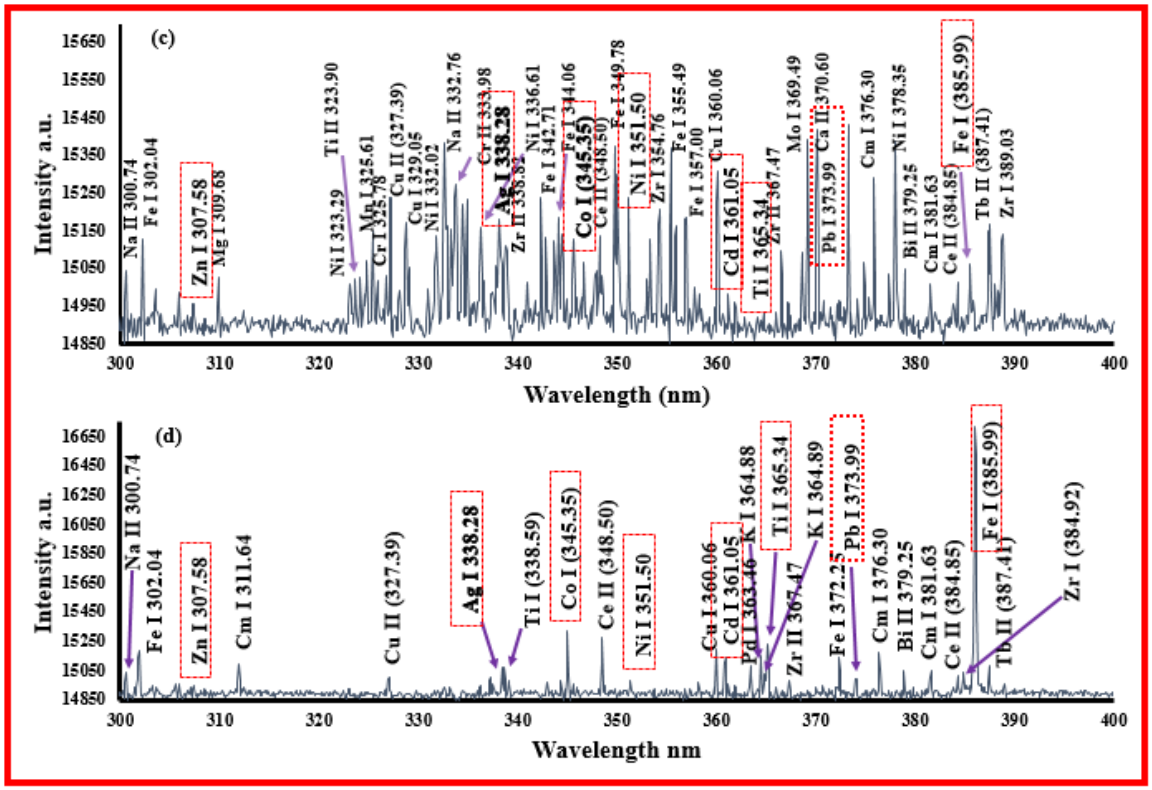

Fig. 5. 16: Spectra illustrated a comparison between health and cancerous tissues in between 200-800 nm (c represents healthy and d represents cancerous)

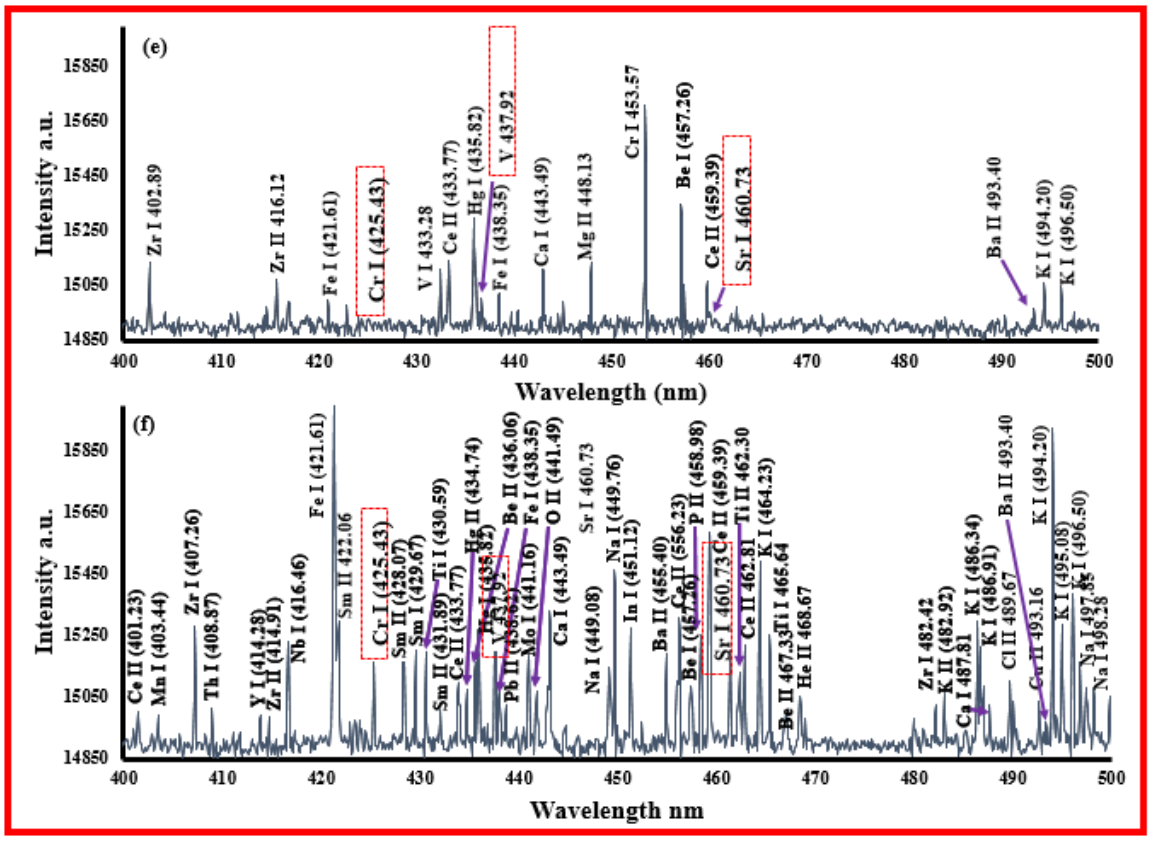

Fig. 5. 17: Spectra illustrated a comparison between health and cancerous tissues in between 200-800 nm (e represents healthy and f represents cancerous)

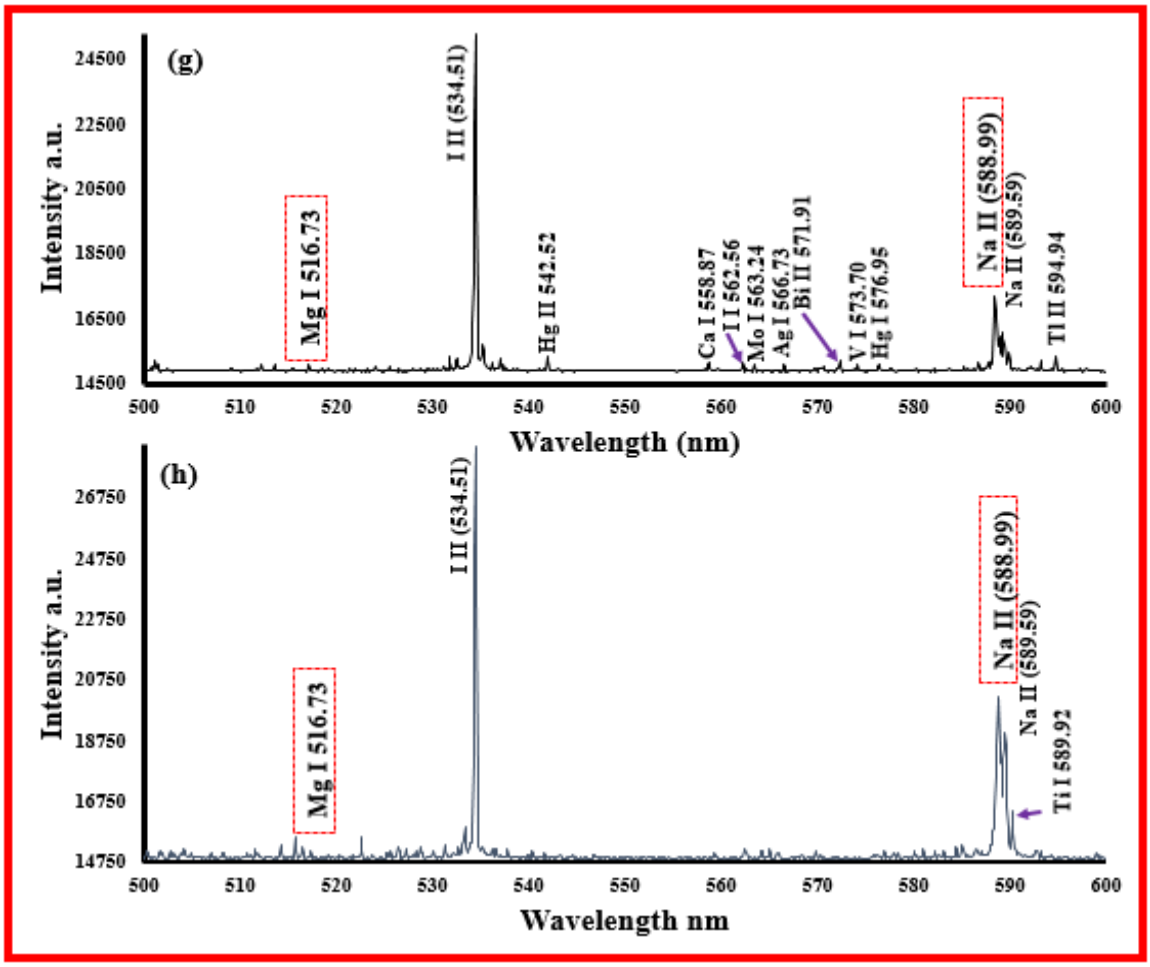

Fig. 5. 18: Spectra illustrated a comparison between health and cancerous tissues in between 200-800 nm (g represents healthy and h represents cancerous)

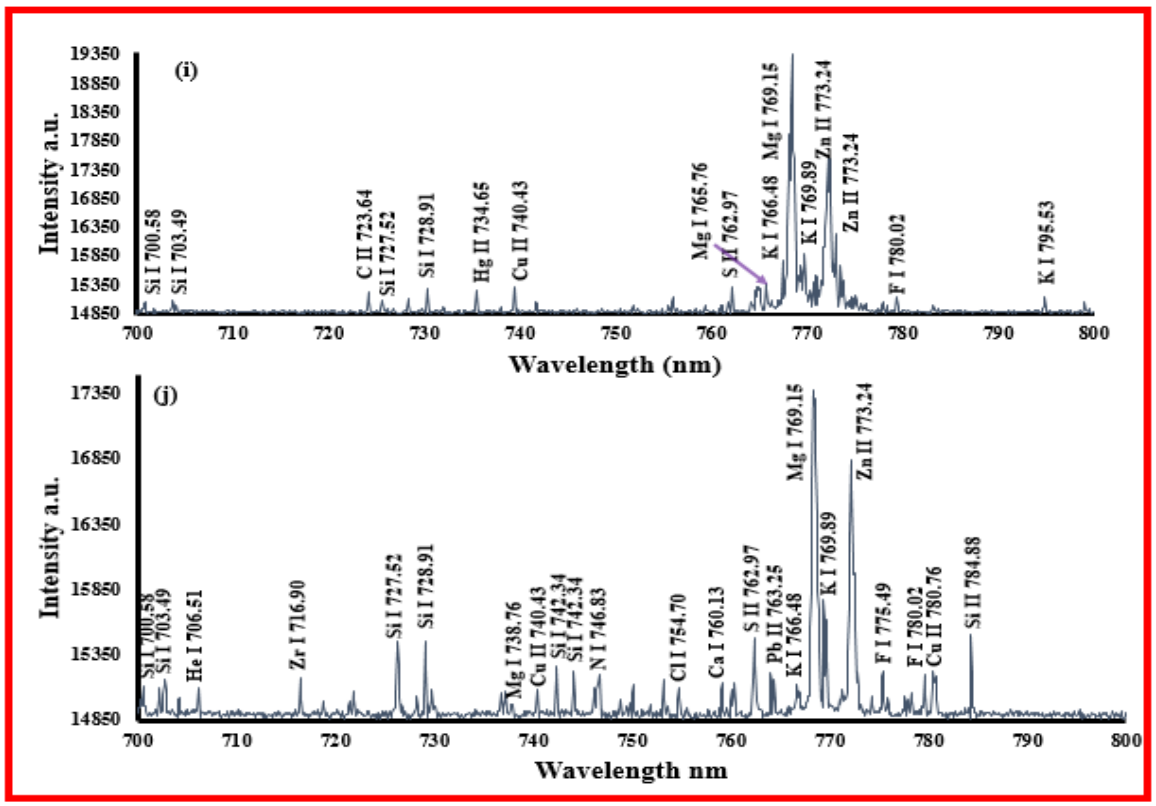

Fig. 5. 19: Spectra illustrated a comparison between health and cancerous tissues in between 200-800 nm (i represents healthy and j represents cancerous)

5.2.4. LIBS Quantitative analysis of the colon samples

We obtained both quantitative and qualitative information for the elements present in colon. The spectral line intensities from the LIBS spectra were converted into ppb using CF-LIBS method., which would allow direct comparison with the ICP-MS results. Standard samples of already known concentrations were used to find the concentration of the elements by using the CF-LIBS method which is well explained in section 3.8. Present elements with their transition lines used to determine the concentrations in colon tissues: Ag, Al, Ba, Be, Ca, Cd, Co, Cr, Cu, Fe, K, Li, Mg, Mn, Mo, Na, Ni, Pb, sb, Sn, Sr, Ti, V and Zn with the wavelengths 338.40, 257.65, 652.74, 264.97, 616.36, 360.92, 345.14, 425.31, 510.78, 386.04, 769.68, 670.84, 516.46, 279.89, 386.14, 588.83, 351.39, 374.11,

214.24, 266.02, 460.82, 365.15, 437.63, and 307.41nm respectively as indicated in Fig.5.11.

This study demonstrating that Ca is drastically decreased from healthy to cancerous tissues of the colon, it decays from 295858.61 ppb to 2700.92 ppb, as depicted in fig. 5.12a. It shows that calcium can be a good marker for the diagnosis of the colon cancer as well as it is good for the protection from the colon cancer. Another variational trend of the elemental concentration also considerable which is, Ba, Cr, Mn, V, Fe, and Na are increasing from healthy to cancerous tissues while Cd, Cu, and Pb have decreasing order from healthy to cancerous colon, illustrated in fig. 5.12a, 5.12b. To further confirm our LIBS quantification results, we determined the concentration of each element in colon tissues using a standard analytical technique like ICP-MS. Which are in excellent agreement with our LIBS results as depicted in Fig.5.12.

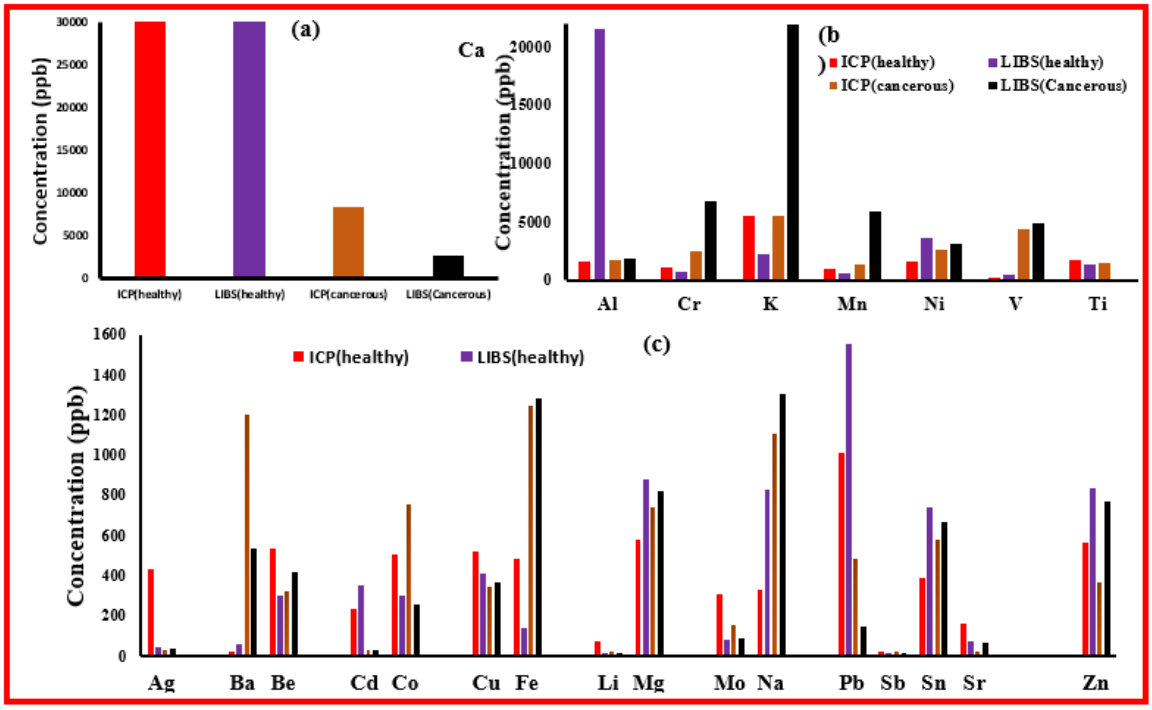

Fig. 5. 20: Shows the comparison of elemental concentration between healthy and cancerous tissues (a). For Ca (b). For major elements (5000-20000 ppb.) (c). Minor elements (20-1600 ppb).

Code has been written for the CF-LIBS analysis is given in appendix.

5.3. Conclusion

This is a detailed study of a commonly consumed beverage drink – different brands of coffee – and one of the most debilitating diseases – colon cancer. In this study five different samples of various coffee brands were analyzed using the locally assembled laser-induced breakdown spectrometer (equipped with a hybrid GSA-SVR chemo-metric for quantitative analysis). The results obtained from our LIBS analysis were verified using the standard ICP-OES technique. LIBS setup was applied for the qualitative detection of all elements in the coffee samples along with a quantitative analysis of elements which are toxic to the human body. Toxic elements detected in coffee brands were Mn, Cr and Ba. The

concentration detected in the examined coffee samples for various elements are given in parentheses: manganese (22.36 –27.74 mg/L), Cr (1.99 –2.13 mg/L) and Ba (3.18 –3.83 mg/L). The concentrations detected for these elements exceed the safe permissible limit set by the World Health Organization (WHO) and European Union (EU). The results obtained from LIBS are in good agreement with the corresponding results obtained using standard techniques by ICP-OES.

In the second part of the study, we analyzed two samples of colon tissues: one healthy and another cancerous by using the LIBS calibration free method. This study shows that Ca decreases from 295858.61 ppb to 2700.92 ppb in cancerous colon tissues from healthy tissues. Hence, calcium can be a good marker for the diagnosis of colon cancer. Furthermore, it is also good for protection from colon cancer. Another variational trend of the elemental concentration, which is also of considerable merit, is that Ba, Cr, Mn, V, Fe, and Na increased from healthy to cancerous tissues in ppb value of 58.61→534.64, 781.30→6780.82, 649.40→5937.43, 517.31→4866.83, 137.35→1282.12 and 831.58→1308.92 respectively while Cd, Cu, and Pb decreased from healthy to cancerous tissues in ppb value of 356.12→32.27, 410.86→371.30 and 1557.62→146.43 respectively. To further confirm our LIBS quantification results, we determined the concentration of each element in colon tissues using a standard analytical technique like ICP-MS, and the results are in excellent agreement with our LIBS results. Such direct comparison provides an assessment of the performance of LIBS, and especially of the procedure of calibration free method, to deal with different biological compounds.

References

[1] N. L. Lanza *et al.*, “Calibrating the ChemCam laser-induced breakdown spectroscopy instrument for carbonate minerals on Mars,” *Appl. Opt.*, vol. 49, no. 13, p. C211, May 2010.

[2] A. K. Knight, N. L. Scherbarth, D. A. Cremers, and M. J. Ferris, “Characterization of Laser-Induced Breakdown Spectroscopy (LIBS) for Application to Space Exploration,” *Appl. Spectrosc.*, vol. 54, no. 3, pp. 331–340, 2000.

[3] G. S. Mungas, C. B. Dreyer, and A. J. Bauer, “Elemental Abundance Measurement Using Micro-LIBS for Space Exploration,” Mar. 2009.

[4] L. C. Trevizan *et al.*, “Evaluation of laser induced breakdown spectroscopy for the determination of micronutrients in plant materials,” *Spectrochim. Acta Part B At. Spectrosc.*, vol. 64, no. 5, pp. 369–377, May 2009.

[5] A. Sarkar, S. K. Aggarwal, and D. Alamelu, “Laser induced breakdownspectroscopy for rapid identification of different types of paper for forensic application,” *Anal. Methods*, vol. 2, no. 1, pp. 32–36, Jan. 2010.

[6] S. H. Wise and J. R. Almirall, “Chemical taggant detection and analysis by laser-induced breakdown spectroscopy,” *Appl. Opt.*, vol. 47, no. 31, p. G15, Jul. 2008.

[7] S. J. Rehse, H. Salimnia, and A. W. Miziolek, “Laser-induced breakdown spectroscopy (LIBS): an overview of recent progress and future potential for biomedical applications.,” *J. Med. Eng. Technol.*, vol. 36, no. 2, pp. 77–89, Mar. 2012.

[8] A. K. Pathak, N. K. Rai, A. Singh, A. K. Rai, P. K. Rai, and P. K. Rai, “Medical Applications of Laser Induced Breakdown Spectroscopy,” *J. Phys. Conf. Ser.*, vol. 548, no. 1, p. 12007, Nov. 2014.

[9] G. Asimellis, N. Michos, I. Fasaki, and M. Kompitsas, “Platinum group metals bulk analysis in automobile catalyst recycling material by laser-induced breakdown spectroscopy,” *Spectrochim. Acta Part B At. Spectrosc.*, vol. 63, no. 11, pp. 1338–1343, Nov. 2008.

[10] S. Carter, A. S. Fisher, P. S. Goodall, M. W. Hinds, S. Lancaster, and S. Shore, “Atomic spectrometry update. Industrial analysis: metals, chemicals and advanced materials,” *J. Anal. At. Spectrom.*, vol. 26, no. 12, p. 2319, Dec. 2011.

[11] R. Gaudiuso, M. Dell’Aglio, O. de Pascale, G. S. Senesi, and A. de Giacomo, “Laser induced breakdown spectroscopy for elemental analysis in environmental, cultural heritage and space applications: A review of methods and results,” *Sensors*, vol. 10, pp. 7434–7468, 2010.

[12] R. Gaudiuso, M. Dell’Aglio, O. De Pascale, G. S. Senesi, and A. De Giacomo, “Laser induced breakdown spectroscopy for elemental analysis in environmental, cultural heritage and space applications: a review of methods and results.,” *Sensors (Basel).*, vol. 10, no. 8, pp. 7434–68, Jan. 2010.

[13] *Laser-Induced Breakdown Spectroscopy*. .

[14] C. Fotakis, D. Anglos, V. Zafiropulos, S. Georgiou, and V. Tornari, *Lasers in the Preservation of Cultural Heritage: Principles and Applications*. CRC Press, 2006.

[15] D. Anglos and J. C. Miller, *Laser-Induced Breakdown Spectroscopy (LIBS)*. Cambridge: Cambridge University Press, 2006.

[16] M. a Gondal, Y. W. Maganda, M. a Dastageer, F. F. Al Adel, a a Naqvi, and T. F. Qahtan, "Detection of carcinogenic chromium in synthetic hair dyes using laser induced breakdown spectroscopy," *Appl Opt*, vol. 53, no. 8, pp. 1636–1643, 2014.

[17] S. Beldjilali, D. Borivent, L. Mercadier, E. Mothe, G. Clair, and J. Hermann, "Evaluation of minor element concentrations in potatoes using laser-induced breakdown spectroscopy," *Spectrochim. Acta Part B At. Spectrosc.*, vol. 65, no. 8, pp. 727–733, Aug. 2010.

[18] F. Mehari *et al.*, "Laser induced breakdown spectroscopy for bone and cartilage differentiation - ex vivo study as a prospect for a laser surgery feedback mechanism," *Biomed. Opt. Express*, vol. 5, no. 11, p. 4013, Nov. 2014.

[19] D. Bulajic *et al.*, "A procedure for correcting self-absorption in calibration free-laser induced breakdown spectroscopy," *Spectrochim. Acta Part B At. Spectrosc.*, vol. 57, no. 2, pp. 339–353, Feb. 2002.

[20] M. Corsi *et al.*, "Double pulse, calibration-free laser-induced breakdown spectroscopy: A new technique for in situ standard-less analysis of polluted soils," *Appl. Geochemistry*, vol. 21, no. 5, pp. 748–755, May 2006.

[21] "H. Griem, Spectral Line Broadening by Plasmas. Elsevier Science, 2012."

[22] B. C. Windom and D. W. Hahn, "Laser ablation—laser induced breakdown spectroscopy (LA-LIBS): A means for overcoming matrix effects leading to

improved analyte response," *J. Anal. At. Spectrom.*, vol. 24, no. 12, p. 1665, 2009.

[23] A. E. Hussein, P. K. Diwakar, S. S. Harilal, and A. Hassanein, "The role of laser wavelength on plasma generation and expansion of ablation plumes in air," *J. Appl. Phys.*, vol. 113, no. 14, p. 143305, Apr. 2013.

[24] J. P. Singh, H. Zhang, F.-Y. Yueh, and K. P. Carney, "Investigation of the Effects of Atmospheric Conditions on the Quantification of Metal Hydrides Using Laser-Induced Breakdown Spectroscopy," *Appl. Spectrosc.*, vol. 50, no. 6, pp. 764–773, Jun. 1996.

[25] M. Autin, A. Briand, P. Mauchien, and J. M. Mermet, "Characterization by emission spectrometry of a laser-produced plasma from a copper target in air at atmospheric pressure," *Spectrochim. Acta Part B At. Spectrosc.*, vol. 48, no. 6–7, pp. 851–862, May 1993.

[26] R. G. Pinnick *et al.*, "Aerosol-induced laser breakdown thresholds: wavelength dependence," *Appl. Opt.*, vol. 27, no. 5, p. 987, Mar. 1988.

[27] "Glow Discharge Spectroscopies. Springer Science & Business Media, 2013."

[28] "D. S. Weiss, B. C. Young, and S. Chu, 'Precision measurement of ?/m Cs based on photon recoil using laser-cooled atoms and atomic interferometry,' Appl. Phys. B Lasers Opt., vol. 59, no. 3, pp. 217–256, Sep. 1994."

[29] and J. S. Yong-Ill Lee, Samuel P. Sawan, Terry L. Thiem, Ye-Yung Teng and F. other works by these Authors, "Interaction of a Laser Beam with Metals. Part II: Space-Resolved Studies of Laser-Ablated Plasma Emission," *Appl. Spectrosc.*, vol.

46, no. 3, pp. 436–441, 1992.

[30] J. G. Jackson, R. W. Fonseca, and J. A. Holcombe, “Mass spectral studies of thermal decomposition of metal nitrates,” *Spectrochim. Acta Part B At. Spectrosc.*, vol. 50, no. 12, pp. 1449–1457, Oct. 1995.

[31] “K. J. Mason and J. M. Goldberg, ‘Production and initial characterization of a laser-induced plasma in a pulsed magnetic field for atomic spectrometry,’ Anal. Chem., vol. 59, no. 9, pp. 1250–1255, May 1987.”

[32] “Xianglei L. Mao, Mark A. Shannon, Alberto J. Fernandez, and Richard E. Russo, ‘Temperature and Emission Spatial Profiles of Laser-Induced Plasmas during Ablation Using Time-Integrated Emission Spectroscopy,’ Appl. Spectrosc. 49, 1054-1062 (1995).”

[33] M. Kuzuya, H. Matsumoto, H. Takechi, and O. Mikami, “Effect of Laser Energy and Atmosphere on the Emission Characteristics of Laser-Induced Plasmas,” *Appl. Spectrosc.*, vol. 47, no. 10, pp. 1659–1664, Oct. 1993.

[34] S. Palanco and J. Laserna, “Spectral analysis of the acoustic emission of laser-produced plasmas,” *Appl. Opt.*, vol. 42, no. 30, p. 6078, Oct. 2003.

[35] J. . Aguilera and C. Aragón, “Multi-element Saha–Boltzmann and Boltzmann plots in laser-induced plasmas,” *Spectrochim. Acta Part B At. Spectrosc.*, vol. 62, no. 4, pp. 378–385, Apr. 2007.

[36] “Laser-Induced Breakdown Spectroscopy. Elsevier, 2007.”

[37] G. Abdellatif and H. Imam, “A study of the laser plasma parameters at different

laser wavelengths," *Spectrochim. Acta Part B At. Spectrosc.*, vol. 57, no. 7, pp. 1155–1165, Jul. 2002.

[38] L. M. Cabalín and J. J. Laserna, "Experimental determination of laser induced breakdown thresholds of metals under nanosecond Q-switched laser operation," *Spectrochim. Acta Part B At. Spectrosc.*, vol. 53, no. 5, pp. 723–730, May 1998.

[39] R. E. Russo, X. L. Mao, O. V. Borisov, and H. Liu, "Influence of wavelength on fractionation in laser ablation ICP-MS," *J. Anal. At. Spectrom.*, vol. 15, no. 9, pp. 1115–1120, Jan. 2000.

[40] X. Mao, W.-T. Chan, M. Caetano, M. A. Shannon, and R. E. Russo, "Preferential vaporization and plasma shielding during nano-second laser ablation," *Appl. Surf. Sci.*, vol. 96–98, pp. 126–130, Apr. 1996.

[41] *Solid-State Laser Engineering*, vol. 1. New York, NY: Springer New York, 2006.

[42] "M. J. Myers, J. D. Myers, and A. G. Myers, 'Laser Induced Breakdown SPectroscopy (LIBS),' Lasers in Chemistry, p1554, 2008."

[43] J.-S. Huang, H.-T. Liu, and K.-C. Lin, "Laser-induced breakdown spectroscopy in analysis of Al3+ liquid droplets: On-line preconcentration by use of flow-injection manifold," *Anal. Chim. Acta*, vol. 581, no. 2, pp. 303–308, Jan. 2007.

[44] X. . Mao, A. . Ciocan, O. . Borisov, and R. . Russo, "Laser ablation processes investigated using inductively coupled plasma–atomic emission spectroscopy (ICP–AES)," *Appl. Surf. Sci.*, vol. 127–129, pp. 262–268, May 1998.

[45] M. J. Myers, J. D. Myers, and A. G. Myers, "Lasers Induced Breakdown

SPectroscopy (LIBS)," *Lasers in Chemestry*, p. 1554, 2008.

[46] "D. a Cremers and L. J. Radziemski, 'Basics of the LIBS plasma,' Handb. Laser-Induced Break. Spectrosc., pp. 23–65, 2006."

[47] R. Agrawal, R. Kumar, S. Rai, A. K. Pathak, A. K. Rai, and G. K. Rai, "LIBS: A Quality Control Tool for Food Supplements," *Food Biophys.*, vol. 6, no. 4, pp. 527–533, Dec. 2011.

[48] A. S. Eppler, D. A. Cremers, D. D. Hickmott, M. J. Ferris, and A. C. Koskelo, "Matrix Effects in the Detection of Pb and Ba in Soils Using Laser-Induced Breakdown Spectroscopy," *Appl. Spectrosc.*, vol. 50, no. 9, pp. 1175–1181, Sep. 1996.

[49] "C. Aragon, J. A. Aguilera, and F. Penalba, 'Improvements in Quantitative Analysis of Steel Composition by Laser-Induced Breakdown Spectroscopy at Atmospheric Pressure Using an Infrared Nd:YAG Laser,' Appl. Spectrosc. 53, 1259-1267 (1999)."

[50] "R. Wisbrun, I. Schechter, R. Niessner, H. Schroeder, and K. L. Kompa, 'Detector for Trace Elemental Analysis of Solid Environmental Samples by Laser Plasma Spectroscopy,' Anal. Chem., vol. 66, no. 18, pp. 2964–2975, Sep. 1994."

[51] R. Krasniker, V. Bulatov, and I. Schechter, "Study of matrix effects in laser plasma spectroscopy by shock wave propagation," *Spectrochim. Acta Part B At. Spectrosc.*, vol. 56, no. 6, pp. 609–618, Jun. 2001.

[52] M. A. Gondal, Y. B. Habibullah, U. Baig, and L. E. Oloore, "Direct spectral

analysis of tea samples using 266nm UV pulsed laser-induced breakdown spectroscopy and cross validation of LIBS results with ICP-MS," *Talanta*, vol. 152, pp. 341–352, May 2016.

[53] F. Anabitarte and A. Cobo, "Laser-Induced Breakdown Spectroscopy : Fundamentals , Applications , and Challenges," vol. 2012, 2012.

[54] D. A. Cremers and A. K. Knight, "Laser-Induced Breakdown Spectroscopy," in *Encyclopedia of Analytical Chemistry*, Chichester, UK: John Wiley & Sons, Ltd, 2000.

[55] M. A. Gondal and T. Hussain, "Determination of poisonous metals in wastewater collected from paint manufacturing plant using laser-induced breakdown spectroscopy," *Talanta*, vol. 71, no. 1, pp. 73–80, Jan. 2007.

[56] K. Y. Yamamoto, D. A. Cremers, M. J. Ferris, and L. E. Foster, "Detection of Metals in the Environment Using a Portable Laser-Induced Breakdown Spectroscopy Instrument," *Appl. Spectrosc.*, vol. 50, no. 2, pp. 222–233, Feb. 1996.

[57] F. Colao, R. Fantoni, V. Lazic, A. Morone, A. Santagata, and A. Giardini, "LIBS used as a diagnostic tool during the laser cleaning of ancient marble from Mediterranean areas," *Appl. Phys. A*, vol. 79, no. 2, pp. 213–219, Jul. 2004.

[58] V. K. Unnikrishnan, K. Alti, V. B. Kartha, C. Santhosh, G. P. Gupta, and B. M. Suri, "Measurements of plasma temperature and electron density in laser-induced copper plasma by time-resolved spectroscopy of neutral atom and ion emissions,"

Pramana, vol. 74, no. 6, pp. 983–993, Sep. 2010.

[59] O. Samek, D. C. S. Beddows, H. H. Telle, G. W. Morris, M. Liska, and J. Kaiser, "Quantitative analysis of trace metal accumulation in teeth using laser-induced breakdown spectroscopy," *Appl. Phys. A Mater. Sci. Process.*, vol. 69, no. S1, pp. S179–S182, Dec. 1999.

[60] B. Le Drogoff *et al.*, "Temporal characterization of femtosecond laser pulses induced plasma for spectrochemical analysis of aluminum alloys," *Spectrochim. Acta Part B At. Spectrosc.*, vol. 56, no. 6, pp. 987–1002, Jun. 2001.

[61] D. a Cremers and L. J. Radziemski, "Basics of the LIBS plasma," *Handb. Laser-Induced Break. Spectrosc.*, pp. 23–65, 2006.

[62] R. Fantoni, L. Caneve, F. Colao, L. Fornarini, V. Lazic, and V. Spizzichino, "Methodologies for laboratory Laser Induced Breakdown Spectroscopy semi-quantitative and quantitative analysis—A review," *Spectrochim. Acta Part B At. Spectrosc.*, vol. 63, no. 10, pp. 1097–1108, Oct. 2008.

[63] "Miziolek AW, Palleschi V, Schechter I (eds) (2006) Laser-induced breakdown spectroscopy: fundamentals and applications. Cambridge University Press, Cambridge."

[64] D. A. Cremers and R. C. Chinni, "Laser-Induced Breakdown Spectroscopy—Capabilities and Limitations," *Appl. Spectrosc. Rev.*, vol. 44, no. 6, pp. 457–506, Nov. 2009.

[65] W. Q. Lei *et al.*, "Comparative measurements of mineral elements in milk powders

with laser-induced breakdown spectroscopy and inductively coupled plasma atomic emission spectroscopy," *Anal. Bioanal. Chem.*, vol. 400, no. 10, pp. 3303–3313, Jul. 2011.

[66] A. A. I. Khalil, M. A. Gondal, and M. A. Dastageer, "Detection of trace elements in nondegradable organic spent clay waste using optimized dual-pulsed laser induced breakdown spectrometer," *Appl. Opt.*, vol. 53, no. 8, p. 1709, Mar. 2014.

[67] M. a. Gondal, Z. S. Seddigi, M. M. Nasr, and B. Gondal, "Spectroscopic detection of health hazardous contaminants in lipstick using Laser Induced Breakdown Spectroscopy," *J. Hazard. Mater.*, vol. 175, pp. 726–732, 2010.

[68] O. Emre1 *et al.*, "Plasma Concentrations of Some Trace Element and Heavy Metals in Patients with Metastatic Colon Cancer," *J. Cancer Ther.*, no. 4, pp. 1085–1090, 2013.

[69] "R. Baran, P. R. Dawber, E. Haneke, A. Tosti and I. a. T. L. Bristow, A text Atlas of Nail Disorders: Techniques in Investigation and Diagnosis, 3rd Edition ed., Martin Duntiz, Taylor and Francis Group, 2005."

[70] V. A. Trunova, N. V. Brenner, and V. V. Zvereva, "Investigation of the Content and of the Distribution of Chemical Elements in Human Nails by SRXRF," *Toxicol. Mech. Methods*, vol. 19, no. 1, pp. 1–18, Jan. 2009.

[71] S. Valente-Campos, M. Yonamine, R. L. de M. Moreau, and O. A. Silva, "Validation of a method to detect cocaine and its metabolites in nails by gas chromatography–mass spectrometry," *Forensic Sci. Int.*, vol. 159, no. 2–3, pp.

218–222, Jun. 2006.

[72] “R. Noll, Laser-Induced breakdown spectroscopy, Springer-Verlag, 2012.”

[73] V. K. Singh and A. K. Rai, “Prospects for laser-induced breakdown spectroscopy for biomedical applications: a review,” *Lasers Med. Sci.*, vol. 26, no. 5, pp. 673–687, Sep. 2011.

[74] M. Bahreini, Z. Hosseinimakarem, and S. Hassan Tavassoli, “A study of association between fingernail elements and osteoporosis by laser-induced breakdown spectroscopy,” *J. Appl. Phys.*, vol. 112, no. 5, p. 54701, Sep. 2012.

[75] M. Bahreini, B. Ashrafkhani, and S. H. Tavassoli, “Discrimination of patients with diabetes mellitus and healthy subjects based on laser-induced breakdown spectroscopy of their fingernails,” *J. Biomed. Opt.*, vol. 18, no. 10, p. 107006, Oct. 2013.

[76] A. O. Mehder *et al.*, “Direct spectral analysis and determination of high content of carcinogenic bromine in bread using UV pulsed laser induced breakdown spectroscopy,” *J. Environ. Sci. Heal. Part B*, vol. 51, no. 6, pp. 358–365, Jun. 2016.

[77] Q. Godoi *et al.*, “Laser-induced breakdown spectroscopy and chemometrics for classification of toys relying on toxic elements,” *Spectrochim. Acta Part B At. Spectrosc.*, vol. 66, no. 2, pp. 138–143, Feb. 2011.

[78] E. C. Ferreira, E. a. Menezes, W. O. Matos, D. M. B. P. Milori, A. R. a Nogueira, and L. Martin-Neto, “Determination of Ca in breakfast cereals by laser induced

breakdown spectroscopy," *Food Control*, vol. 21, no. 10, pp. 1327–1330, 2010.

[79] D. A. Cremers and L. J. Radziemski, *Handbook of Laser-Induced Breakdown Spectroscopy*. John Wiley & Sons, 2013.

[80] W. Demtröder, *Laser Spectroscopy 2*. Berlin, Heidelberg: Springer Berlin Heidelberg, 2015.

[81] W. Demtröder, *Laser Spectroscopy 1: Basic Principles*. Springer, 2014.

[82] "D. E. Kim, K. J. Yoo, H. K. Park, K. J. Oh, and D. W. Kim, 'Quantitative Analysis of Aluminum Impurities in Zinc Alloy by Laser-Induced Breakdown Spectroscopy,' Appl. Spectrosc. 51, 22-29 (1997)."

[83] "X. Hou and B. T. Jones, 'Inductively Coupled Plasma / Optical Emission Spectrometry,' pp. 9468–9485, 2000."

[84] M. A. Gondal, T. Hussain, Z. H. Yamani, and M. A. Baig, "The role of various binding materials for trace elemental analysis of powder samples using laser-induced breakdown spectroscopy," *Talanta*, vol. 72, no. 2, pp. 642–649, 2007.

[85] T. O. Owolabi, K. O. Akande, and S. O. Olatunji, "Estimation of Superconducting Transition Temperature T C for Superconductors of the Doped MgB2 System from the Crystal Lattice Parameters Using Support Vector Regression," *J. Supercond. Nov. Magn.*, Nov. 2014.

[86] "A. Ciucci, M. Corsi, V. Palleschi, S. Rastelli, A. Salvetti, and E. Tognoni, 'New Procedure for Quantitative Elemental Analysis by Laser-Induced Plasma Spectroscopy,' Appl. Spectrosc. 53, 960-964 (1999)."

[87] P. Pohl, E. Stelmach, M. Welna, and A. Szymczycha-madeja, “Determination of the Elemental Composition of Coffee Using Instrumental Methods,” pp. 598–613, 2013.

[88] D. S. Thelle and E. Strandhagen, “Coffee and disease: An overview with main emphasis on blood lipids and homocysteine,” *Scand. J. Nutr.*, vol. 49, no. 2, pp. 50–61, 2005.

[89] “M. E. Gillies and J. A. Birkbeck, ‘Tea and Coffee As Sources of Some Minerals in the New-Zealand Diet,’ Am. J. Clin. Nutr., vol. 38, no. 6, pp. 936–942, 1983.”

[90] J. V Higdon and B. Frei, “Coffee and health: a review of recent human research,” *Crit Rev Food Sci Nutr*, vol. 46, no. 2, pp. 101–123, 2006.

[91] B. Mehari, M. Redi-Abshiro, B. S. Chandravanshi, S. Combrinck, and R. McCrindle, “Characterization of the Cultivation Region of Ethiopian Coffee by Elemental Analysis,” *Anal. Lett.*, vol. 2719, no. March 2017, p. 00032719.2016.1151023, 2016.

[92] U. Thissen, M. Pepers, B. Üstün, W. J. Melssen, and L. M. C. Buydens, “Comparing support vector machines to PLS for spectral regression applications,” *Chemom. Intell. Lab. Syst.*, vol. 73, no. 2, pp. 169–179, Oct. 2004.

[93] I. Barman, C.-R. Kong, N. C. Dingari, R. R. Dasari, and M. S. Feld, “Development of Robust Calibration Models Using Support Vector Machines for Spectroscopic Monitoring of Blood Glucose,” *Anal. Chem.*, vol. 82, no. 23, pp. 9719–9726, 2010.

[94] U. Thissen, B. Ustün, W. J. Melssen, and L. M. C. Buydens, “Multivariate

calibration with least-squares support vector machines.," *Anal. Chem.*, vol. 76, no. 11, pp. 3099–3105, 2004.

[95] E. Rashedi, H. Nezamabadi-pour, and S. Saryazdi, "GSA: A Gravitational Search Algorithm," *Inf. Sci. (Ny).*, vol. 179, no. 13, pp. 2232–2248, 2009.

[96] "http://www.lenntech.com/who-eu-water-standards.htm." .

[97] M. A. Gondal, M. A. Dastageer, A. A. Naqvi, A. A. Isab, and Y. W. Maganda, "Detection of toxic metals (lead and chromium) in talcum powder using laser induced breakdown spectroscopy," vol. 51, no. 30, pp. 7395–7401, 2012.

[98] J. E. Sansonetti, "Wavelengths, transition probabilities, and energy levels for the spectra of sodium (Na I-Na XI)," *J. Phys. Chem. Ref. Data*, vol. 37, no. 4, pp. 1659–1763, 2008.

[99] D. E. Kelleher and L. I. Podobedova, "Atomic transition probabilities of sodium and magnesium. A critical compilation," *J. Phys. Chem. Ref. Data*, vol. 37, no. 1, pp. 267–706, 2008.

[100] A. M. Alhasmi, M. A. Gondal, M. M. Nasr, S. Shafik, and Y. B. Habibullah, "Detection of toxic elements using laser-induced breakdown spectroscopy in smokers' and nonsmokers' teeth and investigation of periodontal parameters.," *Appl. Opt.*, vol. 54, no. 24, pp. 7342–9, 2015.

[101] M. M. Center, A. Jemal, R. A. Smith, and E. Ward, "Worldwide Variations in Colorectal Cancer," *CA. Cancer J. Clin.*, vol. 59, no. 6, pp. 366–378, Nov. 2009.

[102] W. J. Lee, D. P. Sandler, A. Blair, C. Samanic, A. J. Cross, and M. C. R. Alavanja,

"Pesticide use and colorectal cancer risk in the agricultural health study," *Int. J. Cancer*, vol. 121, no. 2, pp. 339–346, Jul. 2007.

[103] U. Majewska, D. Banaś, J. Braziewicz, S. Góźdź, A. Kubala-Kukuś, and M. Kucharzewski, "Trace element concentration distributions in breast, lung and colon tissues," *Phys. Med. Biol.*, vol. 52, no. 13, pp. 3895–3911, Jul. 2007.

[104] J. M. Lutz, "Cancer prevalence in Central Europe: the EUROPREVAL Study," *Ann. Oncol.*, vol. 14, no. 2, pp. 313–322, Feb. 2003.

[105] D.-C. A. Blaszczyk U., "Magnesium: its role in nutrition and carcinogenesis," *Języki Publ.*, 2013.

[106] M. H. Farhat, A. I. Shamseddine, and K. A. Barada, "Small Bowel Tumors: Clinical Presentation, Prognosis, and Outcome in 33 Patients in a Tertiary Care Center," *J. Oncol.*, vol. 2008, pp. 1–5, 2008.

[107] M. Klimczak, A. Dziki, A. Kilanowicz, A. Sapota, J. Duda-Szymańska, and A. Daragó, "Concentrations of cadmium and selected essential elements in malignant large intestine tissue," *Gastroenterol. Rev.*, vol. 1, pp. 24–29, 2016.

[108] "Trace Element Levels in Blood Serum and Colon Tissue in Colorectal Cancer."

[109] B. Bocca *et al.*, "Determination of 30 elements in colorectal biopsies by sector field inductively coupled plasma mass spectrometry: method development and preliminary baseline levels," *Rapid Commun. Mass Spectrom.*, vol. 21, no. 11, pp. 1776–1782, Jun. 2007.

[110] M. A. Gondal, Y. W. Maganda, M. A. Dastageer, F. F. Al Adel, A. A. Naqvi, and

T. F. Qahtan, “Detection of the level of fluoride in the commercially available toothpaste using laser induced breakdown spectroscopy with the marker atomic transition line of neutral fluorine at 731.1nm,” *Opt. Laser Technol.*, vol. 57, pp. 32–38, Apr. 2014.

[111] A. Portnov, S. Rosenwaks, and I. Bar, “Emission following laser-induced breakdown spectroscopy of organic compounds in ambient air,” *Appl. Opt.*, vol. 42, no. 15, p. 2835, May 2003.

[112] R. Barbini *et al.*, “Semi-quantitative time resolved LIBS measurements,” *Appl. Phys. B Lasers Opt.*, vol. 65, no. 1, pp. 101–107, Jul. 1997.

[113] V. Juvé, R. Portelli, M. Boueri, M. Baudelet, and J. Yu, “Space-resolved analysis of trace elements in fresh vegetables using ultraviolet nanosecond laser-induced breakdown spectroscopy,” *Spectrochim. Acta - Part B At. Spectrosc.*, vol. 63, no. 10, pp. 1047–1053, 2008.

[114] S. Pandhija, N. K. Rai, A. K. Rai, and S. N. Thakur, “Contaminant concentration in environmental samples using LIBS and CF-LIBS,” *Appl. Phys. B*, vol. 98, no. 1, pp. 231–241, Jan. 2010.

[115] M. Corsi *et al.*, “Application of laser-induced breakdown spectroscopy technique to hair tissue mineral analysis,” *Appl. Opt.*, vol. 42, no. 30, p. 6133, Oct. 2003.

[116] G. S. Senesi *et al.*, “Heavy metal concentrations in soils as determined by laser-induced breakdown spectroscopy (LIBS), with special emphasis on chromium,” *Environ. Res.*, vol. 109, no. 4, pp. 413–420, May 2009.

Appendix

Code for CF-LIBS

```
%%Conventional CF-LIBS

%% this loads data from excell. the excell should As inside the file

format long

Al=xlsread('coloncancerdata.xlsx',1);

Sb=xlsread('coloncancerdata.xlsx',2);

Ba=xlsread('coloncancerdata.xlsx',3);

Be=xlsread('coloncancerdata.xlsx',4);

Cd=xlsread('coloncancerdata.xlsx',5);

Ca=xlsread('coloncancerdata.xlsx',6);

Cr=xlsread('coloncancerdata.xlsx',7);

Co=xlsread('coloncancerdata.xlsx',8);

Cu=xlsread('coloncancerdata.xlsx',9);

Fe=xlsread('coloncancerdata.xlsx',10);

Pb=xlsread('coloncancerdata.xlsx',11);
```

```
Li=xlsread('coloncancerdata.xlsx',12);

Mg=xlsread('coloncancerdata.xlsx',13);

Mn=xlsread('coloncancerdata.xlsx',14);

Mo=xlsread('coloncancerdata.xlsx',15);

Ni=xlsread('coloncancerdata.xlsx',16);

K=xlsread('coloncancerdata.xlsx',17);

Ag=xlsread('coloncancerdata.xlsx',18);

Na=xlsread('coloncancerdata.xlsx',19);

Sr=xlsread('coloncancerdata.xlsx',20);

Sn=xlsread('coloncancerdata.xlsx',21);

Ti=xlsread('coloncancerdata.xlsx',22);

V=xlsread('coloncancerdata.xlsx',23);

Zn=xlsread('coloncancerdata.xlsx',24);

%%%%%%%%%%%%%%%%%%%%%%%%%%%%%%%%%%%%

%%%%%%%%%%%%%%%%%%%%%%%%%%%%%%%%%%%%

Al2=xlsread('coloncancerdata2.xlsx',1);

Sb2=xlsread('coloncancerdata2.xlsx',2);
```

```
Ba2=xlsread('coloncancerdata2.xlsx',3);

Be2=xlsread('coloncancerdata2.xlsx',4);

Cd2=xlsread('coloncancerdata2.xlsx',5);

Ca2=xlsread('coloncancerdata2.xlsx',6);

Cr2=xlsread('coloncancerdata2.xlsx',7);

Co2=xlsread('coloncancerdata2.xlsx',8);

Cu2=xlsread('coloncancerdata2.xlsx',9);

Fe2=xlsread('coloncancerdata2.xlsx',10);

Pb2=xlsread('coloncancerdata2.xlsx',11);

Li2=xlsread('coloncancerdata2.xlsx',12);

Mg2=xlsread('coloncancerdata2.xlsx',13);

Mn2=xlsread('coloncancerdata2.xlsx',14);

Mo2=xlsread('coloncancerdata2.xlsx',15);

Ni2=xlsread('coloncancerdata2.xlsx',16);

K2=xlsread('coloncancerdata2.xlsx',17);

Ag2=xlsread('coloncancerdata2.xlsx',18);

Na2=xlsread('coloncancerdata2.xlsx',19);
```

```
Sr2=xlsread('coloncancerdata2.xlsx',20);

Sn2=xlsread('coloncancerdata2.xlsx',21);

Ti2=xlsread('coloncancerdata2.xlsx',22);

V2=xlsread('coloncancerdata2.xlsx',23);

Zn2=xlsread('coloncancerdata2.xlsx',24);

%%



%%

[
normAl2izedfunmuhsin,concnt_Al2,concnt_Sb2,concnt_Ba2,concnt_Be2,concnt_Cd2,co
ncnt_Ca2,concnt_Cr2,concnt_Co2,concnt_Cu2,concnt_Fe2,concnt_Pb2,concnt_Li2,conc
nt_Mg2,concnt_Mn2,concnt_Mo2,concnt_Ni2,concnt_K2,concnt_Ag2,concnt_Na2,conc
nt_Sr2,concnt_Sn2,concnt_Ti2,concnt_V2,concnt_Zn2]
=singlycancercolon(Al2,Sb2,Ba2,Be2,Cd2,Ca2,Cr2,Co2,Cu2,Fe2,Pb2,Li2,Mg2,Mn2,Mo
2,Ni2,K2,Ag2,Na2,Sr2,Sn2,Ti2,V2,Zn2)



%%%%%%%%%%%%%%%%%%%%%%%%%%%%%%%%%%%%

%%

%%%%%% This evalute the procedures for the classical CF-LIBS for muhsin
```

```
%%%%%% sample  co cu fe mn ni sisnzn

%%

%% for  Aluminium

%% Neutral

denpro_Al= (Al(:,2).* Al(:,4)).*10^8;

indenpro_Al= Al(:,6)./denpro_Al;

y_Al= log(indenpro_Al);

x_Al=(Al(:,3)./8100);

%figure(1)

%plot(x_Al,y_Al,'ro');

[r_Al,m_Al,b_Al]=regression(x_Al,y_Al,'one');

K_b=8.625E-5;

plas_TemAl=-(1/(m_Al*K_b));

patfun_Al= sum(Al(:,4).*exp(-Al(:,3)./8100)./(K_b.*plas_TemAl));

concnt_Al=patfun_Al.*exp(b_Al);

% % %% singly

% denpro_Al_II= (Al(:,9).* Al(:,11)).*10^8;
```

```
% indenpro_Al_II= Al(:,13)./denpro_Al_II;

% y_Al_II= log(indenpro_Al_II);

% x_Al_II=(Al(:,10)./8100);

% %figure(1)

% %plot(x_Al,y_Al,'ro');

% [r_Al_II,m_Al_II,b_Al_II]=regression(x_Al_II,y_Al_II,'one');

% K_b=8.625E-5;

% plas_TemAl_II=-(1/(m_Al_II*K_b));

% patfun_Al_II= sum(Al(:,11).*exp(-Al(:,10)./8100)./(K_b.*plas_TemAl_II));

% concnt_Al_II=patfun_Al_II.*exp(b_Al_II);



%% Sb

%% Neutral

denpro_Sb= (Sb(:,2).* Sb(:,4)).*10^8;

indenpro_Sb= Sb(:,6)./denpro_Sb;

y_Sb= log(indenpro_Sb);

x_Sb=(Sb(:,3)./8100);
```

```
%figure(1)

%plot(x_Al,y_Al,'ro');

[r_Sb,m_Sb,b_Sb]=regression(x_Sb,y_Sb,'one');

K_b=8.625E-5;

plas_TemSb=-(1/(m_Sb*K_b));

patfun_Sb= sum(Sb(:,4).*exp(-Sb(:,3)./8100)./(K_b.*plas_TemSb));

concnt_Sb=patfun_Sb.*exp(b_Sb);

%%  Barium

%% Neutral

denpro_Ba= (Ba(:,2).* Ba(:,4)).*10^8;

indenpro_Ba= Ba(:,6)./denpro_Ba;

y_Ba= log(indenpro_Ba);

x_Ba=(Ba(:,3)./8100);

%figure(1)

%plot(x_Al,y_Al,'ro');

[r_Ba,m_Ba,b_Ba]=regression(x_Ba,y_Ba,'one');

K_b=8.625E-5;
```

```
plas_TemBa=(1/(m_Ba*K_b));

patfun_Ba= sum(Ba(:,4).*exp(-Ba(:,3)./8100)./(K_b.*plas_TemBa));

concnt_Ba=patfun_Ba.*exp(b_Ba);



%%

%%  Be

%% Neutral

denpro_Be= (Be(:,2).* Be(:,4)).*10^8;

indenpro_Be= Be(:,6)./denpro_Be;

y_Be= log(indenpro_Be);

x_Be=(Be(:,3)./8100);

%figure(1)

%plot(x_Al,y_Al,'ro');

[r_Be,m_Be,b_Be]=regression(x_Be,y_Be,'one');

K_b=8.625E-5;

plas_TemBe=-(1/(m_Be*K_b));

patfun_Be= sum(Be(:,4).*exp(-Be(:,3)./8100)./(K_b.*plas_TemBe));
```

```
concnt_Be=patfun_Be.*exp(b_Be);

%%  Cd

%% Neutral

denpro_Cd= (Cd(:,2).* Cd(:,4)).*10^8;

indenpro_Cd= Cd(:,6)./denpro_Cd;

y_Cd= log(indenpro_Cd);

x_Cd=(Cd(:,3)./8100);

%figure(1)

%plot(x_Al,y_Al,'ro');

[r_Cd,m_Cd,b_Cd]=regression(x_Cd,y_Cd,'one');

K_b=8.625E-5;

plas_TemCd=(1/(m_Cd*K_b));

patfun_Cd= sum(Cd(:,4).*exp(-Cd(:,3)./8100)./(K_b.*plas_TemCd));

concnt_Cd=patfun_Cd.*exp(b_Cd);

%%%

%%  for Ca

denpro_Ca= (Ca(:,2).* Ca(:,4)).*10^8;
```

```
indenpro_Ca= Ca(:,6)./denpro_Ca;

y_Ca= log(indenpro_Ca);

x_Ca=(Ca(:,3)./8100);

%figure(1)

%plot(x_Al,y_Al,'ro');

[r_Ca,m_Ca,b_Ca]=regression(x_Ca,y_Ca,'one');

K_b=8.625E-5;

plas_TemCa=(1/(m_Ca*K_b));

patfun_Ca= sum(Ca(:,4).*exp(-Ca(:,3)./8100)./(K_b.*plas_TemCa));

concnt_Ca=patfun_Ca.*exp(b_Ca);



%%  for Cr

denpro_Cr= (Cr(:,2).* Cr(:,4)).*10^8;

indenpro_Cr= Cr(:,6)./denpro_Cr;

y_Cr= log(indenpro_Cr);

x_Cr=(Cr(:,3)./8100);

%figure(1)
```

```
%plot(x_Al,y_Al,'ro');

[r_Cr,m_Cr,b_Cr]=regression(x_Cr,y_Cr,'one');

K_b=8.625E-5;

plas_TemCr=-(1/(m_Cr*K_b));

patfun_Cr= sum(Cr(:,4).*exp(-Cr(:,3)./8100)./(K_b.*plas_TemCr));

concnt_Cr=patfun_Cr.*exp(b_Cr);

%%

%%  for Cobalt

denpro_Co= (Co(:,2).* Co(:,4)).*10^8;

indenpro_Co= Co(:,6)./denpro_Co;

y_Co= log(indenpro_Co);

x_Co=(Co(:,3)./8100);

%figure(1)

%plot(x_Al,y_Al,'ro');

[r_Co,m_Co,b_Co]=regression(x_Co,y_Co,'one');

K_b=8.625E-5;

plas_TemCo=-(1/(m_Co*K_b));
```

```
patfun_Co= sum(Co(:,4).*exp(-Co(:,3)./8100)./(K_b.*plas_TemCo));

concnt_Co=patfun_Co.*exp(b_Co);

%%

%%  for Copper

denpro_Cu= (Cu(:,2).* Cu(:,4)).*10^8;

indenpro_Cu= Cu(:,6)./denpro_Cu;

y_Cu= log(indenpro_Cu);

x_Cu=(Cu(:,3)./8100);

%figure(1)

%plot(x_Al,y_Al,'ro');

[r_Cu,m_Cu,b_Cu]=regression(x_Cu,y_Cu,'one');

K_b=8.625E-5;

plas_TemCu=-(1/(m_Cu*K_b));

patfun_Cu= sum(Cu(:,4).*exp(-Cu(:,3)./8100)./(K_b.*plas_TemCu));

concnt_Cu=patfun_Cu.*exp(b_Cu);

 %%  for Iron

 %% neutral
```

```
denpro_Fe= (Fe(:,2).* Fe(:,4)).*10^8;

indenpro_Fe= Fe(:,6)./denpro_Fe;

y_Fe= log(indenpro_Fe);

x_Fe=(Fe(:,3)./8100);

%figure(1)

%plot(x_Al,y_Al,'ro');

[r_Fe,m_Fe,b_Fe]=regression(x_Fe,y_Fe,'one');

K_b=8.625E-5;

plas_TemFe=-(1/(m_Fe*K_b));

patfun_Fe= sum(Fe(:,4).*exp(-Fe(:,3)./8100)./(K_b.*plas_TemFe));

concnt_Fe=patfun_Fe.*exp(b_Fe);

%%  for Lead

denpro_Pb= (Pb(:,2).* Pb(:,4)).*10^8;

indenpro_Pb= Pb(:,6)./denpro_Pb;

y_Pb= log(indenpro_Pb);

x_Pb=(Pb(:,3)./8100);

%figure(1)
```

```
%plot(x_Al,y_Al,'ro');

[r_Pb,m_Pb,b_Pb]=regression(x_Pb,y_Pb,'one');

K_b=8.625E-5;

plas_TemPb=(1/(m_Pb*K_b));

patfun_Pb= sum(Pb(:,4).*exp(-Pb(:,3)./8100)./(K_b.*plas_TemPb));

concnt_Pb=patfun_Pb.*exp(b_Pb);



%%  for Lithium

denpro_Li= (Li(:,2).* Li(:,4)).*10^8;

indenpro_Li= Li(:,6)./denpro_Li;

y_Li= log(indenpro_Li);

x_Li=(Li(:,3)./8100);

%figure(1)

%plot(x_Al,y_Al,'ro');

[r_Li,m_Li,b_Li]=regression(x_Li,y_Li,'one');

K_b=8.625E-5;

plas_TemLi=-(1/(m_Li*K_b));
```

```
patfun_Li= sum(Li(:,4).*exp(-Li(:,3)./8100)./(K_b.*plas_TemLi));

concnt_Li=patfun_Li.*exp(b_Li);

%%%

 %%  for Mg

denpro_Mg= (Mg(:,2).* Mg(:,4)).*10^8;

indenpro_Mg= Mg(:,6)./denpro_Mg;

y_Mg= log(indenpro_Mg);

x_Mg=(Mg(:,3)./8100);

%figure(1)

%plot(x_Al,y_Al,'ro');

[r_Mg,m_Mg,b_Mg]=regression(x_Mg,y_Mg,'one');

K_b=8.625E-5;

plas_TemMg=-(1/(m_Mg*K_b));

patfun_Mg= sum(Mg(:,4).*exp(-Mg(:,3)./8100)./(K_b.*plas_TemMg));

concnt_Mg=patfun_Mg.*exp(b_Mg);

 %%  for manganise

denpro_Mn= (Mn(:,2).* Mn(:,4)).*10^8;
```

```
indenpro_Mn= Mn(:,6)./denpro_Mn;

y_Mn= log(indenpro_Mn);

x_Mn=(Mn(:,3)./8100);

%figure(1)

%plot(x_Al,y_Al,'ro');

[r_Mn,m_Mn,b_Mn]=regression(x_Mn,y_Mn,'one');

K_b=8.625E-5;

plas_TemMn=-(1/(m_Mn*K_b));

patfun_Mn= sum(Mn(:,4).*exp(-Mn(:,3)./8100)./(K_b.*plas_TemMn));

concnt_Mn=patfun_Mn.*exp(b_Mn);

 %%  for Mo

denpro_Mo= (Mo(:,2).* Mo(:,4)).*10^8;

indenpro_Mo= Mo(:,6)./denpro_Mo;

y_Mo= log(indenpro_Mo);

x_Mo=(Mo(:,3)./8100);

%figure(1)

%plot(x_Al,y_Al,'ro');
```

```
[r_Mo,m_Mo,b_Mo]=regression(x_Mo,y_Mo,'one');

K_b=8.625E-5;

plas_TemMo=-(1/(m_Mo*K_b));

patfun_Mo= sum(Mo(:,4).*exp(-Mo(:,3)./8100)./(K_b.*plas_TemMo));

concnt_Mo=patfun_Mo.*exp(b_Mo);

%%  for nickel

denpro_Ni= (Ni(:,2).* Ni(:,4)).*10^8;

indenpro_Ni= Ni(:,6)./denpro_Ni;

y_Ni= log(indenpro_Ni);

x_Ni=(Ni(:,3)./8100);

%figure(1)

%plot(x_Al,y_Al,'ro');

[r_Ni,m_Ni,b_Ni]=regression(x_Ni,y_Ni,'one');

K_b=8.625E-5;

plas_TemNi=-(1/(m_Ni*K_b));

patfun_Ni= sum(Ni(:,4).*exp(-Ni(:,3)./8100)./(K_b.*plas_TemNi));

concnt_Ni=patfun_Ni.*exp(b_Ni);
```

```
%%  for K

denpro_K= (K(:,2).* K(:,4)).*10^8;

indenpro_K= K(:,6)./denpro_K;

y_K= log(indenpro_K);

x_K=(K(:,3)./8100);

%figure(1)

%plot(x_Al,y_Al,'ro');

[r_K,m_K,b_K]=regression(x_K,y_K,'one');

K_b=8.625E-5;

plas_TemK=(1/(m_K*K_b));

patfun_K= sum(K(:,4).*exp(-K(:,3)./8100)./(K_b.*plas_TemK));

concnt_K=patfun_K.*exp(b_K);

%%  for Ag

denpro_Ag= (Ag(:,2).* Ag(:,4)).*10^8;

indenpro_Ag= Ag(:,6)./denpro_Ag;

y_Ag= log(indenpro_Ag);

x_Ag=(Ag(:,3)./8100);
```

```
%figure(1)

%plot(x_Al,y_Al,'ro');

[r_Ag,m_Ag,b_Ag]=regression(x_Ag,y_Ag,'one');

K_b=8.625E-5;

plas_TemAg=-(1/(m_Ag*K_b));

patfun_Ag= sum((Ag(:,4).*exp(-Ag(:,3)./8100))./(K_b.*plas_TemAg));

AA=sum(Ag(:,4).*exp(-Ag(:,3)./8100));

concnt_Ag=patfun_Ag.*exp(b_Ag);

%%

%%  for Na

denpro_Na= (Na(:,2).* Na(:,4)).*10^8;

indenpro_Na= Na(:,6)./denpro_Na;

y_Na= log(indenpro_Na);

x_Na=(Na(:,3)./8100);

%figure(1)

%plot(x_Al,y_Al,'ro');

[r_Na,m_Na,b_Na]=regression(x_Na,y_Na,'one');
```

```
K_b=8.625E-5;

plas_TemNa=(1/(m_Na*K_b));

patfun_Na= sum(Na(:,4).*exp(-Na(:,3)./8100)./(K_b.*plas_TemNa));

concnt_Na=patfun_Na.*exp(b_Na);

%%  for Sr

denpro_Sr= (Sr(:,2).* Sr(:,4)).*10^8;

indenpro_Sr= Sr(:,6)./denpro_Sr;

y_Sr= log(indenpro_K);

x_Sr=(Sr(:,3)./8100);

%figure(1)

%plot(x_Al,y_Al,'ro');

[r_Sr,m_Sr,b_Sr]=regression(x_Sr,y_Sr,'one');

K_b=8.625E-5;

plas_TemSr=(1/(m_Sr*K_b));

patfun_Sr= sum(Sr(:,4).*exp(-Sr(:,3)./8100)./(K_b.*plas_TemSr));

concnt_Sr=patfun_Sr.*exp(b_Sr);

%%  for Sn
```

```
denpro_Sn= (Sn(:,2).* Sn(:,4)).*10^8;

indenpro_Sn= Sn(:,6)./denpro_Sn;

y_Sn= log(indenpro_Sn);

x_Sn=(Sn(:,3)./8100);

%figure(1)

%plot(x_Al,y_Al,'ro');

[r_Sn,m_Sn,b_Sn]=regression(x_Sn,y_Sn,'one');

K_b=8.625E-5;

plas_TemSn=-(1/(m_Sn*K_b));

patfun_Sn= sum((Sn(:,4).*exp(-Sn(:,3)./8100))./(K_b.*plas_TemSn));

%AA=sum(Sn(:,4).*exp(-Sn(:,3)./8100));

concnt_Sn=patfun_Sn.*exp(b_Sn);

%%  for Ti

denpro_Ti= (Ti(:,2).* Ti(:,4)).*10^8;

indenpro_Ti= Ti(:,6)./denpro_Ti;

y_Ti= log(indenpro_Ti);

x_Ti=(Ti(:,3)./8100);
```

```
%figure(1)

%plot(x_Al,y_Al,'ro');

[r_Ti,m_Ti,b_Ti]=regression(x_Ti,y_Ti,'one');

K_b=8.625E-5;

plas_TemTi=-(1/(m_Ti*K_b));

patfun_Ti= sum(Ti(:,4).*exp(-Ti(:,3)./8100)./(K_b.*plas_TemTi));

concnt_Ti=patfun_Ti.*exp(b_Ti);

%%  for V

denpro_V= (V(:,2).* V(:,4)).*10^8;

indenpro_V= V(:,6)./denpro_V;

y_V= log(indenpro_V);

x_V=(V(:,3)./8100);

%figure(1)

%plot(x_Al,y_Al,'ro');

[r_V,m_V,b_V]=regression(x_V,y_V,'one');

K_b=8.625E-5;

plas_TemV=-(1/(m_V*K_b));
```

```
patfun_V= sum(V(:,4).*exp(-V(:,3)./8100)./(K_b.*plas_TemV));

concnt_V=patfun_V.*exp(b_V);

%%  for Zn

denpro_Zn= (Zn(:,2).* Zn(:,4)).*10^8;

indenpro_Zn= Zn(:,6)./denpro_Zn;

y_Zn= log(indenpro_Zn);

x_Zn=(Zn(:,3)./8100);

%figure(1)

%plot(x_Al,y_Al,'ro');

[r_Zn,m_Zn,b_Zn]=regression(x_Zn,y_Zn,'one');

K_b=8.625E-5;

plas_TemZn=-(1/(m_Zn*K_b));

patfun_Zn= sum((Zn(:,4).*exp(-Zn(:,3)./8100))./(K_b.*plas_TemZn));

%AA=sum(Zn(:,4).*exp(-Zn(:,3)./8100));

concnt_Zn=patfun_Zn.*exp(b_Zn);

%%


normalizedfunmuhsin=concnt_Al+concnt_Sb+concnt_Ba+concnt_Be+concnt_Cd+concn
```

```
t_Ca+concnt_Cr+concnt_Co+concnt_Cu+concnt_Co+concnt_Fe+concnt_Pb+concnt_Li
+concnt_Mg+concnt_Mn+concnt_Mo+concnt_Ni+concnt_K+concnt_Ag+concnt_Na+co
ncnt_Sr+concnt_Sn+concnt_Ti+concnt_V+concnt_Zn;


 %%

 [
normAl2izedfunmuhsin,concnt_Al2,concnt_Sb2,concnt_Ba2,concnt_Be2,concnt_Cd2,co
ncnt_Ca2,concnt_Cr2,concnt_Co2,concnt_Cu2,concnt_Fe2,concnt_Pb2,concnt_Li2,conc
nt_Mg2,concnt_Mn2,concnt_Mo2,concnt_Ni2,concnt_K2,concnt_Ag2,concnt_Na2,conc
nt_Sr2,concnt_Sn2,concnt_Ti2,concnt_V2,concnt_Zn2]
=singlyhealthycolon(Al2,Sb2,Ba2,Be2,Cd2,Ca2,Cr2,Co2,Cu2,Fe2,Pb2,Li2,Mg2,Mn2,M
o2,Ni2,K2,Ag2,Na2,Sr2,Sn2,Ti2,V2,Zn2)


 ovearllnormalization=normalizedfunmuhsin+normAl2izedfunmuhsin;

 %%

 concnt_percAl=(concnt_Al./ovearllnormalization);

 concnt_percSb=(concnt_Sb./ovearllnormalization);

 concnt_percBa=(concnt_Ba./ovearllnormalization);

 concnt_percBe=(concnt_Be./ovearllnormalization);
```

```
concnt_percCd=(concnt_Cd./ovearllnormalization);

concnt_percCa=(concnt_Ca./ovearllnormalization);

concnt_percCr=(concnt_Cr./ovearllnormalization);

concnt_percCo=(concnt_Co./ovearllnormalization);

concnt_percCu=(concnt_Cu./ovearllnormalization);

concnt_percFe=(concnt_Fe./ovearllnormalization);

concnt_percPb=(concnt_Pb./ovearllnormalization);

concnt_percLi=(concnt_Li./ovearllnormalization);

concnt_percMg=(concnt_Mg./ovearllnormalization);

concnt_percMn=(concnt_Mn./ovearllnormalization);

concnt_percMo=(concnt_Mo./ovearllnormalization);

concnt_percNi=(concnt_Ni./ovearllnormalization);

concnt_percK=(concnt_K./ovearllnormalization);

concnt_percAg=(concnt_Ag./ovearllnormalization);

concnt_percNa=(concnt_Na./ovearllnormalization);

concnt_percSr=(concnt_Sr./ovearllnormalization);

concnt_percSn=(concnt_Sn./ovearllnormalization);
```

```
concnt_percTi=(concnt_Ti./ovearllnormalization);

concnt_percV=(concnt_V./ovearllnormalization);

concnt_percZn=(concnt_Zn./ovearllnormalization);

%%


concnt_percAl2=(concnt_Al2./ovearllnormalization);

concnt_percSb2=(concnt_Sb2./ovearllnormalization);

concnt_percBa2=(concnt_Ba2./ovearllnormalization);

concnt_percBe2=(concnt_Be2./ovearllnormalization);

concnt_percCd2=(concnt_Cd2./ovearllnormalization);

concnt_percCa2=(concnt_Ca2./ovearllnormalization);

concnt_percCr2=(concnt_Cr2./ovearllnormalization);

concnt_percCo2=(concnt_Co2./ovearllnormalization);

concnt_percCu2=(concnt_Cu2./ovearllnormalization);

concnt_percFe2=(concnt_Fe2./ovearllnormalization);

concnt_percPb2=(concnt_Pb2./ovearllnormalization);

concnt_percLi2=(concnt_Li2./ovearllnormalization);
```

```
concnt_percMg2=(concnt_Mg2./ovearllnormalization);

concnt_percMn2=(concnt_Mn2./ovearllnormalization);

concnt_percMo2=(concnt_Mo2./ovearllnormalization);

concnt_percNi2=(concnt_Ni2./ovearllnormalization);

concnt_percK2=(concnt_K2./ovearllnormalization);

concnt_percAg2=(concnt_Ag2./ovearllnormalization);

concnt_percNa2=(concnt_Na2./ovearllnormalization);

concnt_percSr2=(concnt_Sr2./ovearllnormalization);

concnt_percSn2=(concnt_Sn2./ovearllnormalization);

concnt_percTi2=(concnt_Ti2./ovearllnormalization);

concnt_percV2=(concnt_V2./ovearllnormalization);

concnt_percZn2=(concnt_Zn2./ovearllnormalization);

%%

%%%%%%

concnt_allAl=(concnt_percAl+concnt_percAl2)*10^10; %Al %the power is to convert from wt% to ppb

concnt_allSb=((concnt_percSb+concnt_percSb2)/2)*10^6;%Sb  % the division is to cater for element that have  no data for singly ionised species. same data was used in both cases
```

```
concnt_allBa=(concnt_percBa+concnt_percBa2)*10^9; %Ba

concnt_allBe=(concnt_percBe+concnt_percBe2)*10^12; %Be

concnt_allCd=(concnt_percCd+concnt_percCd2)*10^11; %Cd

concnt_allCa=(concnt_percCa+concnt_percCa2)*10^11;%Ca

concnt_allCr=(concnt_percCr+concnt_percCr2)*10^7;%Cr

concnt_allCo=(concnt_percCo+concnt_percCo2)*10^5; %Co

concnt_allCu=(concnt_percCu+concnt_percCu2)*10^9;%Cu

concnt_allFe=(concnt_percFe+concnt_percFe2)*10^6; %Fe

concnt_allPb=((concnt_percPb+concnt_percPb2)/2)*10^11; %Pb

concnt_allLi=(concnt_percLi+concnt_percLi2)*10^8;%Li

concnt_allMg=(concnt_percMg+concnt_percMg2)*10^10; %Mg

concnt_allMn=(concnt_percMn+concnt_percMn2)*10^10; %Mn

concnt_allMo=(concnt_percMo+concnt_percMo2)*10^2; %Mo

concnt_allNi=(concnt_percNi+concnt_percNi2)*10^8;%Ni

concnt_allK=((concnt_percK+concnt_percK2)/2)*10^12;%K

concnt_allAg=((concnt_percAg+concnt_percAg2)/2)*10^12;%Ag

concnt_allNa=(concnt_percNa+concnt_percNa2)*10^11; %Na
```

```
concnt_allSr=(concnt_percSr+concnt_percSr2)*10^9;%Sr

concnt_allSn=(concnt_percSn+concnt_percSn2)*10^8; %Sn

concnt_allTi=(concnt_percTi+concnt_percTi2)*10^3;%Ti

concnt_allV=(concnt_percV+concnt_percV2)*10^7;%V

concnt_allZn=(concnt_percZn+concnt_percZn2)*10^6;%Zn

%% Ag

%%

Resultsh=[concnt_allAl;concnt_allSb;concnt_allBa;concnt_allBe;concnt_allCd;concnt_allCa;concnt_allCr;concnt_allCo;concnt_allCu;concnt_allFe;concnt_allPb;concnt_allLi;concnt_allMg;concnt_allMn;concnt_allMo;concnt_allNi;concnt_allK;concnt_allAg;concnt_allNa;concnt_allSr;concnt_allSn;concnt_allTi;concnt_allV;concnt_allZn]

%%

%Results2h=[concnt_Al;concnt_Sb;concnt_Ba;concnt_Be;concnt_Cd;concnt_Ca;concnt_Cr;concnt_Co;concnt_Cu;concnt_Fe;concnt_Pb;concnt_Li;concnt_Mg;concnt_Mn;concnt_Mo;concnt_Ni;concnt_K;concnt_Ag;concnt_Na;concnt_Sr;concnt_Sn;concnt_Ti;concnt_V;concnt_Zn];

%%
```

Vitae

Name :Mohsin Sarwar

Nationality :Pakistani

Date of Birth :10/28/1987

Email :mohsinsarwarabbasi@gmail.com

Address :H.NO. 1437 Dohke Gulshane Irfan Stadium road Rawalpindi Pakistan

Academic Background :Bachelor of Physics

List of publications :M. A. Gondal, Umair Baig, M. A. Dastageer, and Mohsin Sarwar. Determination of elemental composition of coffee using UV-pulsed laser induced breakdown spectroscopy, AIP Conference Proceedings 1742, 030007 (2016) Published